Coherent Multidimensional Spectroscopy: Development of Efficient Data Acquisition and Analyses of Quantum Dot 2D Spectra

Wang, Zhengjun

2021

Document Version:
Peer reviewed version (aka post-print)

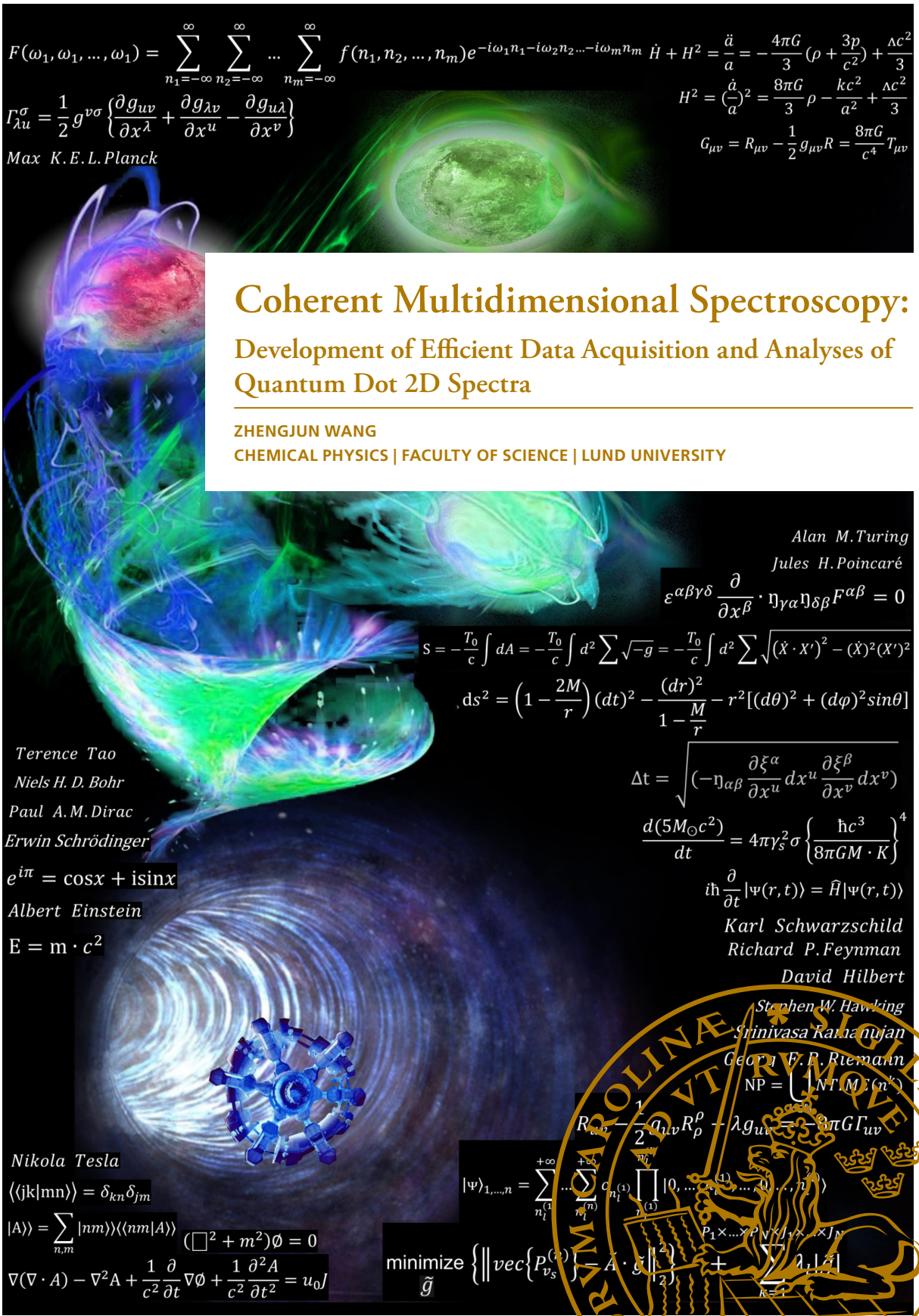
$F(\omega_1,\omega_1,\dots,\omega_1)=\sum_{n_1=-\infty}^{\infty}\sum_{n_2=-\infty}^{\infty}\dots\sum_{n_m=-\infty}^{\infty}f(n_1,n_2,\dots,n_m)e^{-i\omega_1 n_1-i\omega_2 n_2\dots-i\omega_m n_m}$
$\dot{H}+H^2=\frac{\ddot{a}}{a}=-\frac{4\pi G}{3}(\rho+\frac{3p}{c^2})+\frac{\Lambda c^2}{3}$
$H^2=(\frac{\dot{a}}{a})^2=\frac{8\pi G}{3}\rho-\frac{kc^2}{a^2}+\frac{\Lambda c^2}{3}$
$\Gamma^{\sigma}_{\lambda u}=\frac{1}{2}g^{v\sigma}\left\{\frac{\partial g_{uv}}{\partial x^{\lambda}}+\frac{\partial g_{\lambda v}}{\partial x^{u}}-\frac{\partial g_{u\lambda}}{\partial x^{v}}\right\}$
Max K.E.L.Planck
$G_{\mu v}=R_{\mu v}-\frac{1}{2}g_{\mu v}R=\frac{8\pi G}{c^4}T_{\mu v}$
Coherent Multidimensional Spectroscopy:
Development of Efficient Data Acquisition and Analyses of Quantum Dot 2D Spectra
ZHENGJUN WANG
CHEMICAL PHYSICS | FACULTY OF SCIENCE | LUND UNIVERSITY
Alan M.Turing
Jules H.Poincaré
$\varepsilon^{\alpha\beta\gamma\delta}\frac{\partial}{\partial x^{\beta}}\cdot\eta_{\gamma\alpha}\eta_{\delta\beta}F^{\alpha\beta}=0$
$S=-\frac{T_0}{c}\int dA=-\frac{T_0}{c}\int d^2\sum\sqrt{-g}=-\frac{T_0}{c}\int d^2\sum\sqrt{(\dot{X}\cdot X')^2-(\dot{X})^2(X')^2}$
$ds^2=\left(1-\frac{2M}{r}\right)(dt)^2-\frac{(dr)^2}{1-\frac{M}{r}}-r^2[(d\theta)^2+(d\varphi)^2 sin\theta]$
Terence Tao
Niels H. D. Bohr
Paul A.M.Dirac
Erwin Schrödinger
$\Delta t=\sqrt{(-\eta_{\alpha\beta}\frac{\partial\xi^{\alpha}}{\partial x^{u}}dx^{u}\frac{\partial\xi^{\beta}}{\partial x^{v}}dx^{v})}$
$\frac{d(5M_{\odot}c^2)}{dt}=4\pi\gamma_s^2\sigma\left\{\frac{\hbar c^3}{8\pi GM\cdot K}\right\}^4$
$e^{i\pi}=\cos x+i\sin x$
Albert Einstein
$E=m\cdot c^2$
$i\hbar\frac{\partial}{\partial t}|\Psi(r,t)\rangle=\hat{H}|\Psi(r,t)\rangle$
Karl Schwarzschild
Richard P.Feynman
David Hilbert
Stephen W. Hawking
Srinivasa Ramanujan
Georg F.B.Riemann
$NP=\left\{\int NT,MI(n')\right.$
$R_{\mu\nu}-\frac{1}{2}g_{uv}R^{\rho}_{\rho}-\lambda g_{uv}=-8\pi G\Gamma_{uv}$
Nikola Tesla
$\langle(jk|mn)\rangle=\delta_{kn}\delta_{jm}$
$|\Psi\rangle_{1,\dots,n}=\sum_{n_l^{(1)}}^{+\infty}\dots\sum_{n_l^{(n)}}^{+\infty}c_{n_l^{(1)}}\prod_{n_l^{(1)}}^{n_l^{(1)}}|0,\dots,n_l^{(1)},\dots,n_l^{(n)}\rangle$
$|A\rangle\rangle=\sum_{n,m}|nm\rangle\rangle\langle\langle nm|A\rangle\rangle$
$(\square^2+m^2)\emptyset=0$
$\nabla(\nabla\cdot A)-\nabla^2 A+\frac{1}{c^2}\frac{\partial}{\partial t}\nabla\emptyset+\frac{1}{c^2}\frac{\partial^2 A}{\partial t^2}=u_0 J$
$\underset{\tilde{g}}{\text{minimize}}\left\{\left\|vec\left\{P_{v_s}^{(2)}\right\}-\tilde{A}\cdot\tilde{g}\right\|_{\left(\frac{1}{2}\right)}^{\left(\frac{1}{2}\right)}+\sum_{k=1}^{n}\eta_k|\tilde{g}|\right\}$
$P_1\times\dots\times P_N\sqrt{\times J_1\times\dots\times J_N}$

I am not sure how to define science, because science is nothing like the intuitive feelings brought on by music, painting and sports. Science is rather the unique enchantment of amusement. I prefer the rigorousness of mathematics to attractive physics. Even though I have no idea of where science would end, the ending probably lies in more advanced abstractions between mathematics and physics. I do not know how far I can go in my search for truth and soul. However, studying science makes my heart feel worthy.

Zhengjun Wang
Lund, Sweden
2021

Printed by Media-Tryck, Lund 2021 NORDIC SWAN ECOLABEL 3041 0903

LUND UNIVERSITY

Faculty of Science
Department of Chemistry
Division of Chemical Physics

ISBN 978-91-7422-834-2

Coherent Multidimensional Spectroscopy:
Development of Efficient Data Acquisition and Analyses of Quantum Dot 2D Spectra

Coherent Multidimensional Spectroscopy:

Development of Efficient Data Acquisition and Analyses of Quantum Dot 2D Spectra

Zhengjun Wang

DOCTORAL DISSERTATION

by due permission of the Faculty Science, Lund University, Sweden.
To be defended at lecture hall B, Kemicentrum, Naturvetarvägen 14, 22363 Lund.
Friday, the 5th of November 2021 at 09:00 am.

Faculty opponent
Prof. Dr. Jouko Korppi-Tommola

Organization LUND UNIVERSITY Division of Chemical Physics, Department of Chemistry Faculty of Science, P. O. Box 124. SE-221 00 Lund, Sweden	**Document name** Doctoral Dissertation **Date of issue** 2021-11-05
Author(s) Zhengjun Wang	Sponsoring organization

Title and subtitle

Coherent Multidimensional Spectroscopy: Development of Efficient Data Acquisition and Analyzes of Quantum Dot 2D Spectra

Abstract

Coherent multidimensional spectroscopy (CMDS) is the most complete nonlinear optical technique based on the interaction of multiple short laser pulses with matter. It has grown to play a significant role in studies of optoelectronic materials and pigment protein complexes. In this work we apply CMDS to investigate electronic excitations and their dynamics in semiconductor nanocrystals, so called quantum dots (QDs). We also apply modern sparsed sampling algorthms to speed up the data collection in the multidimensional experiments. We test the new methods on CMDS experiments on photosynthetic light harvesting complexes.

In CMDS spectral information is spread in multiple, typically two, dimensions. Such 2D spectra depend on time providing information about dynamics of the processes, both coherent and incoherent. The 2D view enables disentangling spectral features and dynamics which otherwise would be left “behind” the simple 1D spectra and thereby not visible in simpler low-dimensional representation.

In this thesis, we focus on the dynamics and data acquisition of CMDS from five aspects: the excited state dynamics in CdSe QDs at 77 K studied via two-color 2D spectroscopy; the quantum beating of CdSe QDs using 2D electronic spectroscopy (2DES); quantum size effects of CdSe QDs in CMDS; electron-phonon coupling in perovskite nanocrystals, and sparse sampling in the CMDS implemented via the theory of compressed sensing.

Specifically, we characterize the details of the relaxation dynamics of CdSe QDs through two-color 2D Spectroscopy. The beating 2D signal was analysed in terms of coherent LO-phonons of CdSe QDs. Besides, the correlation between the excited state energies and the size of CdSe QDs due to the quantum confinement is also analyzed at 77 K via the 2DES. The phonon coupling with excitons and free carriers in perovskite nanocrystals is characterized. Finally, the compressed sensing theory is used to reconstruct the fluorescence detected 2D spectra of the photosynthetic LH2 complexes.

Keywords

Two-color 2D spectroscopy, 2D electronic spectroscopy, 2D fluorescence spectroscopy, Compressed Sensing theory, CdSe QDs, LH2, Quantum beating

A classification system and/or index terms (if any)

Supplementary bibliographical information		**Language** English
ISSN and key title		**ISBN** 978-91-7422-834-2 (Print) 978-91-7422-835-9 (Digital)
Recipient’s notes	**Number of pages** 176	Price
	Security classification	

Signature 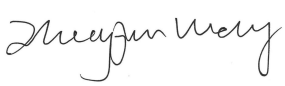 Date 2021-10-01

Coherent Multidimensional Spectroscopy:

Development of Efficient Data Acquisition and Analyses of Quantum Dot 2D Spectra

Zhengjun Wang

Coverphoto designed by Zhengjun Wang

Faculty of Science
Department of Chemistry
Division of Chemical Physics

ISBN 978-91-7422-834-2 (Print)
ISSN 978-91-7422-835-9 (Digital)

Printed in Sweden by Media-Tryck, Lund University
Lund 2021

To my supervisors: Tõnu, Donatas, Andreas

To the scientific truth and soul

Table of Contents

Abstract

Coherent multidimensional spectroscopy (CMDS) is the most complete nonlinear optical technique based on the interaction of multiple short laser pulses with matter. It has grown to play a significant role in studies of optoelectronic materials and pigment protein complexes. In this work we apply CMDS to investigate electronic excitations and their dynamics in semiconductor nanocrystals, so called quantum dots (QDs). We also apply modern sparsed sampling algorthms to speed up the data collection in the multidimensional experiments. We test the new methods on CMDS experiments on photosynthetic light harvesting complexes.

In CMDS spectral information is spread in multiple, typically two, dimensions. Such 2D spectra depend on time providing information about dynamics of the processes, both coherent and incoherent. The 2D view enables disentangling spectral features and dynamics which otherwise would be left “behind” the simple 1D spectra and thereby not visible in simpler low-dimensional representation.

In this thesis, we focus on the dynamics and data acquisition of CMDS from five aspects: the excited state dynamics in CdSe QDs at 77 K studied via two-color 2D spectroscopy; the quantum beating of CdSe QDs using 2D electronic spectroscopy (2DES); quantum size effects of CdSe QDs in CMDS; electron-phonon coupling in perovskite nanocrystals, and sparse sampling in the CMDS implemented via the theory of compressed sensing.

Specifically, we characterize the details of the relaxation dynamics of CdSe QDs through two-color 2D Spectroscopy. The beating 2D signal was analysed in terms of coherent LO-phonons of CdSe QDs. Besides, the correlation between the excited state energies and the size of CdSe QDs due to the quantum confinement is also analyzed at 77 K via the 2DES. The phonon coupling with excitons and free carriers in perovskite nanocrystals is characterized. Finally, the compressed sensing theory is used to reconstruct the fluorescence detected 2D spectra of the photosynthetic LH2 complexes.

Popular Science Summary

The speedy development of science and technology over the past century has been promoting our high-quality lives. Noteworthy examples in these advances are the fields of quantum physics and more recently artificial intelligence. Meanwhile, the development of spectroscopy plays a crucial role in the process of exploration of science. For example, it has been widely used to analyze the characteristics of materials, such as the properties of the excited states, relaxation dynamics, phonon coupling, quantum coherence, vibrational beatings, superposition states, etc. Traditionally, spectroscopy (as shown in Figure 1) is a technique based on the interaction between light and matter and explains the phenomena in the quantum physics field.

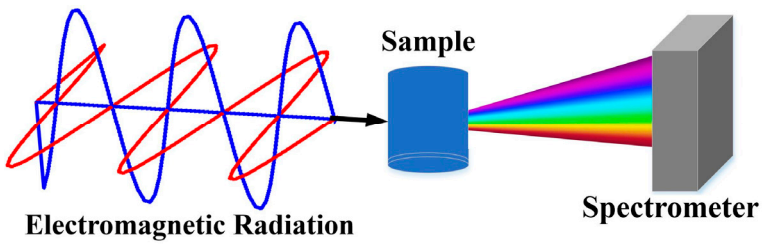

Figure 1. The simple principle of spectroscopy

Among different spectroscopies, coherent multidimensional spectroscopy (CMDS) is one of the most complete ultrafast techniques based on the interaction of multiple pulses to act on the sample and obtain a signal on multiple dimensions in the time and/or frequency domain. Usually, the frequency spectrum is spread in two dimensions and depends parametrically on one or possibly even more time delays. Therefore, it is called multidimensional spectroscopy.[1,2] Specifically, three laser pulses act on the sample and generate a signal. The measured signal is double Fourier transformed to obtain a 2D spectrum. Similarly, 3D spectrum will be obtained, when the signal is triple Fourier transformed using all three time delays. This 2D, 3D, or higher-dimensional spectra are collectively named CMDS.

One of the key factors which have enabled the abovementioned progress in our quality of life is the abundant availability of cheap energy in the form of coal, oil, natural gas, more recently shale gas, nuclear energy, wind energy, and photovoltaics. Many of the conventional energy sources are leading us to potentially devastating climate change while renewable energy sources like wind, hydro and solar have the potential to solve the problem. Particularly the solar energy is so

abundant that photovoltaics do have the true potential to be the major game-changer. For this to occur more efficient and cheaper photovoltaics would be desirable. For that better understanding of the limiting factors of the current and rational design of the new solar materials is needed. In this context, CMDS can help us to understand light-induced processes materials and thereby can help us in optimizing the materials. One of such materials is colloidal semiconductor nanocrystals, so-called quantum dots (QDs). If we can clearly know how the dynamic process works, it will greatly improve the energy utilization for human beings on earth. Moreover, CMDS has recently become an important technology to research the high excitation energy dynamics in the quantum world. Thus, I believe CMDS is a good way to understand the nature of the surrounding world. 2D spectroscopy is the most commonly used CMDS method. The advantage of 2D spectroscopy is more easily to detect information such as quantum coherence that is not as easily available by other spectroscopies. 2D spectroscopy has developed rapidly in recent years. Among the recent developments, we can name artificial intelligence technology developments which have allowed us to optimize the data acquisition algorithms in 2D spectroscopy in terms of experimental data collection and theoretical model establishment. As an outlook, we can name here the recent proposals to use entangled photons in future quantum light spectroscopies where possibilities also for multidimensional spectroscopies have been pointed out. Though, these new exciting developments remain the topic of the future theses.

This thesis is mainly about the development of efficient data acquisition and analyses of the excited state dynamics in quantum dots 2D spectra of CMDS. Specifically, 2D electronic spectroscopy is applied to study the relaxation dynamics and quantum beatings in CdSe QDs (as shown in Figure 2). Additionally, compressed sensing theory with dictionary learning from machine learning is used to reconstruct the 2D fluorescence spectrum of the light-harvesting complexes II (LH2) protein.

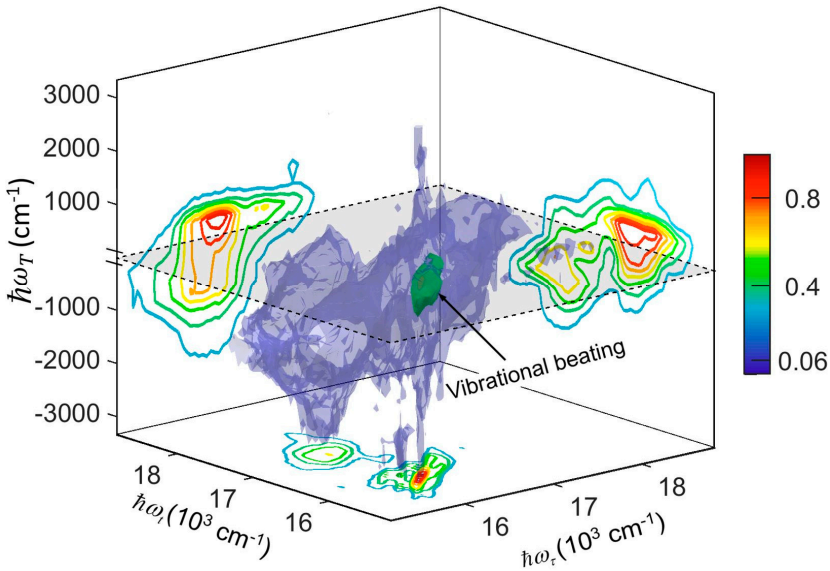

Figure 2. The quantum beating of CdSe QDs was measured using 3D spectroscopy at 77 K. The x and y axes are excitation and detection energy, respectively. The green band is the vibrational beating.

Acknowledgments

Primarily, my appreciation goes to Professor Tõnu Pullerits, Professor Donatas Zigmantas, and Professor Andreas Jakobsson, three important supervisors for my Ph.D. study, who are also the enlightenment of my life in the research field. Thank you very much for guiding me through my Ph.D. journey systematically. Firstly, Professor Tõnu Pullerits, I would like to thank you so much for all conditions that you provided for my Ph.D. study. I enjoyed the relaxing surrounding in our group. You have patiently taught me the knowledge of coherent multidimensional spectroscopy (CMDS) every time. Even if I always ask you the same question repeatedly, you still answer me patiently. Forgive my poor spoken and written English. Thank you very much for your dedication to me in the past five years. Discuss patiently with me and help me with my development of science. I enjoy the process of discussing with you every time. When this doctoral dissertation is submitted, it is like a tree that you have cultivated will grow on its own. I wish I could keep discussing with you. But after all, I have to face everything myself. I believe that your attitude towards life and the spirit of science will always guide me. Your serious and responsible instructions personally guided my Ph.D. research, and your rigorous scientific attitude influenced my future research journey. It is also the wealth of my life. Thank you for bringing me into the quantum world and let me explore the mystery of quantum physics. Secondly, Professor Donatas Zigmantas, thank you so much for your care and help. You always encouraged and praised me, which inspired me very much. Your work attitude, wisdom, and breadth of mind are worth learning for me forever. You've also told me a lot of interesting stories. In every discussion and conversation with you, your knowledge of science, some famous scientists, and the papers published on *Nature* and *Science* show me new insights, and the history of CMDS made me more aware of the development of a science and what I need to do on this road. I will go further if I do the research of my interests. Regarding some of the quantum light insights we discussed earlier, I look forward to discussing with you again after ten years. Thirdly, Professor Andreas Jakobsson, A professor who likes boxing makes me admire your intelligence and have a new understanding of a professor. I also realize how to express a complex mathematical theory with refined formulas. What you did for me makes me experience the charm of mathematics. Thank you for your patient to teach me the compressed sensing theory. Your patience and careful explanation of the compressed sensing theory combined with dictionary learning brought me from the quantum world into the mathematics world. Moreover, I was impressed by the field of artificial intelligence. Importantly, I would like to thank my colleague, Dr. Nils Lenngren. Thank you very much for your patience in introducing me to the research of QDs using 2D spectroscopy and the revision of our paper. Moreover, the collaborators and

researchers like Khadga Jung Karki, Lukas Bruder, Albin Hedse, Edoardo Amarotti, and Pavel Kolesnichenko. Without your kind help, this thesis could not be what it is now. Thanks a lot to the staff and guys in my division, Arkady Yartsev: you are my sports teacher who entered Sweden for my Ph.D. study. My basketball and football skills are under your guidance. Ivan Scheblykin, you are an enthusiastic and friendly professor, and glad to spend five years with you. Ebbe Nordlander. Villy Sundström. Eva Unger. Per Uvdal. Jens Uhlig, you are a delightful and cheerful researcher. Because I enjoy playing basketball together and appreciate your help on my postdoc. Pavel Kolesnichenko, I would say that I enjoy discussing CMDS and chatting together. Eglė Bukartė, a beautiful and passionate girl, who did me a good favor in the experiment of CMDS, really appreciated. Linnea Linda, a beautiful and elegant girl, helped me a lot in study and life. Albin Hedse, a handsome and optimistic boy. I enjoy discussing and doing research with you, especially about entangled photons spectroscopy. Edoardo Amarotti, I like your productive way of doing research, especially when researching CMDS with you. I wish someday we could play football together. Kaibo Zheng, thank you for your concern for me all the time. Qi Shi, I am really grateful to you for help as my officemate. Besides, colleagues like Junsheng Chen, Shiwen Lei, Fan Wu, Zehan Yao, Wei Zhang, Weihua Lin, Lukas Wittenbecher, Jiangbin Zhang, Supriya Ghosh, Pushpendra Kumar, Daniel Finkelstein-Shapiro, Alireza Honarfar, Pavel Chabera, Bin Yang, Yong Li, Meiyuan Guo, Wei Zhou, Ting Sun, Lukas Bruder, and so on, other colleagues in our division are also on my thank-you list. I am very grateful to my good friend, Dr. Dongsheng Wang. We hung out a lot together in Europe and have gone through a lot during our Ph.D. studies. I am also very grateful to my good friend, Jin Li at Cambridge University. We met in Laboratory 1306 of Tsinghua University, and met again at Cambridge University, Bo Ma and Jingjing Zhao at Stanford University, Mingsong Wei and Kaicheng Dong at UC Berkeley, Zhiwei Chang at Massachusetts Institute of Technology, Our Soul-Truth band (Yong, Xing, Jingjing), Fan Liang for my English writing. I would also like to thank my master's supervisor Prof. Jianzhong Yang at Tsinghua University, Prof. Yiyong Yang at the China University of Geosciences (Beijing). I also want to thank NanoLund, Lund University, Tsinghua University, and China University of Geosciences (Beijing), these platforms that created many advanced scientific frontier knowledge. For financial support, I first thank the China Scholarship Council that provided me the Ph.D. study scholarship for my life and accommodation in Sweden. The Swedish Research Council (VR) and the Swedish Foundation are acknowledged for funding the work and visiting studies. I also want to thank the Royal Physiographic Society in Lund and the ÅForsk for supporting me to attend conferences. Finally, yet importantly, I would like to express my special thanks to my family members, my father Renqiang Wang, my mother Limei Shen. I appreciate that your support and care. You may rest assured, that I'll not let you down and am capable of taking good care of myself. Your happiness and health are the best wishes of mine.

List of Publications

This thesis is based on the following publications. All publications have been attached in their current state by the end of the thesis.

Publications are included in the thesis:

I. Zhengjun Wang, Nils Lenngren, Edoardo Amarotti, Karel Zidek, Albin Hedse, Kaibo Zheng, Donatas Zigmantas, Tõnu Pullerits. "Excited states and their dynamics in CdSe quantum dots studied by two-color 2D Spectroscopy" (Submitted).

II. Zhengjun Wang, Nils Lenngren, Karel Zidek, Albin Hedse, Edoardo Amarotti, Kaibo Zheng, Donatas Zigmantas, Tõnu Pullerits. "Beating signals in CdSe quantum dots measured by low-temperature 2D spectroscopy" (Manuscript).

III. Zhengjun Wang, Edoardo Amarotti, Nils Lenngren, Karel Zidek, Kaibo Zheng, Donatas Zigmantas, Tõnu Pullerits. "Quantum size effects in 2D spectroscopy of CdSe quantum dots." (Manuscript).

IV. Zhengjun Wang, Shiwen Lei, Khadga Jung Karki, Andreas Jakobsson, Tõnu Pullerits. "Compressed Sensing for Reconstructing Coherent Multidimensional Spectra", *Journal of Physics Chemistry A*. 2020. 124. 1861-1866.

V. Supriya Ghosh, Qi Shi, Bapi Pradhan, Pushpendra Kumar, **Zhengjun Wang**, Somobrata Acharya, Suman Kalyan Pal, Tõnu Pullerits, Khadga Jung Karki. "Phonon Coupling with Excitons and Free Carriers in Formamidinium Lead Bromide Perovskite Nanocrystals". *Journal of Physics of Physics Chemistry Letters*. 2018. 9. 4245-4250.

Publications are not included in the thesis:

VI. Bin Yang, Junsheng Chen, Qi Shi, **Zhengjun Wang**, Marina Gerhard, Alexander Dobrovolsky, Ivan G. Scheblykin, Khadga Jung Karki, Keli Han, Tõnu Pullerits. "High Resolution Mapping of Two-Photon Excited Photocurrent in Perovskite Microplate Photodetector", *Journal of Physics of Physics Chemistry Letters*, 2018. 9. 5017-5022.

VII. Qi Shi, Supriya Ghosh, Abdus Salam Sarkar, Pushpendra Kumar, **Zhengjun Wang**, Suman Kalyan Pal, Tõnu Pullerits, Khadga Jung Karki. "Variation in the Photocurrent Response Due to Different Emissive States in Methylammonium Lead Bromide Perovskites". *Journal of Physics Chemistry C*. 2018. 122. 3818-3823.

My Contribution to the Publications

Publications are included in the thesis:
I. Zhengjun Wang, Nils Lenngren, Edoardo Amarotti, Karel Zidek, Albin Hedse, Kaibo Zheng, Donatas Zigmantas, Tõnu Pullerits. "Excited states and their dynamics in CdSe quantum dots studied by two-color 2D Spectroscopy".
I processed and analyzed the experimental data, performed theoretical analysis on 2D spectroscopy, performed data processing and analysis, discussion arrangement, and interpretation. I drafted the major part of the paper.

II. Zhengjun Wang, Nils Lenngren, Karel Zidek, Albin Hedse, Edoardo Amarotti, Kaibo Zheng, Donatas Zigmantas, Tõnu Pullerits. "Beating signals in CdSe quantum dots measured by low-temperature 2D spectroscopy".
I processed and analyzed the experimental results, performed theoretical analysis on 2D and 3D spectroscopy, performed data processing and analysis, discussion arrangement, and interpretation. I drafted the manuscript.

III. Zhengjun Wang, Edoardo Amarotti, Nils Lenngren, Karel Zidek, Kaibo Zheng, Donatas Zigmantas, Tõnu Pullerits. "Quantum size effects in 2D spectroscopy of CdSe quantum dots".
I processed and analyzed the experimental results, performed theoretical analysis on the correlation between size and excited states in CdSe QDs, performed data processing and analysis, discussion arrangement, and interpretation. I drafted the major part of the paper.

IV. Zhengjun Wang, Shiwen Lei, Khadga Jung Karki, Andreas Jakobsson, Tõnu Pullerits. Compressed Sensing for Reconstructing Coherent Multidimensional Spectra. *Journal of Physics Chemistry A*. 2020. 124. 1861-1866.
I processed and analyzed the experimental results, performed theoretical analysis on coherent multidimensional spectra and compressed sensing, performed data processing and analysis, discussion arrangement, and interpretation. I drafted the major part of the paper.

V. Supriya Ghosh, Qi Shi, Bapi Pradhan, Pushpendra Kumar, **Zhengjun Wang**, Somobrata Acharya, Suman Kalyan Pal, Tõnu Pullerits, Khadga Jung Karki. "Phonon Coupling with Excitons and Free Carriers in Formamidinium Lead Bromide Perovskite Nanocrystals". *Journal of Physics of Physics Chemistry Letters*. 2018. 9. 4245-4250.
I participated in experiments and discussions, edited and commented on the manuscript.

Abbreviations

1D	One Dimension
2D	Two Dimensions
3D	Three Dimensions
QDs	Quantum Dots
2DES	Two-dimensional Electronic Spectroscopy
2DFS	Two-dimensional Fluorescence Spectroscopy
DFT	Discrete Fourier Transform
FWHW	Full Width at Half Maximum
FFT	Fast Fourier Transform
CB	Conduction Band
VB	Valence Band
GSB	Ground State Bleach
ESA	Excited State Absorption
SE	Stimulated Emission
CS	Compressed Sensing
3DS	Three Dimensional Spectroscopy
Two-color 2DS	Two-color 2D Spectroscopy
CdSe	Cadmium Selenium
S-E	Schrödinger Equation
L-E	Liouville Equation
PC	Planck Constant
HS	Hilbert Space
LS	Liouville Space
LNE	Liouville-von Neumann Equation
DM	Density Matrix
DSFD	Double-sided Feynman Diagram
RF	Response Functions
$\psi(t)$	The Wave function
$\|\rho(t)\rangle\rangle$	The Density Matrix
$\langle\langle\rho(t)\|$	The Hermitian conjugate of the density matrix
H	Hamiltonian

$\|(t)\rangle$	Dirac ket
$\langle(t)\|$	Dirac bra
dFT	double Fourier Transform
tFT	triple Fourier Transform
CMDS	Coherent Multidimensional Spectroscopy
fs	femtosecond (10^{-15}s)
μ	Dipole Operator
Td	Time dimension
Fd	Frequency dimension
SEMA	Sparse Exponential Mode Analysis
LASSO	Least Absolute Shrinkage and Selection Operator
CVX	Matlab-based modeling system for convex optimization
DL	Dictionary Learning
ML	Machine Learning
LH2	Light-harvesting Complexes II of photosynthetic purple bacteria
B800	BChl molecules with an absorption band at about 800 nm
B850	BChl molecules absorbing around 850 nm
$\otimes$	Denoting the outer product
$\omega_k^{(l)}$	Denoting the frequency in the l^{th} dimension of the k^{th} 2D spectral band, where l = 1 or 2.
$\beta_k^{(l)}$	Denoting the width (damping) in the l^{th} dimension of the k^{th} 2D spectral band, where l = 1 or 2.
τ (or t_1)	The coherent time
T (or t_2)	The population time
t (or t_3)	The detection time
CP	Cross Peak
DP	Diagonal Peak
P-P	Pump-Probe
QC	Quantum Coherence
QB	Quantum Beating
R	Rephasing
NR	Non-Rephasing
NOS	Nonlinear Optical Spectroscopy

Chapter 1 Introduction

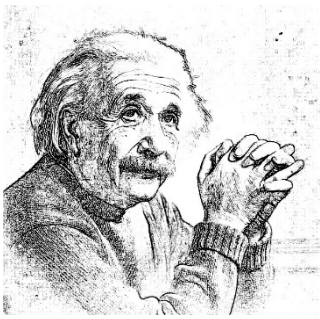

"The true sign of intelligence is not knowledge but imagination."

– Albert Einstein

Boundaries of our knowledge in the fields of biology, chemistry, and physics are expanding with ever-increasing speed. In this astonishing progress, we can identify quantum physics as one of the most important foundations for scientific breakthroughs. In particular, quantum optics theory has promoted the rapid progress of spectroscopy science. Specifically, in terms of nonlinear optical theory, coherent multidimensional spectroscopy (CMDS) is a crucial experimental technology in exploring the fields of materials, biology, physics, and chemistry. One of the fields where CMDS has played an important role is the research of primary processes in photosynthesis. The evolution process has optimized the biological machinery of photosynthesis for hundreds of millions of years. Understanding the essentials of this optimization can give ideas for better man-made devices like, for example, solar cells. Thus, as for the CMDS, these technologies can discover the mysterious quantum world and explore the dynamics in the biological proteins and nanomaterials.

In the above context, this thesis mainly studies the excited states dynamics, quantum beating, and relaxation dynamics in CMDS by testing two nano materials, namely cadmium selenium quantum dots (CdSe QDs) and the light-harvesting antenna complexes II (LH2) of the photosynthetic purple bacteria. This chapter introduces the energy level of the samples and the basics of spectroscopy.

1.1 The Samples

Climate change due to the rapidly growing human energy consumption during the last decades is the most serious current challenge for mankind. Figure 1.1(a) shows how global energy consumption increases in the past decades, while Figure 1.1(b) reveals global environmental pollution. Apparently, it is urgent to find alternative clean energy from some emerging energy technology and materials. Luckily, at the end of 20th century, semiconductors, organic materials, and other materials have been pointed as the significant way out for energy research.

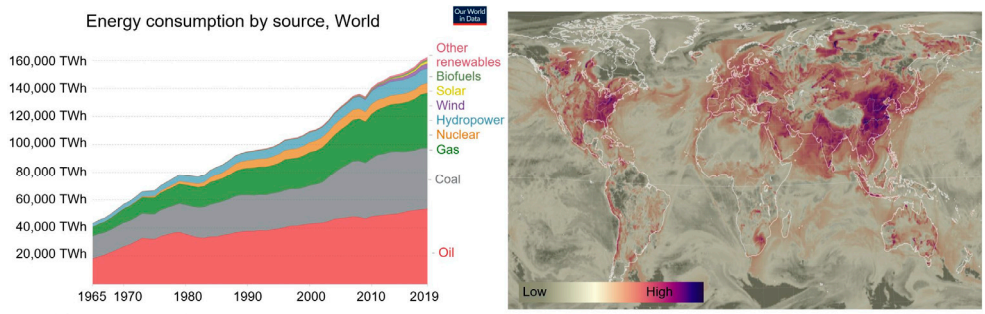

(a) Changes in global energy consumption over time

(b) The world's sulfur dioxide pollution map(2020)

Figure 1.1 Energy consumption (Reproduced from the OurWorldInData and BP Statistical Review of World Energy) and environmental pollution throughout the world (copyright 2020, EarthWindMap, the High-Resolution Global Atmospheric Model). (a). The world energy consumption is from 1965 to 2019. (b). The global sulfur dioxide pollution distribution map is from 2020, among which the darker areas are areas with more pollution.

Semiconductors are the main materials in terms of basic energy research. Currently, these materials such as quantum dots (QDs) and perovskites belong to basic energy research. Moreover, there is no doubt that humans have consumed energy from the sun and nature since ancient times. The daily energy intake of animals in nature mainly comes from the energy absorbed by plants from sunlight. So photosynthesis has been an important energy source since the emergence of life on earth. In a nutshell, photosynthetic protein plays a crucial role in energy absorption in the biological world. Therefore, by studying the mechanism of these materials via CMDS, we can promote the development in terms of material application such as artificial photosynthetic proteins in the efficient use of energy.

1.1.1 Photosynthetic proteins

With the growing energy demand, desirable energy materials will be increasingly needed. Photosynthetic proteins play a vital role in providing energy for biological processes in nature. Primary photosynthetic processes like light absorption and the initial charge separation have very high quantum efficiency – almost every absorbed photon leads to charge separation. While the charge-separating units, the so-called reaction centers (RC), are rather similar, there is large variety of the different light harvesting antennae. An example of the primary photosynthetic machinery of the photosynthetic purple bacteria is shown in Figure 1.2. In our studies, the light-harvesting antenna 2 (LH2),[3–8] is used. The full system includes RC, B875 (BChl an absorbing at 875 nm) antenna called LH1, and two parts of the LH2: B800 (BChl an absorbing at 800 nm), and B850 (BChl an absorbing at 850 nm).[9,10]

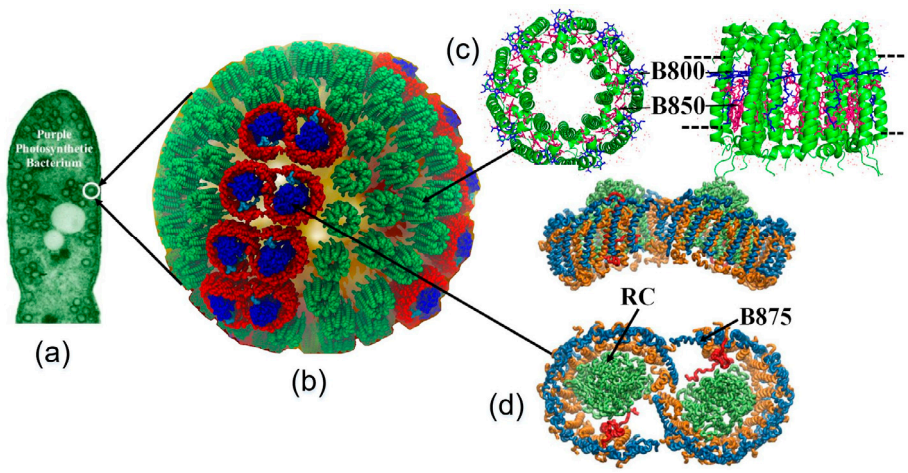

Figure 1.2. (a). Photosynthetic purple bacteria protein.[3,8] (b). The structure of the photosynthetic unit of purple bacteria[5–7,11,12] Copyright from the theoretical and computational biophysics group Beckman institute, the University of Illinois at Urbana-Champaign. (c). LH2 protein. (d). RC and B875 protein.

There are two rings of bacteriochlorophyll a (BChl a) molecules in the LH2. The B800 [9,10] consists of nine well-separated BChl a molecules with an absorption band at about 800 nm. The other ring, named B850, contains eighteen closely packed BChl a molecules absorbing around 850 nm.[9,10,13]

The preparation of our sample is described below. LH2 complexes were isolated from Rhodopseudomonas acidophilus 10050.[14] The isolated LH2 complexes were dispersed in Tris-HCl buffer containing 0.1% N, N-dimethyldodecylamine N-oxide. The LH2 solution is deoxygenated by adding oxygen scavenger to system. For more specific details, please refer to the research literature.[15]

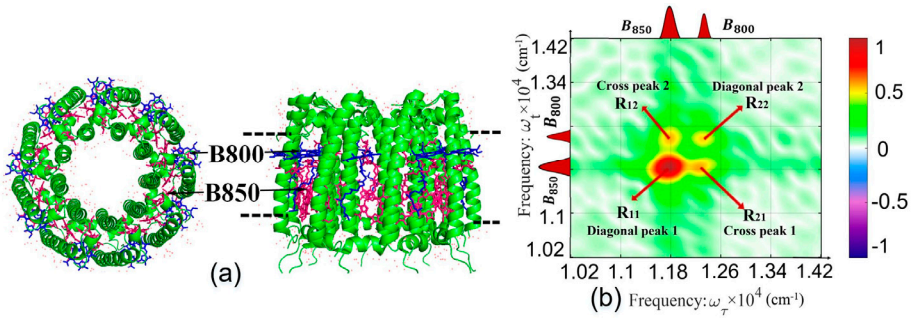

Figure 1.3. The light-harvesting complexes II (LH2) and its corresponding 2D fluorescence spectrum.[16]

In photosynthesis research, many excellent studies have been conducted by applying CMDS, such as Fleming group observed quantum coherence in the FMO protein using 2D spectroscopy.[17,18] These experiments first put forward the idea that quantum coherence can play a role in photosynthesis. In 2014, Zigmantas and Grondelle groups studied the energy conversion of photosynthesis using 2D spectroscopy.[19] Moreover, Zigmantas made a further study on vibrational coherence in RC proteins in 2017.[20]

In our work, we use the fluorescence-detected 2D spectroscopy data measured on LH2 as the testing ground for the new sparse sampling algorithms for optimizing the data acquisition. The 2D spectrum of the LH2 has four pronounced peaks R_{11}, R_{12}, R_{21}, and R_{22} in which correspond to the two clear linear absorption bands,[15,21,22] as shown in Figure 1.3(a) and the 2D spectrum of LH2 protein in Figure 1.3(b).[16] The new compressed sensing method allows to reconstruct the basic features of such 2D spectrum with the drastically reduced amount of the necessary measurement points.

1.1.2 Quantum dots

Quantum dots are semiconductor nanocrystals with quantum confinement effect also known as "artificial atoms". Due to the quantum confinement, they have discrete excited states.[23] Here, our sample CdSe QDs are composed of cadmium and selenium elements in the IIB and VIA groups in the periodic table.

Details of the synthesis of CdSe QDs are described in literature.[24–27] Briefly, the CdO oleic acid as the capping agent is heated to 340°C. Then, Se is injected into the octadecene solution with trioctyl phosphine as a capping agent and cooled rapidly for 2 minutes. Finally, the sample is purified and transferred to the hexane solution.

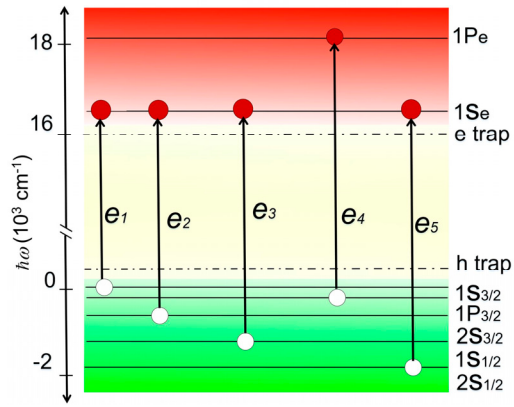

Figure 1.4. Excited states model of CdSe QDs.

Electronic excitations in QDs have been actively studied by many groups. For example, Bawendi at MIT investigated the excited state dynamics of QDs with different sizes,[23,28,29] and Klimov at the Los Alamos National Laboratory studied the relaxation, multiexcitons, and charge transfer in QDs.[30] In the current work, the studies of excited states dynamics in CdSe QDs by Lenngren et al.[24] are further expanded. Especially, we study the relaxation dynamics at the low temperature 77 K. Based on the previous studies,[23,24,31] we describe the excited states in the QDs by the combination of the principal quantum number and the angular momentum state (for example, 1S, 1P, and 1D), adding the total angular momentum term (3/2, 1/2). The combined label of these symbols and numbers constitute a representation method of excited states in CdSe QDs,[29,31] therefore, in this work, there are five excited states of CdSe QDs visible in our 2D spectroscopy measurements. Thus, the following symbols $|e_1\rangle$, $|e_2\rangle$, $|e_3\rangle$, $|e_4\rangle$, and $|e_5\rangle$ correspond to the excited states of $1S_{3/2}(h) - 1S(e)$, $2S_{3/2}(h) - 1S(e)$, $1S_{1/2}(h) - 1S(e)$, $1P_{3/2}(h) - 1S(e)$, and $2S_{1/2}(h) - 1S(e)$,[24] respectively. These excited states of CdSe QDs are visualized in Figure 1.4. These states were identified in previous research[23] and are shown in Figure 1.5 from Bawendi group.

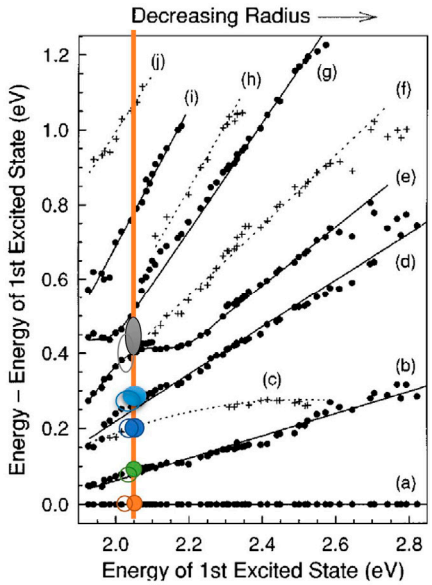

Figure 1.5. The excited states of CdSe QDs.[32] The orange, green, blue, gray, and light gray circles stand for excited states e_1, e_2, e_3, e_4, and e_5, respectively.

The values of excited states in Table 1.1 are obtained by fitting the 2D spectrum in Figure 1.6.

Table 1.1. The excited states of CdSe QDs in the 2DES.

Energy states	$\|e_1\rangle$	$\|e_2\rangle$	$\|e_3\rangle$	$\|e_4\rangle$	$\|e_5\rangle$
The peaks (cm^{-1})	16200	16900	17800	18300	19700

To more clearly study the excited state dynamics among the peaks of CdSe QDs, we fit these excited states by Gaussian in the 2D spectra in Figures 1.6 and 1.7.

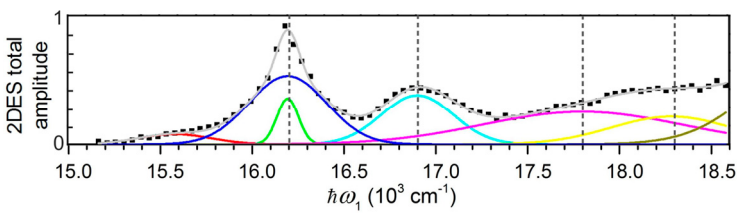

Figure 1.6. A slice of the total 2D spectrum and the absorption spectrum are fitted to find out the excited states of CdSe QDs at ω_3=16200 cm^{-1} at 10 ps. One-color low-energy area. The excited state e_1 is 16200 cm^{-1} in the green curve. The excited state e_2 is 16900 cm^{-1} in the blue curve. The excited state e_3 is 17800 cm^{-1} in the pink curve. The excited state e_4 is 18300 cm^{-1} in the yellow curve.[24]

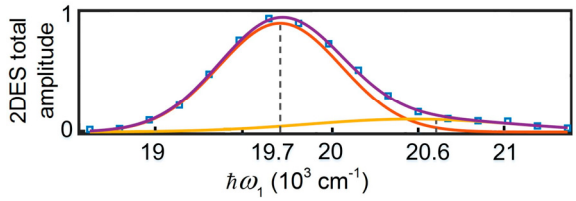

Figure 1.7. A slice of the total 2D spectrum and the absorption spectrum are fitted to find out the excited states of CdSe QDs. One-color high-energy area. The excited state e_5 is 19700 cm^{-1} in the brown curve.

The excited states in Figures 1.6, 1.7, and Table 1.1 are also consistent with the results in Figure 1.5 from Bawendi group.

1.2 Ultrafast Phenomena

To understand ultrafast spectroscopy, it is necessary to consider the time scale. Firstly, we describe the ultrafast phenomenon from the following time scales: nanosecond (10^{-9} s), picosecond (10^{-12} s), femtosecond (10^{-15} s),[33] attosecond (10^{-18} s), zeptosecond (10^{-21} s),[34,35] and yoctosecond (10^{-24} s).[36] To make us feel them more clearly, it is necessary to associate them with some specific physical phenomena.

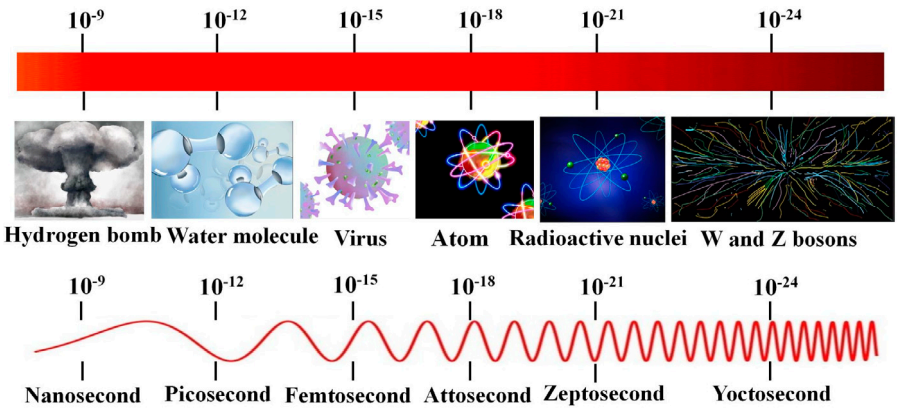

Figure 1.8. The examples of different time scale from nanosecond to yoctosecond. The colorful band on the top simply represents time scales in different time units, which has nothing to do with the color of the light.

Here, for the nanosecond (ns), it takes 20 to 40 ns to complete the fusion in the hydrogen bomb.[37] For the picosecond (ps), the time for water molecules to rotate is about 1.7 ps.[38] For the femtosecond (fs), it takes 1 fs for a beam of light to travel the diameter of the virus about 0.3 um.[39] For the attosecond (as), attosecond spectroscopy can detect basic electronic processes that occur on the attosecond time

scale in condensed matter systems and surfaces.[40] For the zeptosecond (zs), it takes 2 zs for the representative cycle time of gamma radiation released in the decay of radioactive nuclei.[41–43] For the yoctosecond (ys), the average lifespan of W and Z bosons is 0.3 ys.[43,44] These specific examples are summarized in Figure 1.8.
Ultrashort pulses are based on some of the above ultrafast time scales. Ultrafast spectroscopy is a technique that uses ultrashort pulses to study dynamic processes in materials. Besides resolving in time, traditionally, one also measures the energy of light providing spectrum which provides information about the interaction of light acting on the sample.

1.3 Spectroscopy

This part mainly focuses on the understanding of spectroscopy from two aspects: the concept and history of spectroscopy. Then, followed by ultrafast phenomena, the application of spectroscopy, and the current study of 2D spectroscopy.

1.3.1 The concept of spectroscopy

The word “spectroscopy” can be traced back to its Latin suffix, "spectron". It’s stated in Wikipedia that the word “spectroscopy” (“appearance, image, apparition”), from speciō (“look at, view”).[45–47] “Spectrum” is the “image” of the light energies. Before taking the image, the light has interacted with matter, the spectrum gives us information about the matter.[48] This interaction mainly comes from the electric field of light (the effect of the magnetic field is so minimal that can be ignored here). The electric field of light interacts with the sample to obtain a spectrum, including measurable characteristics such as amplitude, frequency, phase, and polarization.

1.3.2 The history of spectroscopy

The development of spectroscopy can date back to the 17th century. Isaac Newton first put forward the description of the colors in the rainbow and published his paper on *Optics*.[49] Later, Joseph von Fraunhofer began to measure the dark lines in the solar spectrum using spectrometers. After that, dozens of scientists have developed spectroscopy in terms of instrumental and theoretical aspects. Especially in 1873, Maxwell proposed the electromagnetic wave equations that provide a basis for the mathematical description of spectroscopy.[50] In 1895, Wilhelm Conrad Röntgen opened up new possibilities by discovering X-rays. In the early twentieth century, physicists like Max Plank, Albert Einstein, Niels Bohr, Wolfgang Pauli, Werner Heisenberg, Erwin Schrödinger, Thomas Young, Ludwig Boltzmann, Max Born, David Hilbert, John von Neumann, and Paul Dirac opened up new horizons for the

basis of the interaction of light and matter.[51] The interaction between light and matter can be observed through spectroscopy technology.[48] The Nobel Prize[52] has also been awarded to many scientists who have contributed to spectroscopy, as shown in Figure 1.9.

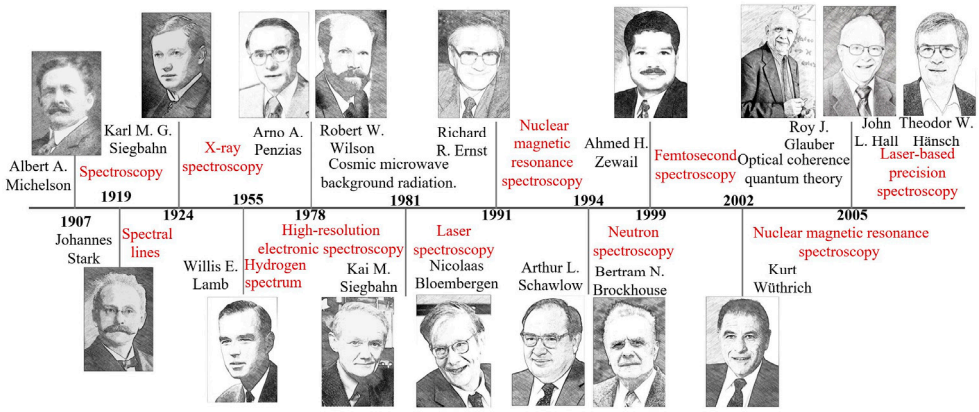

Figure 1.9. Nobel Prize winners related to spectroscopy (Copyright Nobel prizes web).[52]

In the 1980s, Nobel laureate Ahmed H. Zewail used ultrashort pulses to observe chemical reactions at the femtosecond time scale, thus contributing to the development of femtosecond chemistry and ultrafast spectroscopy.[53] Moreover, Graham R. Fleming, Michael Fayer, Shaul Mukamel systematically proposed new nonlinear optical spectroscopy methods. Simultaneously, other scientists, such as R. J. Dwayne Miller, Keith A. Nelson, David M. Jonas, Tobias Brixner, Tõnu Pullerits, Donatas Zigmantas, Andrei Tokmakoff, Jennifer Ogilive, Gregory S. Engle, Kevin Kubarych, Steven Cundiff, Peter Hamm, Minhaeng Cho, Andrew H. Marcus, Yoshitaka Tanimura, Jeffrey Davis, Thomas L. C. Jansen, Oliver Kühn, Howe-Siang Tan, Gabriela S. Schlau-Cohen, and so on, have contributed to CMDS.

1.3.3 The application of 2D spectroscopy

Spectroscopy has been widely used in the fields of astrophysics, quantum physics, biology, and chemistry. Following are some representative examples.

Intuitively, nontrivial quantum effects are likely to be observable in experiments using quantum light, for example, spectroscopy with entangled photons. Besides, CMDS has also been shown to be very useful in investigating quantum effects like quantum beating. For example, Fleming group observed beating signals in 2D spectra of the so-called FMO photosynthetic protein in 2007 as shown in Figure 1.10.[18]

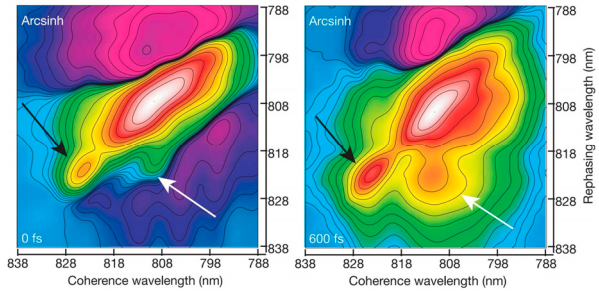

Figure 1.10. The quantum coherence of photosynthetic protein was measured by Fleming's group.[18]

In photosynthetic research, CMDS has been frequently used to study the details of the energy transfer dynamics of pigment protein complexes. For example, Grondelle,[19] Pullerits[15] groups. Sundström[54] groups also researched the dynamics of LH2 protein. Zigmantas[55] group detected the energy transfer time of photosynthetic proteins as illustrated in Figure 1.11.

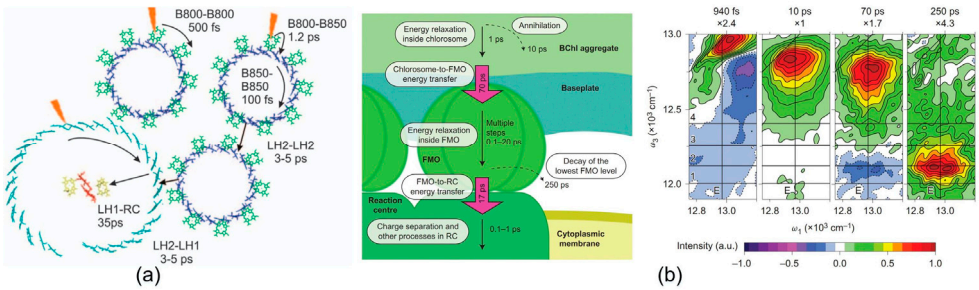

Figure 1.11. (a). The photosynthetic system of purple bacteria is composed of LH1, RC, and LH2 proteins.[56,54] (b). The time scales of energy flow in photosynthesis and the related 2D spectrum.[55]

In the chemistry field, CMDS has been applied to determine compounds, elements, and dynamic processes. For example, Hamm group researched hydrogen-bond dynamics in a β-turn (Figure 1.12).[57]

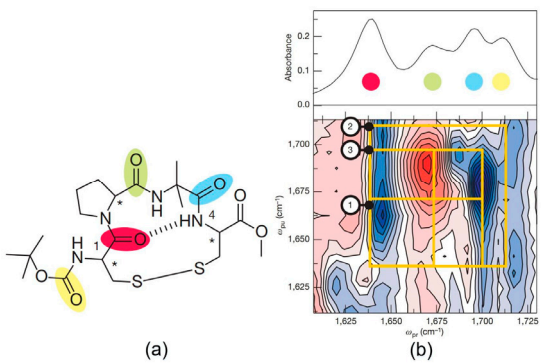

Figure 1.12. (a). The chemical structure of a tetrapeptide ring is bridged by a cyclic disulfide bond (Boc–CPUC–OMe). (b). The corresponding chemical bond changes are detected by 2D infrared spectroscopy.[57]

In the material science, for example, Nelson group measured the high-order electronic correlations for quantum wells using CMDS (Figure 1.13).[58]

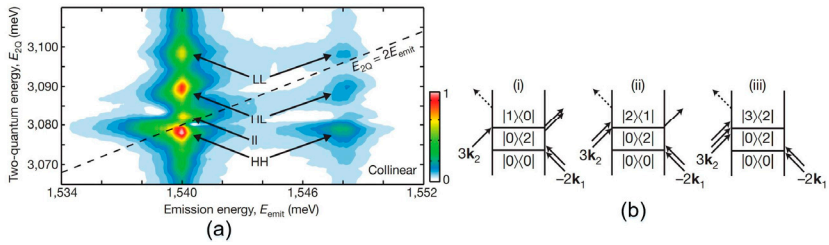

Figure 1.13. The four-particle correlations of quantum wells using 2D spectroscopy. (a). 2D maps of quantum wells. (b). The Feynman pathways ((i)–(iii)) illustrate how the fields create each main feature.[58]

1.3.4 Current study of 2D spectroscopy

The research of 2D spectroscopy mainly can be promoted from three inter-related aspects, namely experiment, data processing, and theoretical description. In this thesis, we mainly address the data processing and theoretical description of the results. We do also summarize the experimental technique but the experiments themselves have been carried out earlier. In terms of experimental data processing, we introduce a novel sparse sampling methodology to 2D spectroscopy. We also apply the so-called least absolute shrinkage and selection operator (LASSO), matching pursuit (MP), and sparse exponential mode analysis (SEMA) methods. These methods can not only drastically decrease the acquisition time in 2D spectroscopy, but they also can improve the measurement resolution of the 2D spectrum. For details, please see Chapter 4.

1.3.5 2D spectroscopy

In this thesis, 2D electronic spectroscopy (2DES) and 2D fluorescence spectroscopy (2DFS) are used. In 2DES, three input beams with wavevectors k_1, k_2, and k_3 interact with the sample and emit various nonlinear signals.[1,59] See for example references.[2,60] All possible phase-matching signals of the third-order nonlinear response are shown in Figure 1.14. Around the 3-rd order signal, one can also see the 5-th and even higher order signals.

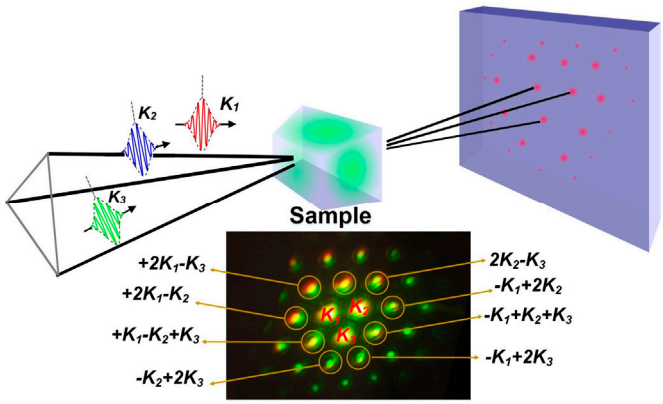

Figure 1.14. Typical phase-matching geometry used in 2D spectroscopy.[2,15,60]

We can obtain 2D spectra by recording different phase-matching directions. Three third-order phase-matching signals, namely rephasing (R), non-rephasing (NR), and double quantum coherence (DQC) can be separated and give valuable information in 2D spectroscopy. The corresponding signal directions are provided in Table 1.2.

Table 1.2. The phase-matching directions of 2D spectroscopy[61]

Direction	2DES	2DFS
R	$\vec{K}_R^E = -\vec{k}_1 + \vec{k}_2 + \vec{k}_3$	$\vec{K}_R^F = -\vec{k}_1 + \vec{k}_2 + \vec{k}_3 - \vec{k}_4$
NR	$\vec{K}_{NR}^E = \vec{k}_1 - \vec{k}_2 + \vec{k}_3$	$\vec{K}_{NR}^F = \vec{k}_1 - \vec{k}_2 + \vec{k}_3 - \vec{k}_4$
DQC	$\vec{K}_{DOC}^E = \vec{k}_1 + \vec{k}_2 - \vec{k}_3$	$\vec{K}_{DOC}^F = \vec{k}_1 + \vec{k}_2 - \vec{k}_3 - \vec{k}_4$

There are three laser pulses and three time delays (t_1, t_2, and t_3. Where t_3 is not really "delay" but time for the signal) in 2DES as shown in Figure 1.15.

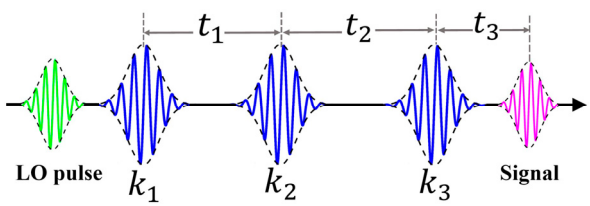

Figure 1.15. The pulses sequence in 2DES.[61] The k_1, k_2, and k_3 are laser pulses.

For analysis of 2D spectroscopy, we use intuitive Feynman diagrams to describe the excited state dynamics over different time periods. Each light-matter interaction acts on one side of the density matrix ρ through absorption or stimulated emission in the Feynman diagram. The bra is the complex conjugate of ket, as shown in Figure 1.16.

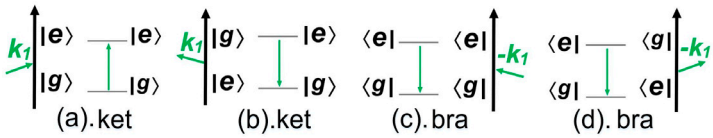

Figure 1.16. The Feynman diagram of the ket and bra sides. (a). The absorption of the ket side. (b). The stimulated emission of ket side. (c). The absorption of bra side. (d). The stimulated emission of bra side.

The third-order nonlinear response function for the 2D spectrum is described in Chapters 2 and 3. In the double-sided Feynman diagrams, three pulses act on both sides of the density matrix at different time delays, the following response function is defined in Figure 1.17. The direction of these response functions are R_1=ket/ket/ket; R_2=bra/ket/bra; R_3=bra/bra/ket; R_4=ket/bra/bra. Here, these double-sided Feynman diagrams represent the pathways of stimulated emission (SE) and ground state bleach (GSB) in the rephrasing (R) and non-rephasing (NR) parts of 2D spectroscopy shown in Figure 1.17.

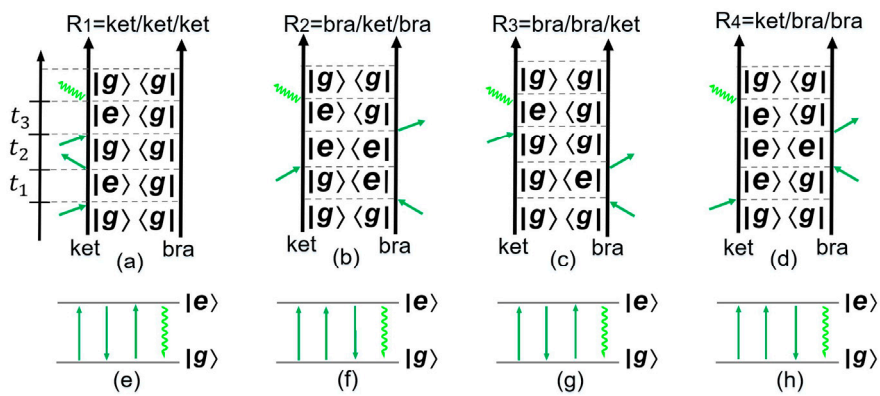

Figure 1.17. The double-sided Feynman diagram with ket and bra sides and the corresponding energy level diagrams are used to explain the 2D spectrum (R and NR parts). (a). The GSB pathway is for the R part. (b). The SE pathway is for the NR part. (c). The GSB pathway is for the R part. (d). The SE pathway is for the NR part. (e)-(h) are the energy level transition diagrams corresponding to (a)-(d) respectively.

A specific example is used to illustrate the 2D spectrum in Figure 1.18. Figure 1.18(a) is a simulated 2D spectrum of LH2 protein data in the time domain. Figure 1.18(b) shows the frequency spectra obtained by double Fourier transform of the same 2D data in Figure 1.18(a) along t_1 and t_3 domains. There are two diagonal

peaks (DP_{11}, DP_{22}) and two cross peaks (CP_{12}, CP_{21}) in the 2D spectrum. The excited states corresponding to these peaks are e_1 and e_2 states.

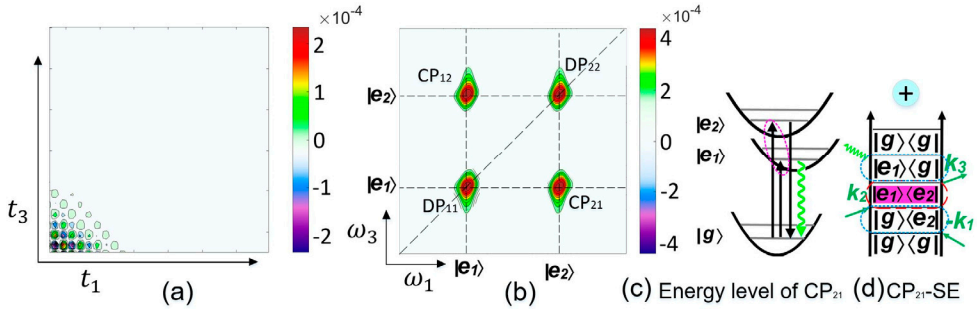

Figure 1.18. The simulated 2D spectrum. (a). 2D spectrum in the time domain (b). 2D spectrum in the frequency domain (c). Energy level diagram of SE pathway corresponding to the CP_{21} peak. (d). The SE pathway corresponding to the CP_{21} peak.

Specifically, we use Figure 1.18(c) to illustrate the dynamics of the CP_{21} peak. The double-sided Feynman diagram of SE corresponding to the CP_{21} peak is shown in Figure 1.18(d). For specific details of these studies, please refer to Chapters 2-4.

1.4 Short Summary

In this chapter, we introduced the research background of samples and spectroscopy. There are two kinds of samples in our research, i.e. LH2 protein and CdSe QDs.

Chapter 2 Nonlinear Optical Spectroscopy Theory

Maybe I did this work with applied mathematician Emmanuel Ken, now so-called compressed sensing, which is a technique for recovering data like an image using many fewer measurements than traditional measurements methods, so it's a very practical problem but Emmanuel had this gift of turning it into a like purely mathematical question which I could help with and this is maybe the one thing that I worked with on which has a very practical application. Maybe that's the thing I am most proud of because of its actual reward impact, most of what I do is very theoretical.

–Terence Tao

The birth of quantum mechanics in the early 20th century enabled people to start understanding the quantum world. Later, this physics field also has been promoted by the development of ultrafast spectroscopy. Therefore, to better understand coherent multidimensional spectroscopy (CMDS), this chapter introduces the mathematical foundations of CMDS. It mainly derives the simple theory about generating CMDS from quantum mechanics, including the basics of nonlinear optical spectroscopy. Firstly, let's start with nonlinear optics as the foundation of CMDS. To explain the nonlinear optics more clearly, we mention Maxwell's equations in Chapter 2.

Here some calculations are based on the theory of the Mukamel studies[1] to explain the basics of nonlinear optical spectroscopy, including some calculations by Hamm and Zanni,[59] and Cho.[62,63]

2.1 Hilbert Space: Wavefunction and Hamiltonians.

To understand the basis of nonlinear optics, we first start with the Hilbert space.
In the quantum mechanical field, the time evolution of the system can be explained by following its time-dependent state. Here the Dirac operator is used to represent the wave function such as Dirac ket $|\psi(t)\rangle$ and bra $\langle\psi(t)|$. These two wave functions are conjugated and shown in equation (2.1).

$$|\psi(t)\rangle = \langle\psi(t)|^* \tag{2.1}$$

The scalar product of the two states is defined by equation (2.2).

$$\langle\psi(t)|\emptyset(t)\rangle = \int \psi^*(x,t)\emptyset(x,t)dx \tag{2.2}$$

The expectation value of any dynamic variable A is given by equation (2.3).

$$\langle \mathrm{A}(t)\rangle = \langle\psi(t)|\mathrm{A}|\psi(\mathrm{t})\rangle = \int \psi^*(x,t)A\psi(x,t)dx \tag{2.3}$$

Hilbert space: The collection of all possible states together with the addition and the scalar product operation forms a linear vector space. In the Hilbert space, the wavefunction $|\psi_n\rangle$ form a complete and orthonormal basis set.
Based on this characteristic of Hilbert space, we can obtain equation (2.4).

$$\sum_n |\psi_n\rangle\langle\psi_n| = 1 \tag{2.4}$$

Thus, we substitute the equation (2.4) into equation (2.1) to obtain equation (2.5).

$$|\psi(t)\rangle = \sum_n |\psi_n\rangle\langle\psi_n|\psi(t)\rangle \tag{2.5}$$

Let us substitute these variables into a linear partial differential equation with a wave function that controls the quantum mechanical system (also known as the Schrödinger equation). The time-dependent Schrödinger is shown in equation (2.6).[1]

$$\frac{\partial|\psi(t)\rangle}{\partial t} = -\frac{i}{\hbar}H|\psi(t)\rangle \tag{2.6}$$

Here, $\hbar$ is Planck's constant; H is the total Hamiltonian of the system; $|\psi(t)\rangle$ is the eigenvectors of the time-independent Schrödinger equation (2.7).

$$H|\psi_n\rangle = E_n|\psi_n\rangle \tag{2.7}$$

E_n is the eigenvalue.
Substitute equation (2.5) into Schrödinger equation (2.7) to get equation (2.8).

$$\frac{\partial|\psi(t)\rangle}{\partial t} = -\frac{i}{\hbar}H|\psi(t)\rangle = -\frac{i}{\hbar}H\sum_n |\psi_n\rangle\langle\psi_n|\psi(t)\rangle \tag{2.8}$$

Multiply equation (2.8) by $\langle\psi_n|$ to obtain equation (2.9).

$$\frac{d}{dt}\langle\psi_n|\psi(t)\rangle = -\frac{i}{\hbar}E_n\langle\psi_n|\psi(t)\rangle \tag{2.9}$$

Thus, the solution of (2.9) is shown in equation (2.10).

$$\langle\psi_n|\psi(t)\rangle = e^{-\frac{i}{\hbar}E_n(t-t_0)}\langle\psi_n|\psi(t_0)\rangle \tag{2.10}$$

Thus,

$$|\psi(t)\rangle = \sum_n e^{-\frac{i}{\hbar}E_n(t-t_0)}|\psi(t_0)\rangle \tag{2.11}$$

Here, we define the time evolution operator $U(t,t_0)$ in the wave function. $U(t,t_0)$ acts on the wavefunction at the time t_0. This can evolve the wave function from t_0 to the time t.

$$|\psi(t)\rangle = U(t,t_0)|\psi(t_0)\rangle \tag{2.12}$$

Comparing equations (2.11) and (2.12), we can obtain equation (2.13).

$$U(t,t_0) = \sum_n |\psi_n\rangle e^{-\frac{i}{\hbar}E_n(t-t_0)}\langle\psi_n| \tag{2.13}$$

Substitute equation (2.12) into equation (2.6) to get equation (2.14).

$$\frac{\partial}{\partial t}U(t,t_0)|\psi(t_0)\rangle = -\frac{i}{\hbar}H(t)U(t,t_0)|\psi(t_0)\rangle \tag{2.14}$$

Thus,

$$\frac{\partial}{\partial t}U(t,t_0) = -\frac{i}{\hbar}H(t)U(t,t_0) \tag{2.15}$$

From this definition of time evolution operator $U(t,t_0)$ immediately follows that,

$$U(t_0,t_0) = 1 \tag{2.16}$$

Integrate and sum both sides of equation (2.14) from time τ to time t_0. Moreover, get equation (2.17).

$$U(t,t_0) = 1 - \frac{i}{\hbar}\int_{t_0}^{t} d\tau H(\tau)U(\tau,t_0) = U(t_0,t_0) - \frac{i}{\hbar}\int_{t_0}^{t} d\tau H(\tau)U(\tau,t_0) \tag{2.17}$$

Therefore, equation (2.17) is obtained by deriving to the n^{th} as shown in equation (2.18).

$$U(t,t_0) = 1 + \sum_{n=1}^{\infty} (-\frac{i}{\hbar})^n \int_{t_0}^{t} d\tau_n \int_{t_0}^{\tau_n} d\tau_{n-1} \dots \int_{t_0}^{\tau_2} d\tau_1 H(\tau_n) H(\tau_{n-1}) \dots H(\tau_1) \quad (2.18)$$

The time variable is expressed as equation (2.19) and Figure 2.1.

$$t_1 = \tau_2 - \tau_1, t_2 = \tau_3 - \tau_2, \dots, t_n = t - \tau_n \quad (2.19)$$

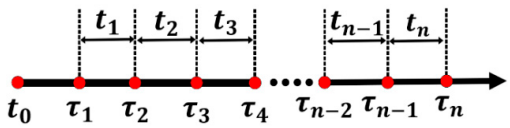

Figure 2.1. Time variables in the time-ordered expansion[1].

2.2 Liouville Space: Density matrix, Time evolution.

To describe the CMDS more clearly, here is an introduction of the Liouville space. The Liouville space more widely describes the optical lineshapes of the spectrum, such as mixed states, and represents the multi-time nonlinear correlation function. Therefore, it is necessary to introduce the Liouville space in nonlinear optical spectroscopy. Before that, let's start with an overview of the wave function from the Hilbert space.

The wave function in Hilbert space is defined as equation (2.20).

$$|\psi_n\rangle = \begin{bmatrix} \psi_1 \\ . \\ . \\ . \\ \psi_n \end{bmatrix} \quad (2.20)$$

Therefore, the conjugate of wave function $|\psi_n\rangle$ is equation (2.21).

$$\langle\psi_n| = [\psi_1, \dots \dots \dots, \psi_n] \quad (2.21)$$

Hence, we construct the density matrix based on equations (2.20) and (2.21) to express it as equation (2.22).

$$\rho_{nn} = |nn\rangle\rangle = |\psi_n\rangle\langle\psi_n| = \begin{bmatrix} \psi_1 \\ . \\ . \\ . \\ \psi_n \end{bmatrix} [\psi_1, \dots \dots \dots, \psi_n]$$
$$= \begin{bmatrix} \psi_1\psi_1, \psi_1\psi_2, \dots, \psi_1\psi_n \\ \dots, \dots, \dots, \dots, \dots, \dots \\ \dots, \dots, \dots, \dots, \dots, \dots \\ \dots, \dots, \dots, \dots, \dots, \dots \\ \dots, \dots, \dots, \dots, \dots, \dots \\ \psi_n\psi_1, \dots, \dots, \psi_n\psi_n \end{bmatrix}_{n\times n} \tag{2.22}$$

For the density matrix, we use the density operator to represent the state of the system by a matrix (rather than a vector). Thus, in the Liouville space, the density operator is a vector in the quantum mechanics field. Hilbert space: for the wavefunction, a vector represents the excited state of the system and an operator is represented by a matrix.

Therefore, we can also write the density matrix as equation (2.23).

$$\rho(t) = |\psi(t)\rangle\langle\psi(t)| \tag{2.23}$$

Here, we have the matrix elements in equation (2.24).

$$\rho_{nm} = \sum_k P_k \langle n|\psi_k\rangle\langle\psi_k|m\rangle \tag{2.24}$$

P_k represents the probability that the system is in state $|\psi(t)\rangle$.
Thus, the density matrix is as equation (2.25).

$$\rho_{nm}(t) = \sum_k P_k \langle n(t)|\psi_k(t)\rangle\langle\psi_k(t)|m(t)\rangle$$
$$= \begin{bmatrix} \sum_k P_k \langle n(t)|\psi_k(t)\rangle\langle\psi_k(t)|m(t)\rangle \propto \langle\psi_n|\psi_m\rangle \; n \neq m \\ \sum_k P_k \langle n(t)|\psi_k(t)\rangle\langle\psi_k(t)|n(t)\rangle \propto \langle\psi_n|\psi_n\rangle \;\; n = m \end{bmatrix} \tag{2.25}$$

From the density matrix of equation (2.25), there are two kinds of elements in the density matrix: population ($n = m$) and coherence ($n \neq m$), respectively.

Thus, we add the electromagnetic field ($\vec{E}$) and transition dipole ($\vec{\mu}$) to the density matrix to get equation (2.26).

$$|\langle\psi_e|\vec{E}\cdot\vec{\mu}|\psi_g\rangle|^2 = \langle\psi_e|\vec{E}\cdot\vec{\mu}|\psi_g\rangle\langle\psi_e|\vec{E}\cdot\vec{\mu}|\psi_g\rangle^*$$
$$= \langle\psi_e|\vec{E}\cdot\vec{\mu}|\psi_g\rangle\langle\psi_g|\vec{E}\cdot\vec{\mu}|\psi_e\rangle \tag{2.26}$$

The time-dependent of the density operator can be derived as equation (2.27).

$$\frac{\partial \rho_m(t)}{\partial t} = \sum_m [\frac{\partial |\psi_m\rangle}{\partial t}\langle\psi_m| + |\psi_m\rangle\langle\frac{\partial \langle\psi_m|}{\partial t}] \tag{2.27}$$

Back to Hilbert space, we can get two parts (bra and ket) of the Schrödinger equation.

$$\frac{\partial |\psi_m(t)\rangle}{\partial t} = -\frac{i}{\hbar} H|\psi_m(t)\rangle \tag{2.28}$$

Based on equation (2.28), the conjugate equation is (2.29).

$$\frac{\partial \langle\psi_m(t)|}{\partial t} = \frac{i}{\hbar} H\langle\psi_m(t)| \tag{2.29}$$

Based on equations (2.28) and (2.29), we also establish the Liouville-von Neumann equation (2.30).

$$\begin{aligned} \frac{\partial \rho_m(t)}{\partial t} &= -\frac{i}{\hbar} H|\psi_m(t)\rangle\langle\psi_m(t)| + \frac{i}{\hbar}|\psi_m(t)\rangle\langle\psi_m(t)|H \\ &= -\frac{i}{\hbar}[H, \rho_m(t)] \end{aligned} \tag{2.30}$$

By integrating on both sides from t_0 to t we obtain the first-order equation of motion.

$$\rho(t) = \rho(t_0) - \frac{i}{\hbar}\int_{t_0}^{t} d\tau [H(\tau), \rho(\tau)] \tag{2.31}$$

By inserting (2.30) and (2.31) and integrating again, one gains the second-order equation. Repeating these procedure n times give the equation of motion in the nth order, as follows in the equation (2.32).

$$\begin{aligned} \rho(\mathrm{t}) = \rho(t_0) + \sum_{n=1}^{\infty} \left(-\frac{i}{\hbar}\right)^n \int_{t_0}^{t} d\tau_n \int_{t_0}^{\tau_n} d\tau_{n-1} \dots \\ \int_{t_0}^{\tau_2} d\tau_1 [H(\tau_n), \dots [H(\tau_2), [H(\tau_1), \rho(t_0)]] \dots] \end{aligned} \tag{2.32}$$

2.3 Nonlinear Optical Spectroscopy

Based on the response functions in the Hilbert space and Liouville space, the calculations of the nonlinear optical spectrum can be found as follows. When the laser pulses act on the sample, we can use the dipole approximation of the radiation-matter interaction Hamiltonian.

$$H_{int}(t) = -E(t)\mu(t) \tag{2.33}$$

Here, $E(t)$ is the external field, $\mu(t)$ is the dipole operator.
The polarization function is expressed in equation (2.34).

$$P(r,t) = Tr[\mu\rho(t)] = \langle\langle\mu|\rho(t)\rangle\rangle \tag{2.34}$$

Incorporating equation (2.32) into equation (2.34) we obtain the relationship between the polarization function and the electric field.

$$P^{(n)}(t) = \int_0^\infty dt_n \int_0^\infty dt_{n-1} \dots \int_0^\infty dt_1 R^{(n)}(t_n, t_{n-1}, \dots, t_1) E(t - t_n) E(t - t_n - t_{n-1}) \dots E(t - t_n - t_{n-1} \dots - t_1) \tag{2.35}$$

With

$$R^{(n)}(t_n, t_{n-1}, \dots, t_1) = (\frac{i}{\hbar})^n \langle\langle\mu|\rho(t_n)\mu(t_{n-1})\mu \dots \rho(t_1)\mu|\rho(-\infty)\rangle\rangle \tag{2.36}$$

Here, the n[th]-order nonlinear response function is the equation of $R^{(n)}(t_n, t_{n-1}, \dots, t_1)$.
The Green function in Liouville space for the material system is shown in equation (2.37).

$$\mathrm{G}(\tau) = \theta(\tau) e^{-\frac{i}{\hbar}\hat{G}\tau} \tag{2.37}$$

By inserting the Green function (2.37) enter in the response function we obtain the equation (2.36) in the Liouville space.

$$\begin{aligned} &R^{(n)}(t_n, t_{n-1}, \dots, t_1) \\ &= \left(\frac{i}{\hbar}\right)^n \theta(t_1)\theta(t_2) \dots \theta(t_n) \times \langle\langle\mu(t_n + \cdots \\ &+ t_1)|\mu(t_{n-1} + \cdots + t_1) \dots \mu(t_1)\mu(0)|\rho(-\infty)\rangle\rangle \end{aligned} \tag{2.38}$$

By converting the response function from the Liouville space to the Hilbert space, we obtain equations (2.39) and (2.40).

$$
\begin{aligned}
&R^{(n)}(t_n, t_{n-1}, \dots, t_1) \\
&= \left(\frac{i}{\hbar}\right)^n \theta(t_1)\theta(t_2) \dots \theta(t_n) \times \langle \mu(t_n + \cdots \\
&+ t_1)[\mu(t_{n-1} + \cdots \\
&+ t_1), \left[\dots \left[\mu(t_1), [\mu(0), \rho(-\infty)]\right] \dots\right]]\rangle
\end{aligned}
\tag{2.39}
$$

Alternatively, similar to the left side.

$$
\begin{aligned}
&R^{(n)}(t_n, t_{n-1}, \dots, t_1) \\
&= \left(\frac{i}{\hbar}\right)^n \theta(t_1)\theta(t_2) \dots \theta(t_n) \\
&\times [\left[\left[\dots [\mu(t_n + \cdots + t_1), \mu(t_{n-1} + \cdots \right.\right. \\
&\left.\left. + t_1)], \dots\right], \mu(t_1)\right], \mu(0)]\rho(-\infty)\rangle
\end{aligned}
\tag{2.40}
$$

Through these n^{th} order nonlinear response functions, we can clearly express the basic theoretical model of coherent nonlinear spectroscopy in Chapter 3. Please see Chapter 3 for details.

2.4 Short Summary

This chapter mainly focuses on the basics of the wavefunction, density matrix, response function, how to express the nonlinear response functions and nonlinear optical spectroscopy. Moreover, based on this section, Chapter 3 will also provide further analysis for the description of CMDS.

Chapter 3 Coherent Multidimensional Spectroscopy (CMDS)

I worked on extending the Liouville space pathway approach to nonlinear spectroscopy. My entire career has been a series of adventures in Liouville space. Also like the British astrophysicist, A. Eddington (proving the general theory of Einstein's theory of relativity through experiments) stated: "No experimental result should be accepted before being confirmed by theory".

–Shaul Mukamel

Spectroscopy is a measurement technique performed in the time domain or frequency domain. Generally, the frequency spectrum is a function of multiple time delays. Therefore, two or more time delays in the spectrum are usually called multidimensional in the frequency domain.[1] For the understanding of coherent multidimensional spectroscopy (CMDS), there are more than two-time delays from interaction signals of light acting on the matter in Liouville space. Moreover, the signal undergoes a double Fourier transform, which is called 2D spectroscopy.

Similarly, the 3D spectrum can be obtained by a triple Fourier transform. 2D, 3D, or higher dimensions are collectively referred to as CMDS. It comes from the fifth or higher order of signal based on the interaction of multiple pulses acting on matter. In this chapter, the 3D spectrum comes from the Fourier transform of the 2D spectrum along population time T.

In terms of studying excited state dynamics, quantum beating, and coherence, CMDS[16,64,73–82,65,83–85,66–72] has successfully been used to investigate different materials such as light-harvesting complexes,[17,20,54,55,86–91] QDs,[24,31] quantum wells,[92–94] and molecular aggregates.[95] Mukamel,[1,76,78,81,96,97] Cho,[98,99] and Hamm[57,59,78,100–103] et al. have developed theories for 2D spectroscopy. 2D spectroscopy in the IR region was introduced by Hochstrasser[104] and further developed by Tokmakoff group.[57,105–110] More recently, 2D spectroscopy has been

further developed so that the spectra are detected via various incoherent "action" signals, such as fluorescence,[16,21,22,61,109,111–114] photocurrent,[114] photoelectron,[115,116] and photoions[73]. This chapter mainly discusses three kinds of CMDS, namely the 2D fluorescence spectroscopy (2DFS),[16] 2D electronic spectroscopy (2DES),[24,117] and the expansion of 2DES (two-color 2D spectroscopy[90,106,118–121]).

3.1 2D Electronic Spectroscopy (2DES)

In the 2DES, the signal is generated based on three non-collinear ultrafast pulses (Φ_1, Φ_2, Φ_3). There are also three time delays in 2DES in Figure 3.1. The time delay between the first pulse Φ_1 and the second pulse Φ_2 is called the coherence time τ (or t_1), while the time delay between the second Φ_2 and the third pulse Φ_3 is the population time T (or t_2). The detection time t (or t_3) is between the second pulse Φ_3 and the signal.[17]

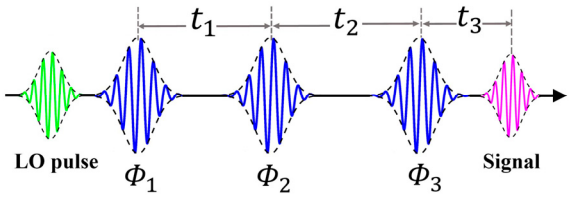

Figure. 3.1. The schematics of pulses for 2DES.

According to the nonlinear optical spectrum derived in Chapter 2, we continue the calculation of the 2DES with the polarization from equation (2.35). The third-order polarization of 2DES is expressed as equation (3.1).[1]

$$P^{(3)}(t) = \int_0^\infty dt_3 \int_0^\infty dt_2 \int_0^\infty dt_1 E(t-t_3)E(t-t_2-t_1)E(t-t_3-t_2-t_1)R^{(3)}(t_3,t_2,t_1) \tag{3.1}$$

The third-order response function of 2DES is based on the equation (2.39) in Chapter 2. Thus, the response function is calculated as equation (3.2).

$$R^{(3)}(t_3,t_2,t_1) = -\left(\frac{-i}{\hbar}\right)^3 \langle \hat{\mu}_{It}, [\hat{\mu}_I(t_3+t_2+t_1), [\hat{\mu}_I(t_2+t_1), [\hat{\mu}_I(t_1), \hat{\rho}(-\infty)]]]\rangle = \left(\frac{i}{\hbar}\right)^3 \langle \hat{\mu}_{It}[\hat{\mu}_{I3}, [\hat{\mu}_{I2}, [\hat{\mu}_{I1}, \hat{\rho}(-\infty)]]]\rangle \tag{3.2}$$

The electric field of three laser pulses in 2DES is explained as equation (3.3).

$$\begin{aligned} E_1(t) &= e^{i(k_1\cdot x-\omega_1\cdot t+\emptyset_1)} + e^{-i(k_1\cdot x-\omega_1\cdot t+\emptyset_1)} \\ E_2(t) &= e^{i(k_2\cdot x-\omega_2\cdot t+\emptyset_2)} + e^{-i(k_2\cdot x-\omega_2\cdot t+\emptyset_2)} \\ E_3(t) &= e^{i(k_3\cdot x-\omega_3\cdot t+\emptyset_3)} + e^{-i(k_3\cdot x-\omega_3\cdot t+\emptyset_3)} \end{aligned} \tag{3.3}$$

The extended commutator from the response function of 2DES is shown in equation (3.4).

$$
\begin{aligned}
&\langle \hat{\mu}_{It}, \left[\hat{\mu}_{I3}, \left[\hat{\mu}_{I2}, [\hat{\mu}_{I1}, \hat{\rho}(-\infty)]\right]\right]\rangle \\
&= \langle \hat{\mu}_{It}\hat{\mu}_{I3}\hat{\mu}_{I2}\hat{\mu}_{I1}\hat{\rho}(-\infty)\rangle - \langle \hat{\mu}_{It}\hat{\mu}_{I3}\hat{\mu}_{I2}\hat{\rho}(-\infty)\hat{\mu}_{I1}\rangle \\
&\quad - \langle \hat{\mu}_{It}\hat{\mu}_{I3}\hat{\mu}_{I1}\hat{\rho}(-\infty)\hat{\mu}_{I2}\rangle + \langle \hat{\mu}_{It}\hat{\mu}_{I3}\hat{\rho}(-\infty)\hat{\mu}_{I1}\hat{\mu}_{I2}\rangle \\
&\quad - \langle \hat{\mu}_{It}\hat{\mu}_{I2}\hat{\mu}_{I1}\hat{\rho}(-\infty)\hat{\mu}_{I3}\rangle + \langle \hat{\mu}_{It}\hat{\mu}_{I2}\hat{\rho}(-\infty)\hat{\mu}_{I1}\hat{\mu}_{I3}\rangle \\
&\quad + \langle \hat{\mu}_{It}\hat{\mu}_{I1}\hat{\rho}(-\infty)\hat{\mu}_{I2}\hat{\mu}_{I3}\rangle - \langle \hat{\mu}_{It}\hat{\rho}(-\infty)\hat{\mu}_{I1}\hat{\mu}_{I2}\hat{\mu}_{I3}\rangle \\
&\quad - \langle \hat{\mu}_{I3}\hat{\mu}_{I2}\hat{\mu}_{I1}\hat{\rho}(-\infty)\hat{\mu}_{It}\rangle + \langle \hat{\mu}_{I3}\hat{\mu}_{I2}\hat{\rho}(-\infty)\hat{\mu}_{I1}\hat{\mu}_{It}\rangle \\
&\quad + \langle \hat{\mu}_{I3}\hat{\mu}_{I1}\hat{\rho}(-\infty)\hat{\mu}_{I2}\hat{\mu}_{It}\rangle - \langle \hat{\mu}_{I3}\hat{\rho}(-\infty)\hat{\mu}_{I1}\hat{\mu}_{I2}\hat{\mu}_{It}\rangle \\
&\quad + \langle \hat{\mu}_{I2}\hat{\mu}_{I1}\hat{\rho}(-\infty)\hat{\mu}_{I3}\hat{\mu}_{It}\rangle - \langle \hat{\mu}_{I2}\hat{\rho}(-\infty)\hat{\mu}_{I1}\hat{\mu}_{I3}\hat{\mu}_{It}\rangle \\
&\quad - \langle \hat{\mu}_{I1}\hat{\rho}(-\infty)\hat{\mu}_{I2}\hat{\mu}_{I3}\hat{\mu}_{It}\rangle + \langle \hat{\rho}(-\infty)\hat{\mu}_{I1}\hat{\mu}_{I2}\hat{\mu}_{I3}\hat{\mu}_{It}\rangle
\end{aligned}
\tag{3.4}
$$

According to the above equation (3.4), the corresponding double-sided Feynman diagram is shown in Figure 3.2.

Here, it is necessary to explain the double-sided Feynman diagrams. The four arrows in the double-sided Feynman diagrams represent the interaction based on the electric field acting on the sample. Generally, there are mainly three kinds of dynamics pathways of 2DES, namely ground state bleach (GSB), stimulated emission (SE), and excited state absorption (ESA). For the SE pathway in Figure 3.2(a), the first pulse of k_1 generates coherent superposition between |g⟩ and |e⟩ states. The second pulse k_2 converts this coherence to the population state |e⟩. In addition, the third pulse k_3 acts on the sample and the signal from the |e⟩ state to the |g⟩ state. Finally, the emission from the |e⟩ state to the |g⟩ state. As for the GSB pathway in Figure 3.2(b), the pulse k_1 creates the coherence between the state |g⟩ and the state |e⟩; Pulse k_2 relaxation returns to the state |g⟩; Pulse k_3 creates a coherent superposition between the state |g⟩ and the state |e⟩. The emission signal generates from the |e⟩ state to the |g⟩ state. Similarly, the ESA pathway corresponds to Figure 3.2(c).

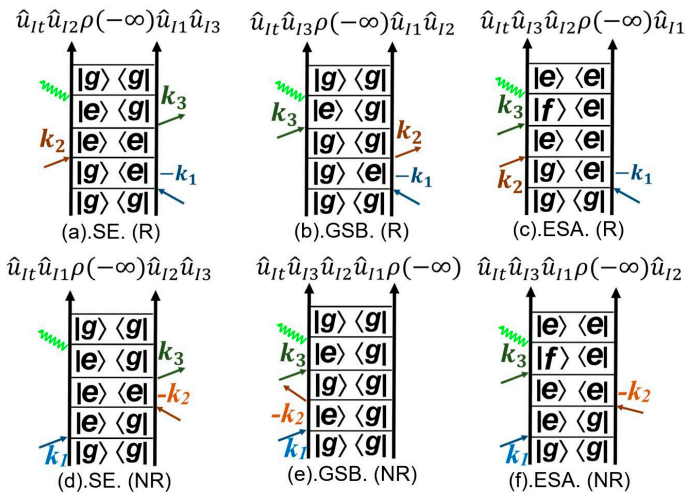

Figure 3.2. Corresponding Feynman diagrams of 2DES.

The laser beams in 2DES experiment[117] is shown in Figure 3.3.

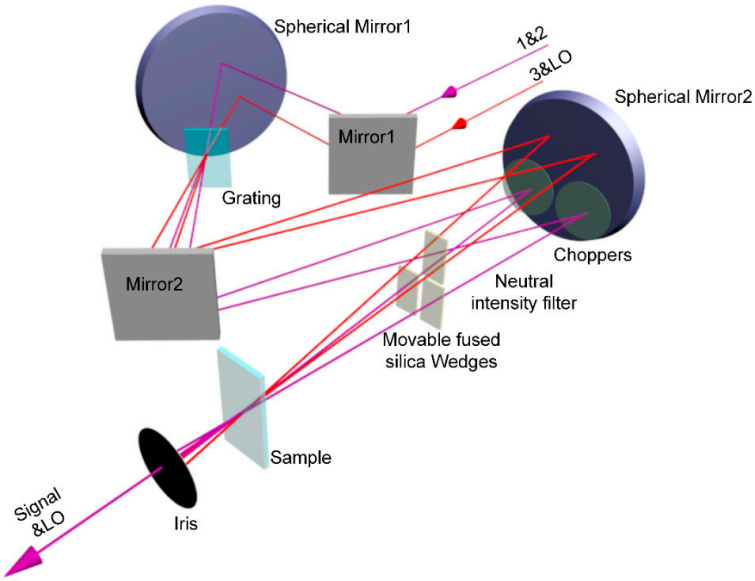

Figure 3.3. The schematics of the 2DES experiment setup.[117]

The main part of the setup is pumped by a laser system which is produced by KGW amplified laser (Pharos, Light Conversion) and laboratory-made NOPA to generate ultra-short (15-20 fs) laser pulses. The adjustable range of this device is 450-850 nm, and the maximum repetition frequency is 200 kHz. Each pulse is divided into two parts by the beam splitter. The time delay between the generated pulses is set by the mechanical delay line. Each pulse is further divided into two parts through the transmission diffraction grating which is optimized for ±1st order diffraction. The four laser pulses generated are labeled as 1, 2, 3, and local oscillators (LO). The resulting four pulse sequences are focused on the same point of the sample in the geometry of a box car. After passing through the spectrometer, a nonlinear third-order signal is detected in the LO direction by the CCD camera. For specific details, please refer to the literature.[117]

3.2 Two-color 2D Spectroscopy

In our experiment, two-color 2D spectroscopy is an extension of conventional 2DES. Traditionally, 2D spectroscopy is based on a single energy region while our 2D spectroscopy is further broadened on the different energy of 2DES, which is also called two-color 2D spectroscopy in Figure 3.4.[119]

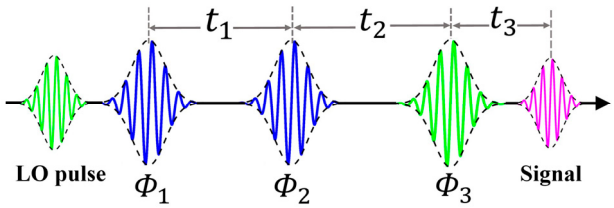

Figure. 3.4. The pulses sequence of two-color 2D spectroscopy.

In this technique, the first two excitations (pump pulses) resonate with the high energy level of the sample whose low energy level also resonates with the third excitation (probe pulse) and local oscillator (LO) frequency simultaneously. Therefore, the two-color 2D spectrum presents the different ranges of energy along the ω_1 and ω_3 (x- and y-axis) domains. For our two-color 2D spectroscopy, where the first two laser pulses (pump pulses) are used to resonate with the high-energy state of the sample, and the third laser pulse (probe pulse) and local oscillator (LO) are employed to low-energy state resonance.

3.3 2D Fluorescence Spectroscopy (2DFS)

Two-dimensional fluorescence-detected coherent spectroscopy can also be called 2D fluorescence spectroscopy (2DFS). Different groups are using 2DFS, such as Marcus,[109] Pullerits,[114] Brixner,[112] and so on. In conventional 2DFS, an incoherent signal is generated by four non-collinear ultrafast pulses ($\Phi_1, \Phi_2, \Phi_3, \Phi_4$), which interact and resonate with the material system. In the 2DFS experiment, there are three time delays among four pulses: the first time delay between pulses Φ_1 and Φ_2 is called coherence time τ (or t_1), the second between pulses Φ_3 and Φ_4 is called the detection time t (or t_3), and the last between pulses Φ_2 and Φ_3 is called the population time T (or t_2). Besides, the relationship between the pulses and the time delays of 2DFS is shown in Figure 3.5.

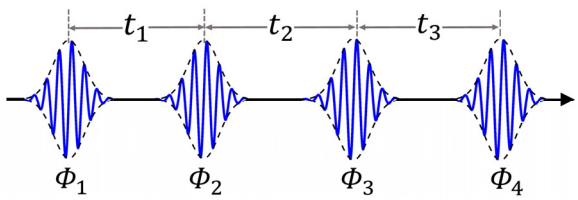

Figure. 3.5. The pulses sequences of 2DFS.

Based on the nonlinear optical spectroscopy derived in Chapter 2, we continue the calculation of the 2DFS from equation (2.35). The signal based on the fourth-order population in 2DFS is expressed as equation (3.5).[110]

$$P^{(4)}(t) = \int_0^\infty dt_4 \int_0^\infty dt_3 \int_0^\infty dt_2 \int_0^\infty dt_1 E(t-t_1)E(t-t_2-t_1)E(t-t_3-t_2-t_1)E(t-t_4-t_3-t_2-t_1)R^{(4)}(t_4,t_3,t_2,t_1) \quad (3.5)$$

The response function of 2DFS is based on the third order population. Thus, the nonlinear response function is calculated as equation (3.6).

$$R^{(4)}(t_4,t_3,t_2,t_1) = -\left(\frac{-i}{\hbar}\right)^4 [\hat{\mu}_I(t_4+t_3+t_2+t_1),[\hat{\mu}_I(t_3+t_2+t_1),[\hat{\mu}_I(t_2+t_1),[\hat{\mu}_I(t_1),\hat{\rho}(-\infty)]]]] = -\left(\frac{i}{\hbar}\right)^4 [\hat{\mu}_{I4},[\hat{\mu}_{I3},[\hat{\mu}_{I2},[\hat{\mu}_{I1},\hat{\rho}(-\infty)]]]] \quad (3.6)$$

The electric fields of four pulses in 2DFS are calculated as equation (3.7).

$$\begin{aligned} E_1(t) &= e^{i(k_1\cdot x-\omega_1\cdot t+\emptyset_1)} + e^{-i(k_1\cdot x-\omega_1\cdot t+\emptyset_1)} \\ E_2(t) &= e^{i(k_2\cdot x-\omega_2\cdot t+\emptyset_2)} + e^{-i(k_2\cdot x-\omega_2\cdot t+\emptyset_2)} \\ E_3(t) &= e^{i(k_3\cdot x-\omega_3\cdot t+\emptyset_3)} + e^{-i(k_3\cdot x-\omega_3\cdot t+\emptyset_3)} \\ E_4(t) &= e^{i(k_4\cdot x-\omega_4\cdot t+\emptyset_4)} + e^{-i(k_4\cdot x-\omega_4\cdot t+\emptyset_4)} \end{aligned} \quad (3.7)$$

The extended commutator from the response function of 2DFS is shown in equation (3.8).

$$\begin{aligned} &[\hat{\mu}_{I4},[\hat{\mu}_{I3},[\hat{\mu}_{I2},[\hat{\mu}_{I1},\hat{\rho}(-\infty)]]]] \\ &= \langle\hat{\mu}_{I4}\hat{\mu}_{I3}\hat{\mu}_{I2}\hat{\mu}_{I1}\hat{\rho}(-\infty)\rangle - \langle\hat{\mu}_{I4}\hat{\mu}_{I3}\hat{\mu}_{I2}\hat{\rho}(-\infty)\hat{\mu}_{I1}\rangle \\ &\quad - \langle\hat{\mu}_{I4}\hat{\mu}_{I3}\hat{\mu}_{I1}\hat{\rho}(-\infty)\hat{\mu}_{I2}\rangle + \langle\hat{\mu}_{I4}\hat{\mu}_{I3}\hat{\rho}(-\infty)\hat{\mu}_{I1}\hat{\mu}_{I2}\rangle \\ &\quad - \langle\hat{\mu}_{I4}\hat{\mu}_{I2}\hat{\mu}_{I1}\hat{\rho}(-\infty)\hat{\mu}_{I3}\rangle + \langle\hat{\mu}_{I4}\hat{\mu}_{I2}\hat{\rho}(-\infty)\hat{\mu}_{I1}\hat{\mu}_{I3}\rangle \\ &\quad + \langle\hat{\mu}_{I4}\hat{\mu}_{I1}\hat{\rho}(-\infty)\hat{\mu}_{I2}\hat{\mu}_{I3}\rangle - \langle\hat{\mu}_{I4}\hat{\rho}(-\infty)\hat{\mu}_{I1}\hat{\mu}_{I2}\hat{\mu}_{I3}\rangle \\ &\quad - \langle\hat{\mu}_{I3}\hat{\mu}_{I2}\hat{\mu}_{I1}\hat{\rho}(-\infty)\hat{\mu}_{I4}\rangle + \langle\hat{\mu}_{I3}\hat{\mu}_{I2}\hat{\rho}(-\infty)\hat{\mu}_{I1}\hat{\mu}_{I4}\rangle \\ &\quad + \langle\hat{\mu}_{I3}\hat{\mu}_{I1}\hat{\rho}(-\infty)\hat{\mu}_{I2}\hat{\mu}_{I4}\rangle - \langle\hat{\mu}_{I3}\hat{\rho}(-\infty)\hat{\mu}_{I1}\hat{\mu}_{I2}\hat{\mu}_{I4}\rangle \\ &\quad + \langle\hat{\mu}_{I2}\hat{\mu}_{I1}\hat{\rho}(-\infty)\hat{\mu}_{I3}\hat{\mu}_{I4}\rangle - \langle\hat{\mu}_{I2}\hat{\rho}(-\infty)\hat{\mu}_{I1}\hat{\mu}_{I3}\hat{\mu}_{I4}\rangle \\ &\quad - \langle\hat{\mu}_{I1}\hat{\rho}(-\infty)\hat{\mu}_{I2}\hat{\mu}_{I3}\hat{\mu}_{I4}\rangle + \langle\hat{\rho}(-\infty)\hat{\mu}_{I1}\hat{\mu}_{I2}\hat{\mu}_{I3}\hat{\mu}_{I4}\rangle \end{aligned} \quad (3.8)$$

Based on equation (3.8), the expression in this equation can be understood as follows in the double-sided Feynman diagram. For the above equation (3.8), the corresponding Feynman diagram is summarized as follows in Figure 3.6.

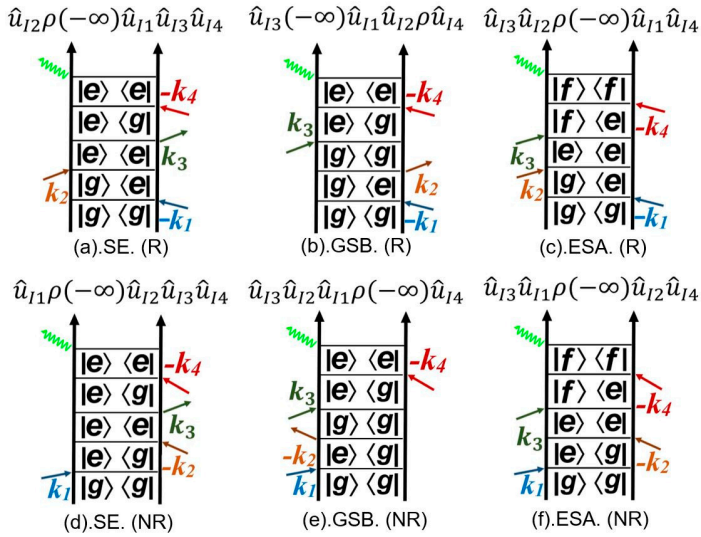

Figure 3.6. Corresponding Feynman diagrams of 2DFS.

It is important to point out that the last signal arrow here is not a coherent polarization signal as in 2DES but incoherent signal like fluorescence.
Our 2DFS setup[15] is based on the optical path of Figure 3.7.

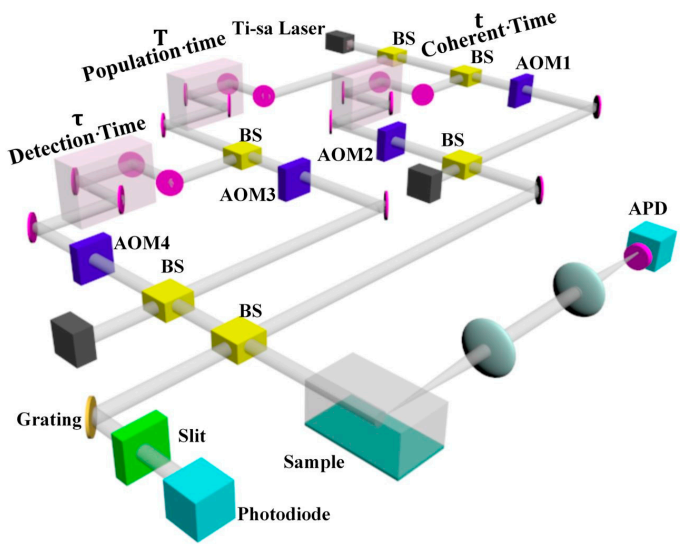

Figure 3.7. The optical path of 2DFS. BS: beam splitter; AOM: A cousto-optic Bragg cell; APD: avalanche photodiode.

Ti:Sa oscillator provides a repetition frequency of 70 MHz (set to pulses of 8-10 fs). The beam splitter (BS) separates two equal copies. There are four AOMs driven by

radio frequency generators with four different modulation frequencies. The used four frequencies are $\boldsymbol{\Phi_1}$=54.70 MHz, $\boldsymbol{\Phi_2}$= 54.75 MHz, $\boldsymbol{\Phi_3}$= 54.92 MHz, and $\boldsymbol{\Phi_4}$=55.00 MHz. For specific details, please refer to the literature.[15]

3.4 Short Summary

In this chapter, three kinds of 2D spectroscopy have been briefly introduced, namely, 2DES, 2DFS, and two-color 2D spectroscopy. Besides, based on the theoretical calculations in Chapter 2, we also briefly discussed Feynman diagrams of these spectra and their corresponding mathematical equations.

Chapter 4 Analyses of Excitation Dynamic in QDs and Data Acquisition with Coherent 2D Spectroscopy

Zhengjun, I am concerned. These are elementary things. When are we getting any close to real science?

-Tõnu Pullerits

Here we summarize the research articles which have been organized during my doctoral study in the theses. Specifically, the first part (Subsection 4.1, the paper I) concerns excited states and their dynamics in CdSe QDs studied by two-color 2D spectroscopy. The second part (Subsection 4.2, paper II) analyses the beating signals in CdSe QDs measured by low-temperature 2D spectroscopy. The third section (Subsection 4.3, paper III) mainly studies the quantum size effects in 2D spectroscopy of CdSe QDs. The fourth part (Subsection 4.4, paper IV) focuses on the compressed sensing (CS) theory to enable sparse sampling and reconstruct the 2DFS. The last section (Subsection 4.5, paper V) investigates the phonon coupling with excitons and free carriers in nanocrystals.

4.1 The Excited State Dynamics of CMDS

Coherent multidimensional spectroscopy (CMDS) can detect details of the dynamic processes of samples,[16,57,76–78,81,82,84,110,122,123,64,65,67,69,71,73–75] such as excited state dynamics, relaxation dynamics, and quantum beating dynamics. In our research, the excited state dynamics of CdSe QDs are mainly researched through CMDS.

4.1.1 Excited states of CdSe QDs by two-color 2D spectroscopy

Traditionally, three ultrafast pulses of 2DES are all in the same energy region. In this subproject, we measured the excited state dynamics of CdSe QDs using two-color 2D spectroscopy[118,124–128] in Figure 4.1 (B_1 and B_2).

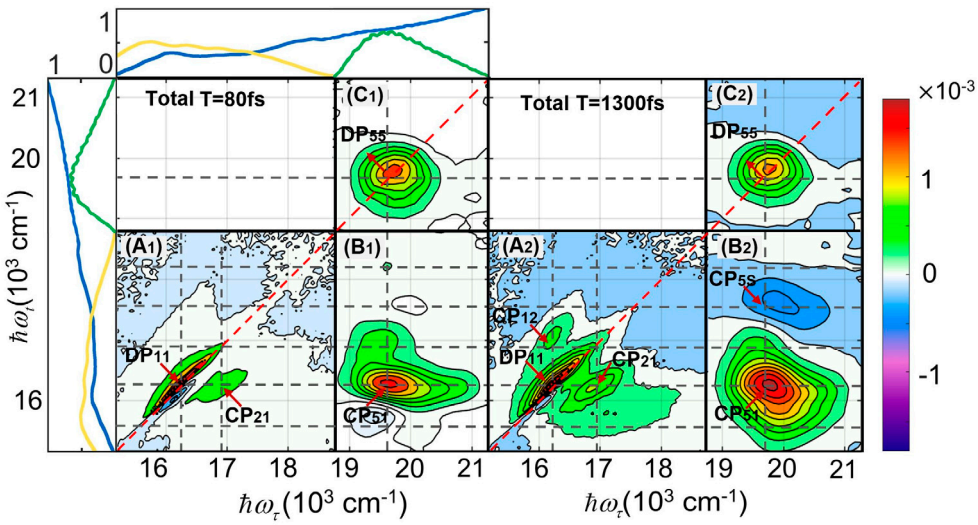

Figure 4.1. The real part of the total 2D spectrum. Panel A, B, and C represent the low-energy area, two-color area, and high-energy area, respectively. The range of low energy area goes from 15500 cm^{-1} to 18800 cm^{-1}. The range of high-energy areas goes from 18800 cm^{-1} to 21300 cm^{-1}. The yellow line in the box on the right represents the low-energy laser intensity of absorption. The green curve represents the high-energy laser intensity of absorption. The blue line stands for the sample absorbance.

In the 2D spectrum at 80 fs, four excited states $|e_1\rangle$, $|e_2\rangle$, $|e_3\rangle$, and $|e_4\rangle$ share the same low-energy area (panel A_1 and A_2), while the state $|e_5\rangle$ remains in the high-energy area (panels C_1 and C_2). According to previous researches[29,31] and our 2D spectrum, the excited state transition system of CdSe QDs is established in Figure 4.2. Besides, the $|f\rangle$ region, biexcitons, need to be considered to describe the excited state absorption signal.

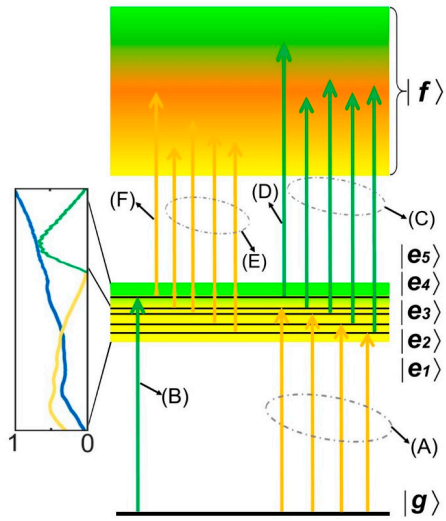

Figure 4.2. The absorption of a laser pulse by excited state transition system of a simple CdSe QDs. Inside the left box, the yellow and green curves represent the excited state transitions in the low-energy and high-energy areas, respectively. The blue line represents the sample absorbance.

In our two-color 2D spectrum, colors yellow and green are used to mark low-energy and high-energy areas in Figure 4.2. The yellow arrows between the excited states imply that the transition process is excited from the low-energy area. Besides, the green arrowed lines show the transition process from the high-energy area. Thus, there are six areas (A), (B), (C), (D), (E), and (F), respectively, in our system. Among them, areas (A), (E), and (F) are excited by the low-energy area, while the remaining areas (B), (C), and (D) are excited by the high-energy area. Unlike areas (A) and (B), areas (C), (D), (E), (F) are excited to the higher energy level of $|f\rangle$ where it contains some biexciton process.

4.1.2 The relaxation dynamics of CdSe QDs

To understand the details of the relaxation dynamics in CdSe QDs, it is necessary to analyze the real part of the rephasing 2D spectrum. The different size distribution of CdSe QDs may also affect the extension of these peaks. Therefore, these elongated and uneven wide peaks like DP_{11} are revealed, as shown in Figure 4.3.

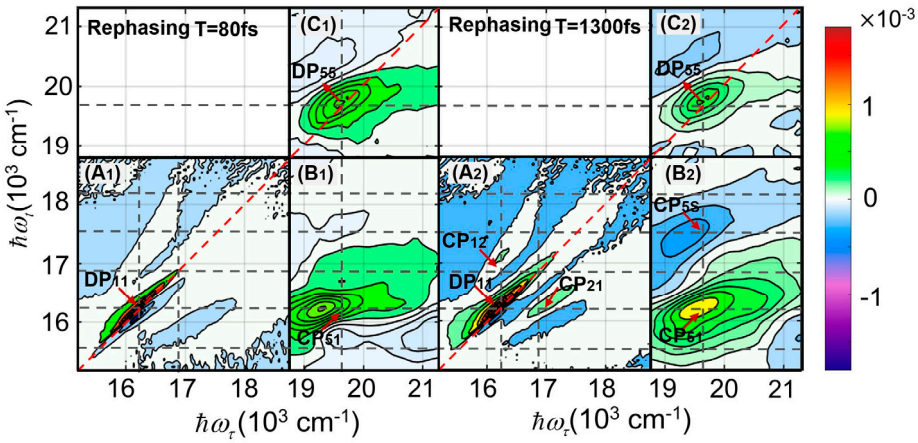

Figure 4.3. The real part of the rephasing 2D spectrum. The A_1, A_2, B_1, B_2, C_1, and C_2 panels represent low-energy, high-energy, and two-color areas at 80 fs and 1300 fs, respectively.

In this subproject, to reveal the relaxation dynamics between the excited states $|e_1\rangle$ and $|e_5\rangle$, three peaks have been selected: CP_{51}, CP_{5S}, and DP_{55} (Figure 4.4). The CP_{51} and CP_{5S} peaks are displayed in panels B_1 and B_2. The DP_{55} peak arises in the C_1 and C_2 panels. The energy of the DP_{55} peak decreases progressively, while the energy of CP_{51} and CP_{5S} increases along with population time T. The energy changes of the three peaks are shown in Figure 4.4(c). Simultaneously, the previous research[24] has shown some relaxation processes between states $|e_1\rangle$ and $|e_3\rangle$. However, this work mainly studies the relaxation dynamics between the states $|e_1\rangle$ and $|e_5\rangle$.

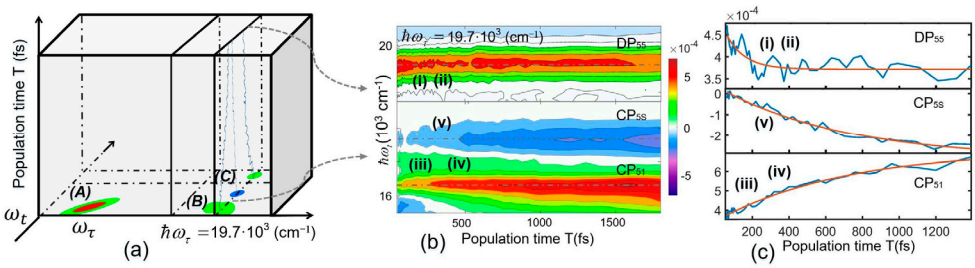

Figure 4.4. Schematic diagrams of extracting peaks from 2D maps. (a). Schematic diagram of 3D data. (b). The 2D slice is from Figure (a) along $\boldsymbol{\omega_\tau}$ at 19700 cm^{-1}. (c). The curves of three peaks DP_{55}, CP_{5S}, and CP_{51} are fitted at 16200 cm^{-1}, 17500 cm^{-1}, and 19700 cm^{-1}. The lifetimes of DP_{55}, CP_{5S}, and CP_{51} are 100 fs, 700 fs, and 700 fs respectively.

The processing of the experimental data is explained as follows. The 2D map in Figure 4.4(a) is obtained from a 2D slice of 3D data located at $\hbar\omega_\tau$=19700 cm^{-1}, where the excited states are $|e_1\rangle$ and $|e_5\rangle$. Moreover, to obtain lifetimes of the three peaks, we extract the curves at $\hbar\omega_t$ =16200 cm^{-1}, 17500 cm^{-1}, and 19700 cm^{-}

[1]. Thus, the data in Figure 4.4(a) is extracted from Figure 4.4(b) in the peaks DP_{55}, CP_{5S}, and CP_{51}.

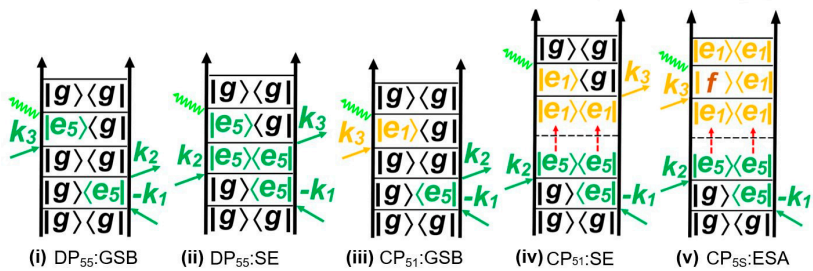

Figure 4.5. The relaxation dynamics among the excited states of CdSe QDs using double-sided Feynman diagrams.

The dynamics among the DP_{55}, CP_{5S}, and CP_{51} peaks in the 2D spectrum are discussed below. The GSB(i) and SE(ii) pathways occur in the DP_{55} decay band. The contribution of SE(ii) to peak DP_{55} is gradually decreasing, while the contribution of GSB remains relatively constant from 0 to 100 fs. Besides, the GSB continues to contribute steadily to the DP_{55} after 100 fs. The CP_{5S} band increases mainly as a function of the contribution of ESA(v). Here, the subscript S from CP_{5S} stands for the possible transition from excited states R_2, characterized by an electron trap (For specific details, refer to the literature.[24]). It takes 700 fs for state $|e_5\rangle$ to relax to $|e_1\rangle$, and this pathway of ESA(v) makes the state S stays in an increased negative band. The GSB(iii) and SE(iv) pathways are shown in the increasing band CP_{51}. The relaxation dynamics of SE(iv) grows in 700 fs, while GSB(iii) provides a stable contribution to CP_{51} during its whole lifetime. Specifically, when the DP_{55} band stabilizes after 100 fs, the signals in CP_{5S} and CP_{51} bands begin to increase from 0 to 700 fs. So, cascade transitions occur between the $|e_5\rangle$ and $|e_1\rangle$ states. In the CdSe QDs system, there are many phonons with energy at 200 cm^{-1}.[129,130] Thus, it is estimated that some jumps of phonon energy have been taken from state $|e_5\rangle$ to state $|e_1\rangle$. It takes much longer time to see the signal from where it disappears.

4.1.3 Short generalization

In this subproject, the relaxation dynamics of CdSe QDs were measured at 77 K by two-color 2D spectroscopy. Specifically, we analyzed the dynamic processes among the peaks DP_{55}, CP_{5S}, and CP_{51}.

4.2 Quantum Beating in CMDS.

First, it is good practice to introduce the basics of quantum coherence.[131–134] The description of coherence goes back to the work by Tonnoudji in 1962.[134] In molecular systems, one needs to distinguish between electronic and vibrational coherence. Electronic coherence is formed between electronic states, while vibrational coherence is formed between vibrational states.[135] The generation of quantum coherence can lead to oscillating signals in the experiment. Such quantum coherence can be observed in a 2D spectrum. This is the beating from the oscillator coherence between the different excited states, and for this reason, this phenomenon is called quantum beating. Specifically, In the 2DES, there are three time delays which are defined as t, T, τ in Figure 4.6(a). Figure 4.6(b) shows a positive signal in the rephasing 2D map. Correspondingly, the SE pathway is used to illustrate the dynamics of positive B peak in Figure 4.6(c). The energy level diagram of the SE pathway is shown in Figure 4.6(d).

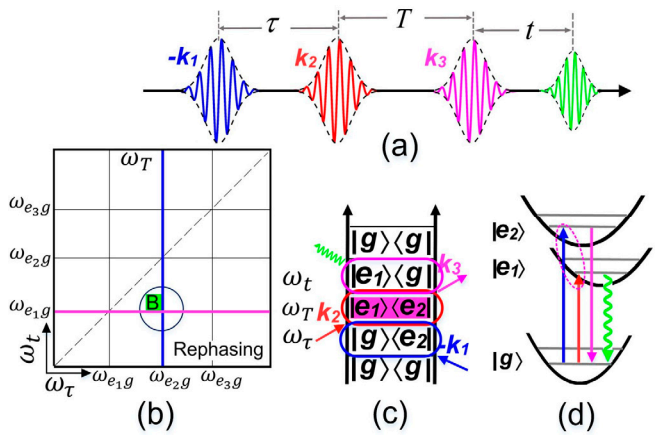

Figure 4.6. The illustration of quantum beating in the 2D spectrum. (a). 2D spectral pulse sequence. (b). 2D beating map. (c) the SE pathway corresponding to the blue peak of the 2D beating map. (d). The energy level diagram corresponding to the quantum beating from SE pathway.

If the Fourier transform is performed on the complex signal in the 3D spectrum along the population time T, the positive and negative frequencies of 2D maps are obtained, as shown in Figure 4.7.

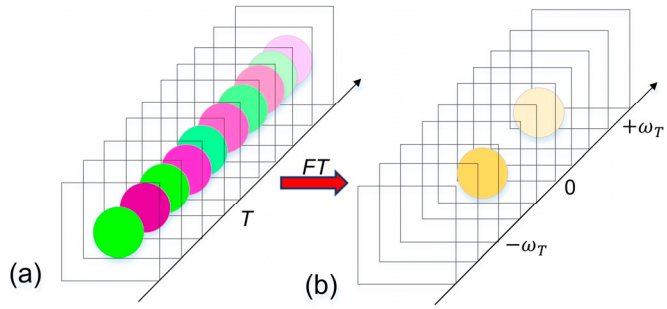

Figure 4.7. The Fourier analysis of oscillation beating from 3D spectra. (a). 3D spectrum with the population time T. (b). 3D spectrum with the frequency domain.

When the 2D spectrum varies with the population time T, the quantum beating from the oscillating signal can be clearly obtained from 2D beating maps. The positive and negative parts of 2D maps are shown in Figure 4.8.

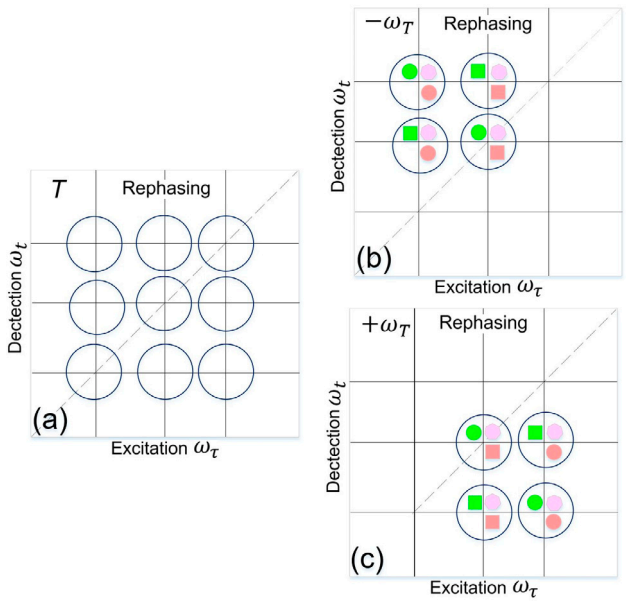

Figure 4.8. The 2D beating map model. (a). 2D spectrum. (b). The negative beating of 2D maps. (c). The positive beating of the 2D spectrum.

Generally, the Fourier transform of the signal in the complex domain can result in an asymmetric quantum beating between the positive and negative frequencies in the 2D maps, as visible in Figure 4.8.

4.2.1 Vibrational beating of CdSe QDs revealed by 2DES

Some groups have studied the quantum coherence of CdSe QDs using 2D spectroscopy.[136] Here we study the vibrational coherence of CdSe QDs at low temperatures.

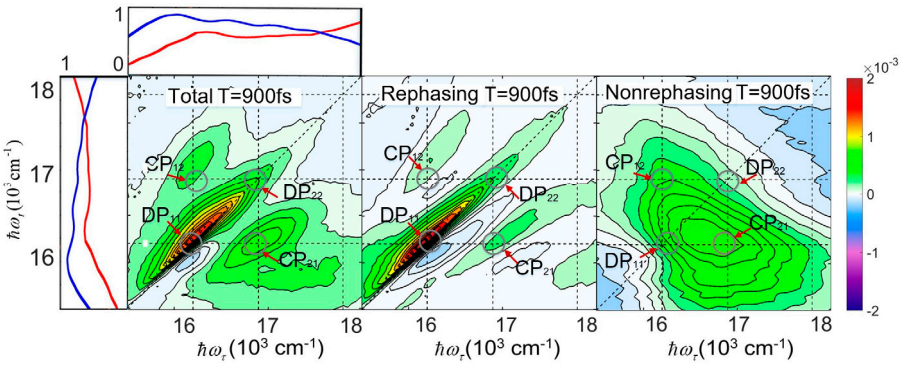

Figure 4.9. The real part of the 2D spectrum of CdSe QDs. (a). The real part of total 2D spectrum. (b). The real part of rephasing 2D spectrum. (c). The real part of non-rephasing 2D spectrum.

In the 2D spectrum in Figure 4.9, there are four peaks, namely DP_{11}, DP_{22}, CP_{12}, and CP_{21}. The excitation energies of DP_{11} and DP_{22} peaks are 16200 cm^{-1} and 16900 cm^{-1}, respectively, which is also reported by theoretical works.[23,24] The excited states of CdSe QDs are shown in Table 4.1.

Table 4.1. The excited states of CdSe QDs.

	$\|g\rangle$	$\|e_1\rangle$	$\|e_2\rangle$	$\|v_0\rangle$	$\|v_1\rangle$
Signal	ω_g	$\omega_{e_1 g}$	$\omega_{e_2 g}$	ω_{v_0}	ω_{v_1}
(cm^{-1})	0	16200	16900	0	230

To illustrate these quantum beatings clearly, the whole dynamic process of the 2D spectrum is shown in Figure 4.10.

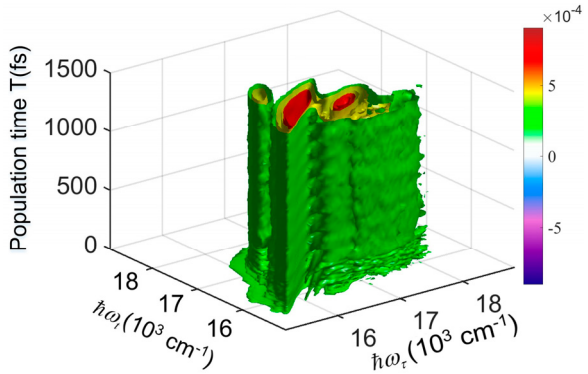

Figure 4.10. The real part of the rephasing 3D spectrum in the CdSe QDs.

A main vibrational beating band (green band) is visible in the 3D spectrum in Figure 4.11. Quantum beating of QDs exists between the vibrational states $|v_1\rangle$ and $|v_2\rangle$. As the quantum beating in the 3D spectrum is very complicated to decode, it's necessary to analyze its 2D slices.

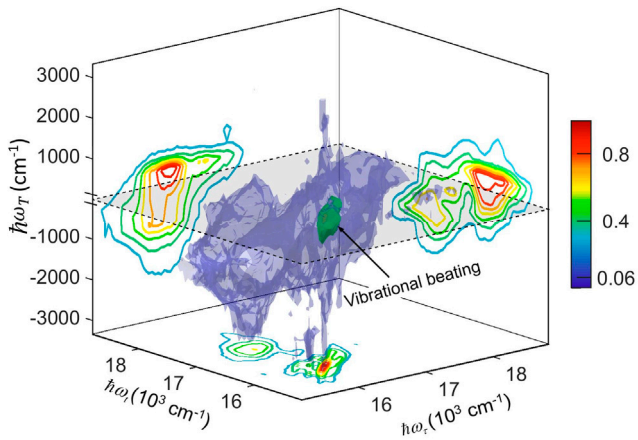

Figure 4.11. Oscillatory components in the real part of the rephasing 3D spectrum

Considering the rephasing 2D spectrum in Figure 4.12, it is obtained from the 3D spectrum, the oscillating features occur at ±230 cm^{-1}.
These beating bands appear in this 2D spectrum, namely A, C, DP_{11}, and D peaks.

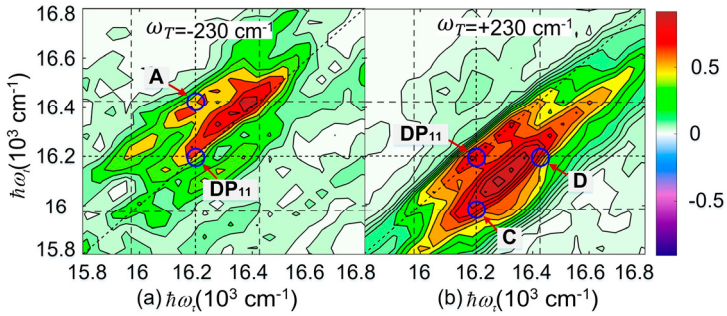

Figure 4.12. The vibrational beating of CdSe QDs.in the rephasing part of 2D beating maps. (a). There are two vibrational beating peaks A and DP_{11}, respectively at ω_T=-230 cm^{-1}. (b). There are three vibrational beating peaks, C, D, and DP_{11}, respectively at ω_T=+230 cm^{-1}.

Based on the above experimental results and previous researches,[137,138] the model diagram is established in Figure 4.13. Here, the red and blue circles indicate the excitation signals arising from QDs with different sizes. The DP_{11} peak of the 2D map is elongated due to distinctive sizes excitation of QDs, which has also been verified in Bawendi's research.[23] Specifically, the vibrational beating of peaks A and DP_{11} originates from the contribution of coherence $|e_1, v_1\rangle\langle e_1, v_0|$ visible in Figure 4.13(a1) and (a2), respectively. Considering the 2D map at +230 cm^{-1}, the vibrational beating from the coherence $|g, v_0\rangle\langle g, v_1|$ by the pathway of C-GSB, contributes to the ground state coherence as shown in Figure 4.13(a6). Similarly, pathways of the vibrational beating of DP_{11}-GSB and D-GSB are shown in Figure 4.13(a3), and (a4), respectively.

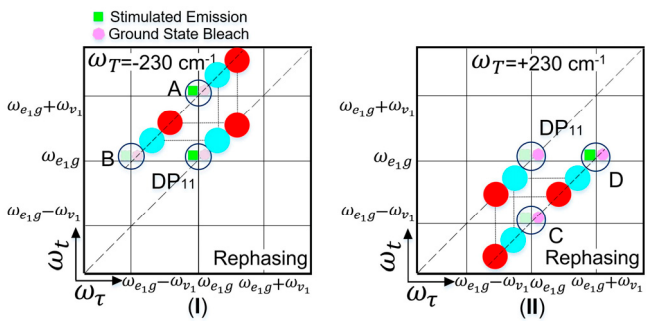

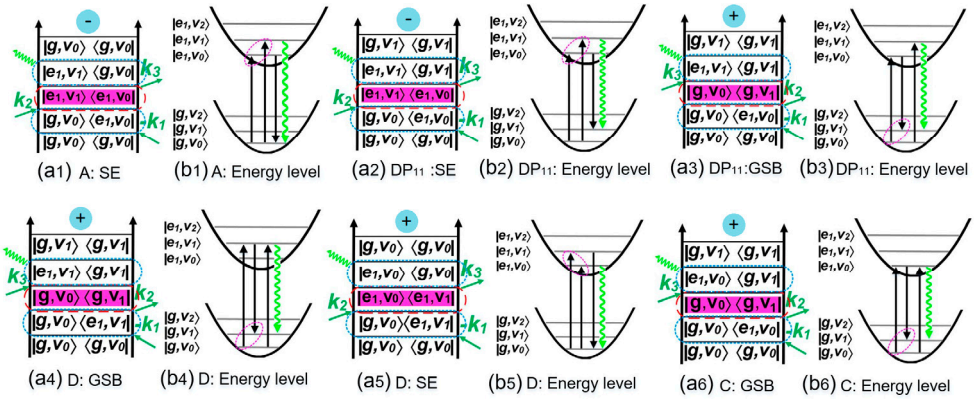

Figure 4.13. The vibrational beating of the CdSe QDs in the rephasingof 2D spectrum (ω_T=±230 cm^{-1}). (I). 2D beating maps at -230 cm^{-1}. (II). 2D beating maps at +230 cm^{-1}. (a). The related double-sided Feynman diagrams. (b). The corresponding energy level diagram.

Similarly, for the non-rephasing part of the 2D beating map at ±230 cm^{-1}, there are four beating peaks namely the DP_{11}, M, N, and E.

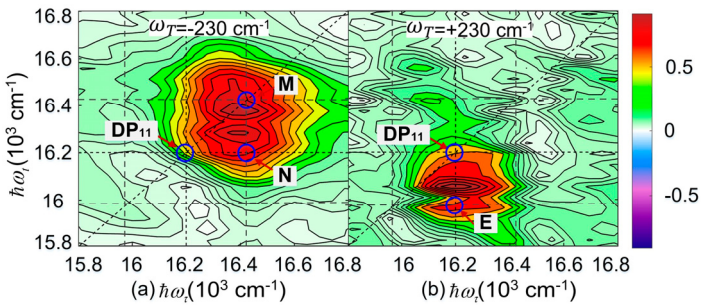

Figure 4.14. The vibrational beating of CdSe QDs in 2D spectrum (non-rephasing part). (a). The vibrational beating of 2D map at -230 cm^{-1}. (b) The vibrational beating of the 2D map at +230 cm^{-1}.

When the 2D map is at -230 cm^{-1}, the contribution of vibrational beating comes from the ground state coherence $|g, v_1\rangle\langle g, v_0|$ as shown in DP_{11}-GSB in Figure 4.15(a1). Besides, the vibrational beating in the M and N peaks mainly stems from the excited state coherence $|e_1, v_1\rangle\langle e_1, v_0|$ in Figure 4.15(a2) and (a3).

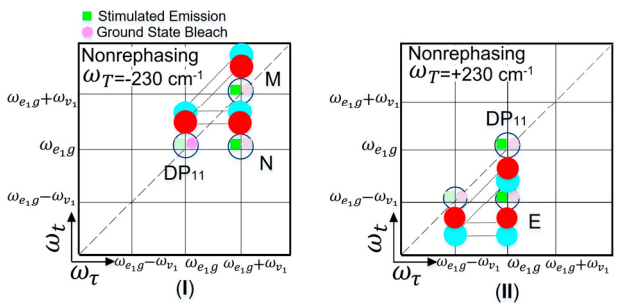

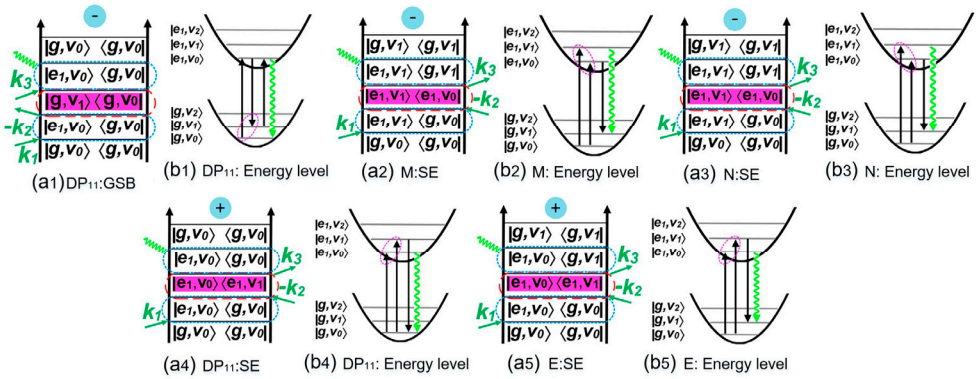

Figure 4. 15. The vibrational beating of non-rephasing 2D spectrum in the CdSe QDs (ω_T=±230 cm^{-1}). (I). 2D beating model map at -230 cm^{-1}. (II). 2D beating model map at +230 cm^{-1}. (a). The related double-sided Feynman diagrams. (b). Corresponding energy level diagrams.

As the 2D map is at +230 cm^{-1} as shown in Figure 4.15, the vibrational beating comes from the $|e_1, v_0\rangle\langle e_1, v_1|$ in DP$_{11}$-SE in Figure 4.15(a4). Therefore, the vibrational beating of peak E results from the contribution of the excited state coherence $|e_1, v_0\rangle\langle e_1, v_1|$ in Figure 4.15(a5). All the vibrational beating results are summarized in Tables 4.2 and 4.3.

Table 4.2. The vibrational beating of CdSe QDs in 2D (ω_τ, ω_t) cuts

	Vibrational beating (Rephasing)				
Peak	A	DP$_{11}$	DP$_{11}$	C	D
ω_τ, ω_t	$\omega_{e_1}, \omega_{e_1}+\omega_{v_1}$	$\omega_{e_1}, \omega_{e_1}$	$\omega_{e_1}, \omega_{e_1}$	$\omega_{e_1}, \omega_{e_1}+\omega_{v_1}$	$\omega_{e_1}+\omega_{v_1}, \omega_{e_1}$
ω_τ, ω_t (cm^{-1})	16200, 16430	16200, 16200	16200, 16200	16200, 159700	16430, 16200
ω_T (cm^{-1})	-230	-230	+230	+230	+230
Pathway	SE	SE	GSB	GSB	SE
Signal	$\|e_1, v_1\rangle\langle e_1, v_0\|$	$\|e_1, v_1\rangle\langle e_1, v_0\|$	$\|g, v_0\rangle\langle g, v_1\|$	$\|g, v_0\rangle\langle g, v_1\|$	$\|g, v_0\rangle\langle g, v_1\|$
Beating	Excited state coherence		Ground state coherence		

Table 4.3. The vibrational beating of CdSe QDs in 2D (ω_τ, ω_t) cuts

	Vibrational beating (Non-rephasing)				
Peak	DP$_{11}$	M	N	DP$_{11}$	E
ω_τ, ω_t	$\omega_{e_1}, \omega_{e_1}$	$\omega_{e_1}+\omega_{v_1}, \omega_{e_1}+\omega_{v_1}$	$\omega_{e_1}+\omega_{v_1}, \omega_{e_1}$	$\omega_{e_1}, \omega_{e_1}$	$\omega_{e_1}, \omega_{e_1}-\omega_{v_1}$
ω_τ, ω_t (cm^{-1})	16200,16200	16430, 16430	16430, 16200	16200,16200	16200,15970
ω_T (cm^{-1})	-230	-230	-230	+230	+230
Pathway	GSB	SE	SE	SE	SE
Signal	$\|g, v_1\rangle\langle g, v_0\|$	$\|e_1, v_1\rangle\langle e_1, v_0\|$	$\|e_1, v_1\rangle\langle e_1, v_0\|$	$\|e_1, v_0\rangle\langle e_1, v_1\|$	$\|e_1, v_0\rangle\langle e_1, v_1\|$
Beating	Ground state coherence		Excited state coherence		

Based on the above Table 4.2 and 4.3, 2DES can clearly distinguish the vibrational beatings in the CdSe QDs system. Specifically, there are two types of quantum beating contribution at 230 cm^{-1}: the vibrational coherence in the ground state $|g\rangle$ and excited state $|e_1\rangle$ at 77 K.

4.2.2 Short generalization

The 2D slices can be obtained from the 3D Fourier spectrum. In this subproject, we figured out which kind of excited states can produce the vibrational beating of CdSe QDs using 2DES. It can also be found that the stable quantum beating occurs in the vibrational states at ±230 cm^{-1}.

4.3 Quantum size effects in 2D spectroscopy of CdSe QDs

In this subproject, we find that when the size of CdSe QDs reduces, the energy band gap between excited states increases. This is mainly due to the change of the energy absorption bands for QDs with different sizes.

4.3.1 Excited states of CdSe QDs by 2DES

Based on the previous research,[23] the most remarkable property of QDs is the size dependence of the energy bandgap: when the nanostructure size decreases, the bandgap increases as shown in Figure 4.16.

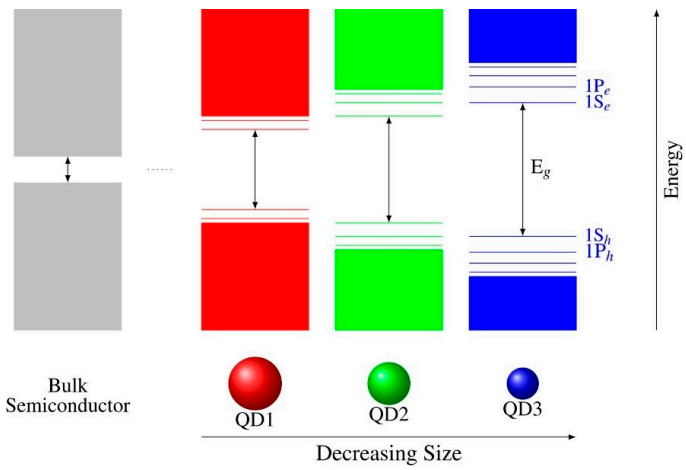

Figure 4.16. Comparison of energy levels of different sizes of CdSe QDs.

Although there have been many reports[23,29,31,66,136,139–141] about the excited state dynamics of QDs, there hasn't been research on the excited state dynamics of QDs with different sizes performed by 2DES at 77 K yet. This subproject mainly uses 2DES to detect the correlation between excited states and sizes of CdSe QDs at 77 K. The diameter of our CdSe QDs samples ranges from 6.3 nm to 11 nm.[24] The detailed 2D maps are recorded in Figure 4.17.

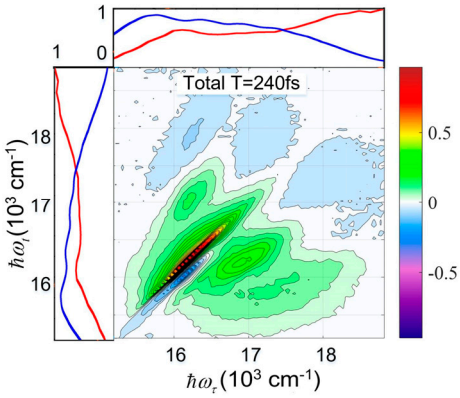

Figure 4.17. The real part of the total 2D spectrum of CdSe QDs at 240 fs. The x and y axes respectively represent the excitation wavelength and the detection wavelength from 15500 cm^{-1} to 18800 cm^{-1}.

4.3.2 The correlation between excited states and sizes in CdSe QDs

According to the shape of the peaks in Figure 4.17, it is necessary to determine whether the angle is constant between the cross peaks and the diagonal peaks for different sizes of CdSe QDs. To describe the relationship more clearly between excited states and the different sizes of QDs, the 2D spectra are shown in Figure 4.18.

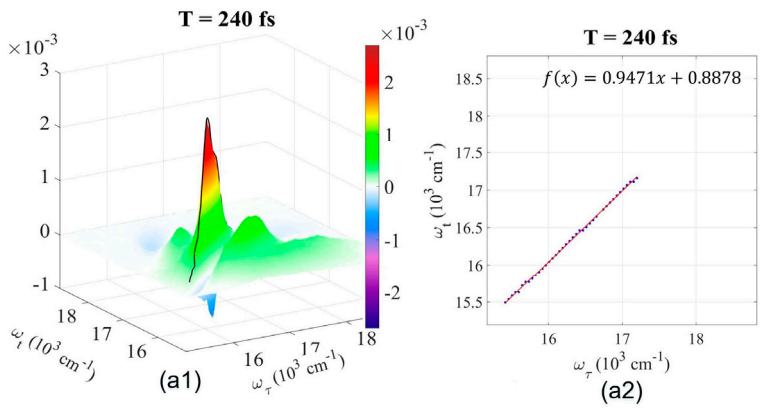

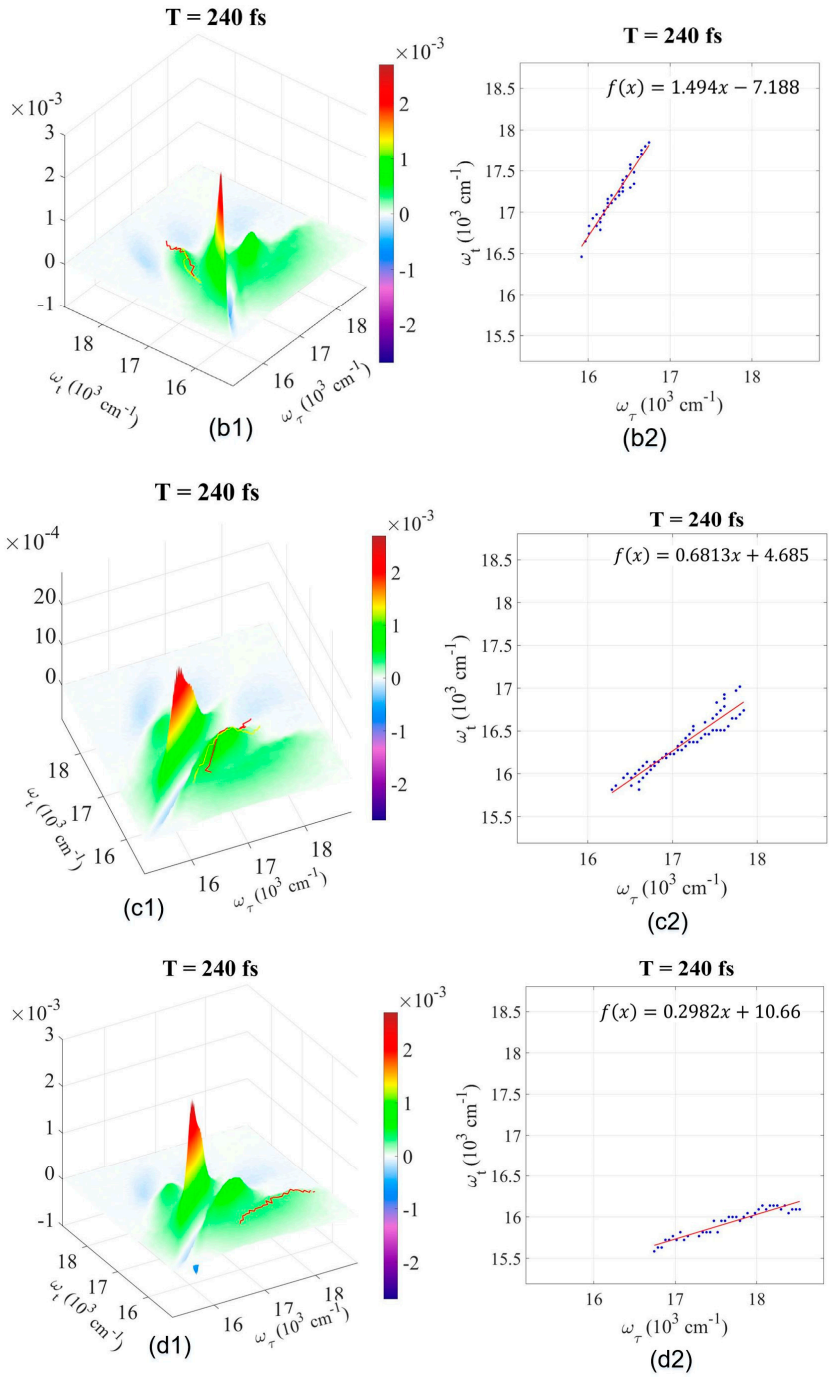

Figure 4.18. The fitting of different peaks of CdSe QDs of different sizes in the 2D spectrum. (a). The fitting of the diagonal peak varies with different sizes. (b). The fitting of cross peak CP_{12} varies with different sizes. (c). The fitting of cross peak CP_{21} varies with different sizes. (d). The fitting of cross peak CP_{31} varies with different sizes.

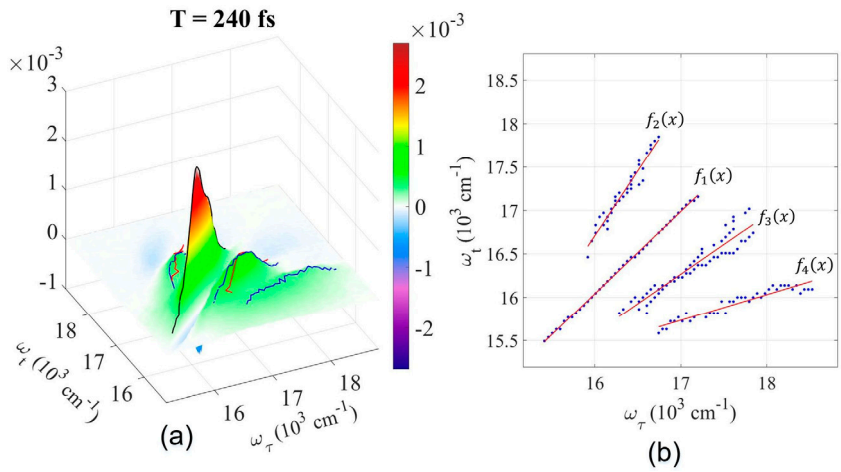

Figure 4.19. The fitting of different peaks of CdSe QDs in the 3D map. (a). the fitting of cross peaks and diagonal peaks in the 3D map at 240 fs. (b). The fitted peaks in the 2D map.

In 2D spectra of CdSe QDs in Figure 4.18, the diagonal peak DP_{11} (DP_{22}) is referred to as the cross peak between the first excited state $|e_1\rangle$ and the second excited state $|e_2\rangle$ in (b1) and (c1). As shown in Figure 4.19, the cross peaks are tilted with a certain angle relative to the diagonal peak. This correlation is likely to be the broad size distribution presenting in the CdSe QDs sample. Besides, we summarize the excited states of different sizes of CdSe QDs from Table 4.4 based on the previous research.[23]

Table 4.4. Summary of the excited states of different sizes of CdSe QDs

Diameter (nm)	7.96	6.78	6.5
$\|e_1\rangle$ (cm^{-1})	15490	16131	16330
$\|e_2\rangle$ (cm^{-1})	15890	16736	17000
$\|e_3\rangle$ (cm^{-1})	16700	17462	18631

In Figure 4.20, we marked these peaks based on Table 4.4. A negative peak N appears below DP_{11}. This is a biexciton produced by the e_1 excited state.

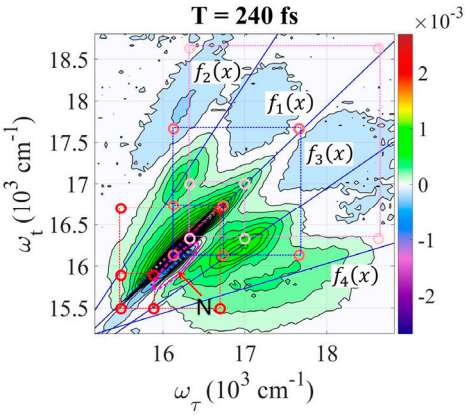

Figure 4.20. The excited states of the different sizes of CdSe QDs and the circles marked with the excited states from the three CdSe QDs are shown in Table 4.4 based on previous research.[23]

4.3.3 The biexciton shift changes with different sizes of CdSe QDs

Based on the experimental results in Figure 4.20 and previous studies,[23] we find that the 2D spectral peaks of CdSe QDs at 77 K are linear. The negative peak N is mainly from the contribution of biexciton. The dynamic process of N peak is shown in Figure 4.21(a) and (b).

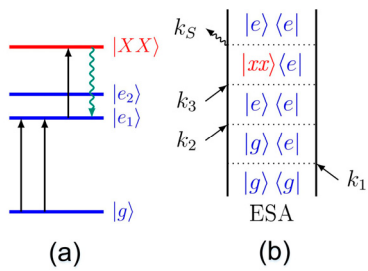

Figure 4.21. The dynamic pathway of the N peak. (a). The energy level of the ESA pathway of N peak. (b). The ESA pathway of N peak.

In order to be more clear about the change of biexciton shift as the size decreases, we select the 1D spectrum at ω_τ=16147 cm^{-1} and 16330 cm^{-1} for comparison in Figure 4.22. From the biexciton shift comparison of Figure 4.22(b) and (c), it can be seen that as the size of the QDs decreases, the biexciton shift gradually increases linearly. These are due to the quantum confinement effect of QDs.

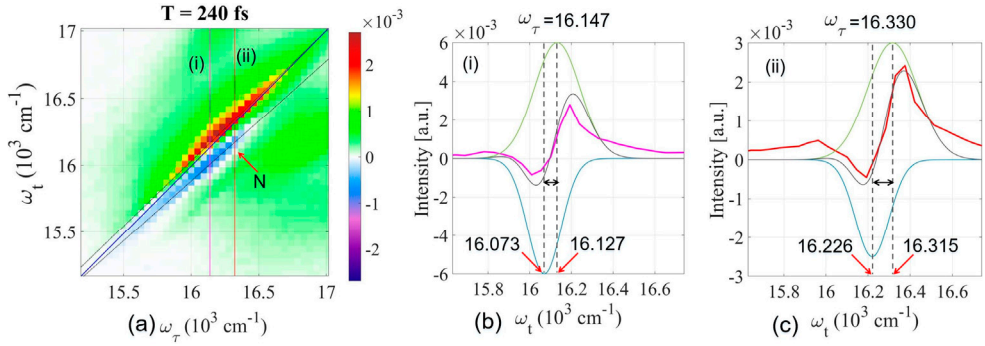

Figure 4.22. The biexciton shift in 2D spectra. (a). The biexciton shift of 2D spectra at 240 fs. (b). The Gaussian fitting of the 1D spectra at ω_τ=16147 cm^{-1}. (c). The Gaussian fitting of the 1D spectra at ω_τ=16330 cm^{-1}.

The above analysis shows that the angles are constant between the cross peaks and the diagonal peaks in the 2D spectrum. Simultaneously, as the sizes of QDs decrease, the biexciton shift also increases gradually. This means that the energy difference between the first two excited states increases linearly. As the size of the CdSe QDs decreases, the bandgap of the CdSe QDs increases in Figure 4.22. For details, please refer to paper III.

This entire discussion has been based on CdSe QDs. However, considering other samples of QDs (for example, CdTe, GaAs, InP), the discussion could be similar. If we observe a regular variation of the energy differences of the excited states as the sizes vary for different kinds of QDs, this model should still be valid. Here, we only study the relationship between e_1 and e_2 excited states. Further experiments are required to verify the discussion and conclusion.

4.3.4 Short generalization

In this chapter, we studied the correlation between excited states and different sizes in CdSe QDs.

4.4 Spare Sampling in CMDS

CMDS can detect complex dynamic systems, which also requires its complex experiment. Especially in the era of artificial intelligence (AI), the detection of N-dimensional spectroscopy demands advanced mathematical theories to sparsely sample experimental data to reduce the experimental time and data storage. With the above background, this subproject uses compressed sensing theory combined with dictionary learning from AI to achieve the data acquisition of CMDS.

In 2004, Candès, Romberg, Tao, and Donoho proved that if the signal satisfies the sparsity, the signal can be reconstructed with fewer samples. This optimal sampling theory is called compressed sensing (CS)[142–144] (also called compressed sampling, or sparse sampling). CS theory can effectively reconstruct the signal by finding the solution to the underdetermined nonlinear system.[142–144] That is, the sparse signal can be used to reconstruct the signal with fewer samples than that the Nyquist-Shannon sampling theorem requires. The signal can be reconstructed by CS when it meets the following conditions: (1) the signal is sparse in some domains; (2) the incoherence is that which is applied through the isometric property.

The early CS application was a single-pixel camera.[145] Initially, CS theory is based on the least absolute shrinkage and selection operator ((LASSO) proposed by Tibshirani in 1996,[146] and matching pursuit (MP) algorithms were applied to CMDS.[85,147–149] For example, Marcus and Aspuru-Guzik groups used CS theory to reconstruct the 2DFS signal.[85] Brixner group also applied CS theory on 2DES signal.[147] In our CMDS, we mainly use two CS methods to reconstruct the 2D fluorescence spectrum of LH2 protein in Figure 4.23.[16]

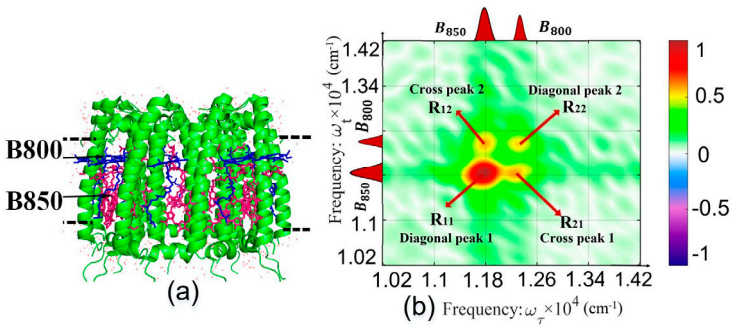

Figure 4.23. The LH2 protein and related 2D map.[16] (a). The LH2 protein. (b). Corresponding 2D spectrum.

4.4.1 Compressed sensing method

In our 2DFS experiment,[15] we have collected 20 points of T (from 0 fs to 73 fs) and 40 points for both t_1 and t_3 among the pulses sequence. The pulses sequence of 2DFS is as shown in Figure 4.24. 2D maps were obtained applying a double Fourier transform along t_1 and t_3 for a given population time T.[15]

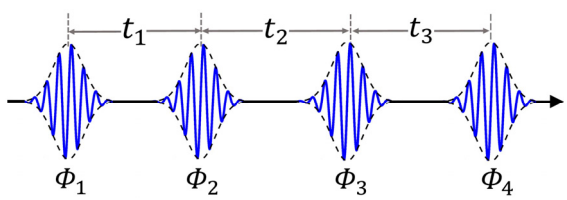

Figure 4.24. Pulses sequence of 2DFS

In this subproject, we reconstructed the 2DFS signal through two CS methods: the LASSO[146] and the sparse exponential mode analysis (SEMA).[150] To describe the CS method, we use a simple mathematical model. The 2D estimators are described as:

$$\mathrm{s} = \left[t_{i_1}^{(1)}, t_{i_2}^{(2)}\right]^T \tag{4.6}$$

$t_{i_1}^{(1)}$ and $t_{i_2}^{(2)}$ represent the 2D sampling time of the signal, the i_1-th sampling point in the first dimension, and the i_2-th sampling point in the two-dimensional. These time delays were represented by the τ and t symbol.

$$\mathrm{x(s)} = \sum_{k=1}^{K} g_k e^{\left[i\omega_k^{(1)} - \beta_k^{(1)}\right]\cdot t_{i_1}^{(1)}} \cdot e^{\left[i\omega_k^{(2)} - \beta_k^{(2)}\right]\cdot t_{i_1}^{(2)}} + u(s) \tag{4.7}$$

$\omega_k^{(l)}$ and $\beta_k^{(l)}$ respectively represent the frequency and width (damping) in the l (l=1,2) dimension of the k[th] 2D spectral band. g_k denotes the amplitude of the spectral band k. The noise term $u(s)$ is modeled as a Gaussian distributed random number.

The signal can be reconstructed by determining the most suitable penalty to minimize the problem,

$$\underset{\tilde{g}}{\text{minimize}} \left\{ \left\| vec\{x(s)\} - \tilde{A}\tilde{g} \right\|_2^2 + \sum_{m=1}^{P_1\times P_2\times J_1\times J_2} \lambda \left| \tilde{g}_m \right| \right\} \tag{4.8}$$

The spectral band $\tilde{A}$ is composed of all possible candidates in the dictionary. Please, refer to the literature[16] for more details.

$$\tilde{\mathrm{A}} = vec\{e^{\left[i\omega_{p1}^{(1)} - \beta_{j1}^{(1)}\right]\cdot t_{i1}^{(1)}} \otimes e^{\left[i\omega_{p2}^{(2)} - \beta_k^{(2)}\right]\cdot t_{j2}^{(2)}}\} \tag{4.9}$$

The symbol ⊗ denotes the outer product. With the above model, we use equation (4.8) to construct model data sets, which is aiming to test the efficiency of LASSO, SEMA and recover the parameters $\{\omega_p, \beta_j\}$ from the data sets. Different densities of sampling data sets are down to just a few original points through this model. For the calculation of the LASSO algorithm, Table 4.5 describe the process to perform the LASSO method, in which the sparse dictionary is mainly to solve the frequency in function (4.8).

Table 4. 5. The main steps of the LASSO algorithm

	LASSO algorithm
Step A:	Define a two-dimensional frequency grid dictionary and estimate the frequency peaks using the regularized least-squares method.
Step B:	Successive iterated step (A), until convergence.
Step C:	After Fourier transforms, obtained corresponding frequency and the damping value.

For the SEMA algorithm, the candidate frequencies and the consideration grid over the damping coefficients are updated in an alternating manner. A standard nonlinear least squares estimator is utilized. Then, using the improved parameter estimation, the model is subtracted again, and the next model is also improved. The improved pattern is used to update the dictionary so that it is divided into n dictionaries, one for each dimension. Then each dictionary moves in a fine grid around each found frequency. As a result, unused dictionary elements have zero amplitude and are excluded from the updated dictionary. This also means that closely spaced patterns can be generated after dictionary elements. After deleting these duplicate dictionary elements, scaling the dictionary elements of each grid point is avoided according to the corresponding mode of the found damping coefficient. In the end, it will ensure that all dictionary elements have the same specification.

Table 4. 6. The main steps of the SEMA algorithm

	SEMA algorithm
Step A:	Start with setting the damping $\beta_j^{(l)} = 0$, and the frequency ω_p is a roughly known estimate.
Step B:	For iter=1,…, do
Step C:	For $\mathrm{m} = 1, \ldots, P_1 \times P_2 \times J_1 \times J_2$ do
Step D:	Calculate frequency and damping, based on function (4.3) and (4.4) frequency using the dictionary damping by the dictionary (here including the sparse dictionary learning algorithm)
Step E:	End for.
Step F:	End for.
Step G:	Refine the grids and repeat steps (B) - (D) until convergence.

The estimated frequency values in the SEMA method can be obtained through function (4.4) using the frequency dictionary (a). The SEMA algorithm can select fewer sparse signals because the designed dictionary can be iteratively learned, which allows for a more accurate reconstruction of CMDS. The general steps for the dictionary learning in the SEMA algorithm are shown in Table 4.6. and Figure 4.23.

Table 4. 7. The main steps of the dictionary-learning algorithm

	The sparse dictionary learning algorithm
1:	Set all damping factors to zero and then use (4.3) Preliminary estimate.
2:	For i=1,…, intermix do
3:	Calculated residual using the function (dictionary learning R): $\mathrm{R} = \widetilde{\mathrm{A}} - G \times \widetilde{A_1} \times \widetilde{A_2}$ (Gis the sparse dictionary learning)
4:	For $\mathrm{k} = 1, \ldots, P_1 \times P_2 \times J_1 \times J_2$. Add the pattern of the current calculation mode to the residual.
5:	Estimate the frequency and damping of the mode (from the 4 calculated).
6:	Delete the acquired mode (in step 4)
7:	End for i
8:	Create a new dictionary using the frequency and damping factor (from step 5.)
9:	Recalculate using dictionary learning R .
10:	End

The upper part is a theoretical description of the LASSO and SEMA algorithms. Figure 4.25 shows the process of SEMA. Please, check the reference for details.[16,146,150]

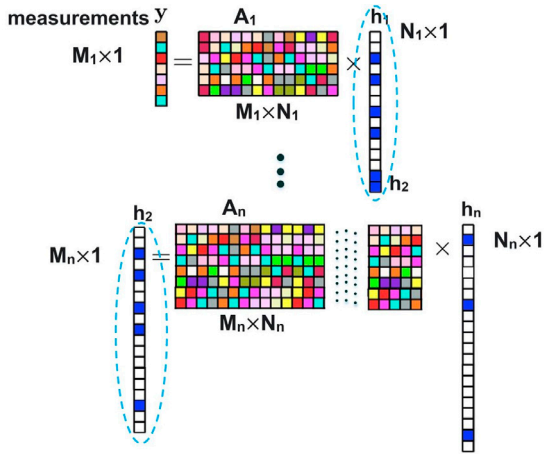

Figure 4.25. The process of dictionary learning in the Compressed sensing.

Based on the calculations of SEMA and LASSO above, we reconstructed the 2D spectrum as shown in Figure 4.26.

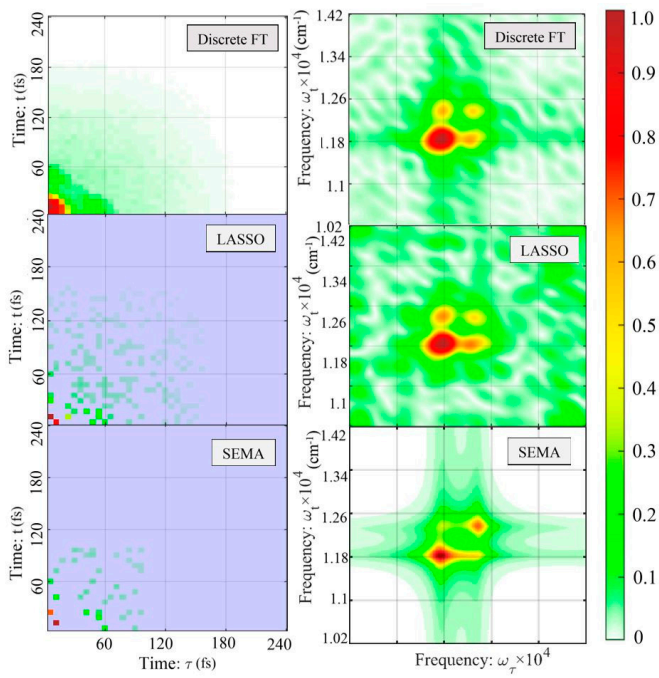

Figure 4. 26. Comparison of LASSO and SEMA methods for reconstruction of 2D spectrm.

We perform the following steps to reconstruct the CMDS signal. The first step is to sparsely sample the data in the time domain in Figure 4.27(b), and then use these time signals to reconstruct the 3D spectrum in Figure 4.27(c1) and (c2).

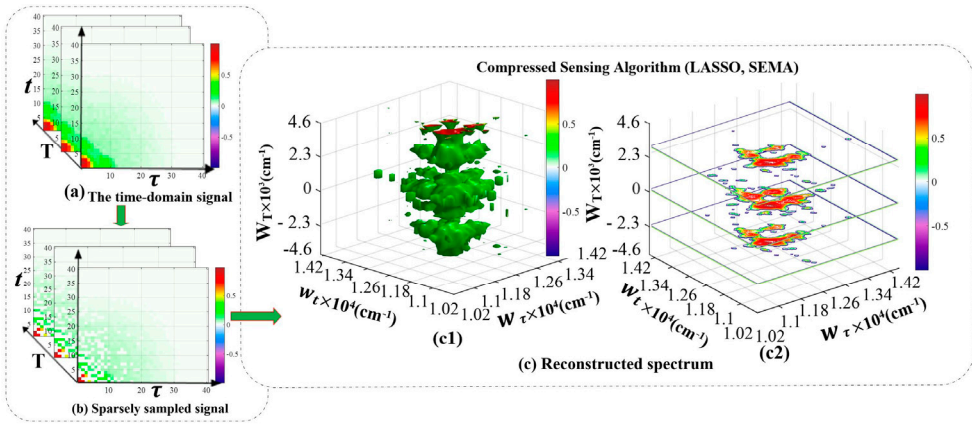

Figure 4.27. Compressed sensing for reconstruction 3D spectrum

Figure 4.27 shows the reconstruction of 3D spectra using the CS method including the LASSO and SEMA algorithms. For details, please refer to paper IV.

4.4.2 Short generalization

In summary, this section discusses some details of CS theory for CMDS. In this subproject, there are two CS methods (LASSO and SEMA algorithms) to sparsely reconstruct the 2DFS signal.

4.5 Phonon Coupling with Excitons and Free Carriers in Nanocrystals.

In this subsection, the temperature dependence of emission linewidth broadening in formamidinium lead bromide (FAPbBr3) perovskite nanocrystals (NCs) are examined as shown in Figure 4.28. The experiment provides information about electron-phonon interaction in these nanocrystals. Coupling between the electronic and nuclear degrees of freedom – the electron-phonon coupling – is the main origin of the relaxation between the energy levels in materials, included QDs.

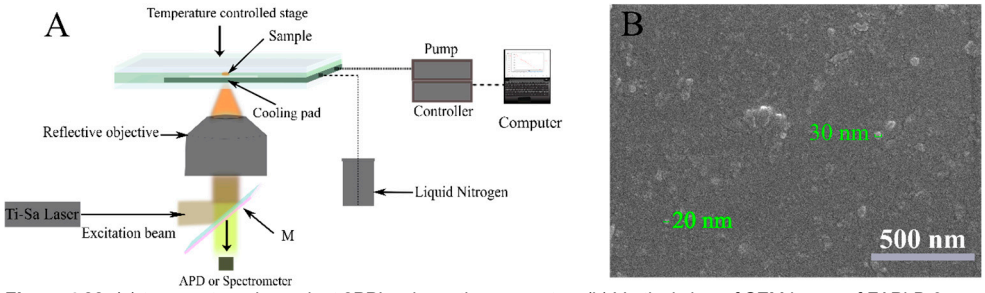

Figure 4.28. (a) temperature-dependent 2PPL schematics apparatus. (b) Vertical view of SEM image of FAPbBr3 perovskite NCs.

In our research, we observed that the orthorhombic phase is the origin of most of the emissions. The Fröhlich interaction between the free charge carriers and the optical phonons determines the PL linewidth broadening at high temperatures. At low temperatures, it is clear that a continuous redshift shows the growth of the exciton contribution from the peak of the PL spectrum and the reduction of the line-width because of the inhibition of the optical phonons. The exciton phonon interaction is determined based on the temperature-dependent measurement. The results show that the charge phonon coupling is stronger than that of the exciton phonon coupling in Figure 4.29. For details, please refer to paper V.

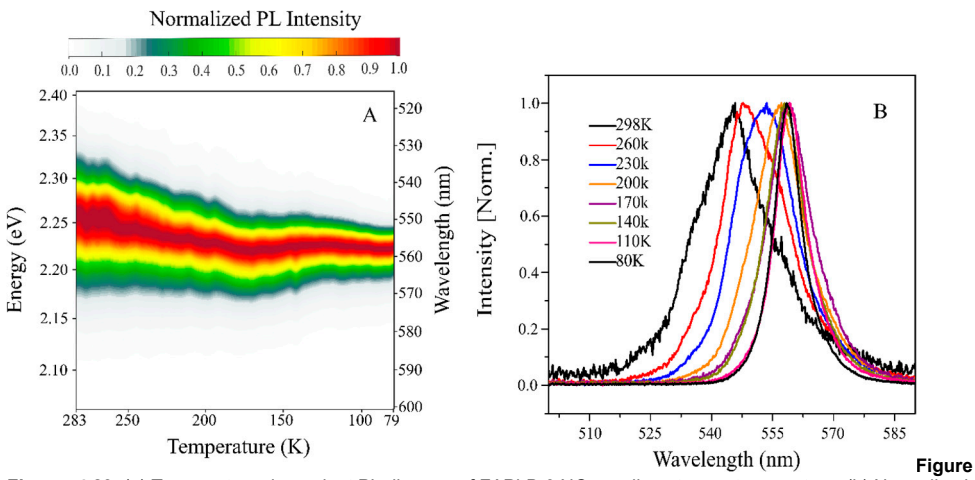

Figure

Figurre 4.29. (a) Temperature-dependent PL diagram of FAPbBr3 NCs cooling at room temperature. (b) Normalized PL spectra of FAPbBr3 of different temperatures (from RT to 80 K).

4.6 Short Summary

In this chapter, we measured CdSe QDs using CMDS, analyzed the dynamics of the sample, and collect LH2 data by 2DFS. Specifically, this section covers how to measure the excited state dynamics using two-color 2D spectroscopy, the quantum beating of CdSe QDs by 2DES, the correlation between excited state and sizes of CdSe QDs by 2DES, and use CS theory to reconstruct CMDS, the phonon coupling in nanocrystals.

Chapter 5 Conclusions and Outlook

Learn to be a decent person before learn to do things; don't discredit your country.

-Jianzhong Yang

This thesis we apply CMDS to study excited state dynamics in colloidal semiconductor nanocrystals. We also implement sparse sampling ideas to speed up the data collection in fluorescence detected 2D spectroscopy.

The first subproject mainly studies relaxation dynamics of CdSe QDs via two-color 2D spectroscopy. The second subproject is mainly about beating signals in the QD 2DES. We interpret the beatings as vibrational coherences. The third subproject studies the effect of the correlation between excited state energies and the QD size and how this correlation appears in 2DES. We also investigate the ways to obtain information about electron-phonon interaction in nanocrystals through the temperature dependence of fluorescence spectra. The last subproject employs the CS theory to reconstruct sparsely sampled 2D spectra of photosynthetic antenna complex LH2.

5.1 Conclusions

- The two-colour 2D measurements show that the initially high energy excitation in CdSe QDs relaxes with time-constant of 100 fs while the excitation arrives at the band edge with the time constant of 700 fs.
- The clear beating signals in 2DES of QDs are interpreted as coherent LO phonons.
- The quantum confinement related size effect is clearly visible in 2DES providing a nice illustration of the correlation of the different excited states.
- With the application of CS theory to the CMDS, we have successfully reconstructed the 2D spectrum of the LH2 protein.

5.2 Outlook

With coherent multidimensional spectroscopy technology, I am looking forward to laying the foundation for my future research on nonlinear optical spectroscopy and also exploring the mysteries of the quantum world.

Coherent multidimensional spectroscopy is still rapidly advancing. If given the chance, I would like to continue to studies of the new developments in coherent multidimensional spectroscopy. Also, for example, entangled photon spectroscopy, quantum light, and compressed sensing theory. I will continue to seek the truth and the soul.

References

(1) Mukamel, S. *Principles of Nonlinear Optical Spectroscopy*; Oxford University Press, 1995.

(2) Hamm, P. *Concepts and Methods of 2D Infrared Spectroscopy*; Cambridge University Press, 2011.

(3) Singharoy, A.; Maffeo, C.; Delgado-Magnero, K. H.; Swainsbury, D. J. K.; Sener, M.; Kleinekathöfer, U.; Vant, J. W.; Nguyen, J.; Hitchcock, A.; Isralewitz, B.; Teo, I.; Chandler, D. E.; Stone, J. E.; Phillips, J. C.; Pogorelov, T. V.; Mallus, M. I.; Chipot, C.; Luthey-Schulten, Z.; Tieleman, D. P.; Hunter, C. N.; Tajkhorshid, E.; Aksimentiev, A.; Schulten, K. Atoms to Phenotypes: Molecular Design Principles of Cellular Energy Metabolism. *Cell* **2019**, *179* (5), 1098-1111.e23. https://doi.org/10.1016/j.cell.2019.10.021.

(4) Ritz, T.; Hux, X.; Damjanović, A.; Schulten, K. Excitons and Excitation Transfer in the Photosynthetic Unit of Purple Bacteria. *J. Lumin.* **1998**, *76–77* (96), 310–321. https://doi.org/10.1016/S0022-2313(97)00286-X.

(5) Strümpfer, J.; Şener, M.; Schulten, K. How Quantum Coherence Assists Photosynthetic Light-Harvesting. *J. Phys. Chem. Lett.* **2012**, *3* (4), 536–542. https://doi.org/10.1021/jz201459c.

(6) Şener, M.; Strümpfer, J.; Timney, J. A.; Freiberg, A.; Hunter, C. N.; Schulten, K. Photosynthetic Vesicle Architecture and Constraints on Efficient Energy Harvesting. *Biophys. J.* **2010**, *99* (1), 67–75. https://doi.org/10.1016/j.bpj.2010.04.013.

(7) Şener, M. K.; Olsen, J. D.; Hunter, C. N.; Schulten, K. Atomic-Level Structural and Functional Model of a Bacterial Photosynthetic Membrane Vesicle. *Proc. Natl. Acad. Sci. U. S. A.* **2007**, *104* (40), 15723–15728. https://doi.org/10.1073/pnas.0706861104.

(8) Schulten, K. [Illinois] Phys550 Lecture 2: Photosynthesis I https://nanohub.org/resources/19300.

(9) McDermott, G.; Prince, S. M.; Freer, A. A.; Hawthornthwaite-Lawless, A. M.; Papiz, M. Z.; Cogdell, R. J.; Isaacs, N. W. Crystal Structure of an Integral Membrane Light-Harvesting Complex from Photosynthetic Bacteria. *Nature* **1995**, *374* (6522), 517–521. https://doi.org/10.1038/374517a0.

(10) Bandilla, M.; Ücker, B.; Ram, M.; Simonin, I.; Gelhaye, E.; McDermott, G.; Cogdell, R. J.; Scheer, H. Reconstitution of the B800 Bacteriochlorophylls in the Peripheral Light Harvesting Complex B800-850 of Rhodobacter Sphaeroides 2.4.1 with BChl a and Modified (Bacterio-)Chlorophylls. *Biochim. Biophys. Acta - Bioenerg.* **1998**, *1364* (3), 390–402. https://doi.org/10.1016/S0005-2728(98)00086-3.

(11) Atomic Energy Level Structure of the Photosynthetic Unit of Purple Bacteria https://www.ks.uiuc.edu/Research/psures/.

(12) How Does the Purple Bacteria Photosynthesize? Beckman Institute-UIUC (2015) http://naturedocumentaries.org/10031/purple-bacteria-photosynthesis-chromatophore-molecular-structure/.

(13) Thyrhaug, E.; Schröter, M.; Bukartė, E.; Kühn, O.; Cogdell, R.; Hauer, J.; Zigmantas, D. Intraband Dynamics and Exciton Trapping in the LH2 Complex of Rhodopseudomonas Acidophila. *J. Chem. Phys.* **2021**, *154* (4). https://doi.org/10.1063/5.0033802.

(14) Papiz, M. Z.; Hawthornthwaite, A. M.; Cogdell, R. J.; Woolley, K. J.; Wightman, P. A.; Ferguson, L. A.; Lindsay, J. G. Crystallization and Characterization of Two Crystal Forms of the B800-850 Light-Harvesting Complex from Rhodopseudomonas Acidophila Strain 10050. *J. Mol. Biol.* **1989**, *209* (4), 833–835. https://doi.org/10.1016/0022-2836(89)90612-8.

(15) Karki, K. J.; Chen, J.; Sakurai, A.; Shi, Q.; Gardiner, A. T.; Kühn, O.; Cogdell, R. J.; Pullerits, T. Before Förster. Initial Excitation in Photosynthetic Light Harvesting. *Chem. Sci.* **2019**, *10* (34), 7923–7928. https://doi.org/10.1039/c9sc01888c.

(16) Wang, Z.; Lei, S.; Karki, K. J.; Jakobsson, A.; Pullerits, T. Compressed Sensing for Reconstructing Coherent Multidimensional Spectra. *J. Phys. Chem. A* **2020**, *124* (9), 1861–1866. https://doi.org/10.1021/acs.jpca.9b11681.

(17) Brixner, T.; Stenger, J.; Vaswani, H. M.; Cho, M.; Blankenship, R. E.; Fleming, G. R. Two-Dimensional Spectroscopy of Electronic Couplings in Photosynthesis. *Nature* **2005**, *434* (7033), 625–628. https://doi.org/10.1038/nature03429.

(18) Engel, G. S.; Calhoun, T. R.; Read, E. L.; Ahn, T. K.; Mančal, T.; Cheng, Y. C.; Blankenship, R. E.; Fleming, G. R. Evidence for Wavelike Energy Transfer through Quantum Coherence in Photosynthetic Systems. *Nature* **2007**, *446* (7137), 782–786. https://doi.org/10.1038/nature05678.

(19) Romero, E.; Augulis, R.; Novoderezhkin, V. I.; Ferretti, M.; Thieme, J.; Zigmantas, D.; Van Grondelle, R. Quantum Coherence in Photosynthesis for Efficient Solar-Energy Conversion. *Nat. Phys.* **2014**, *10* (9), 676–682. https://doi.org/10.1038/NPHYS3017.

(20) Paleček, D.; Edlund, P.; Westenhoff, S.; Zigmantas, D. Quantum Coherence as a Witness of Vibronically Hot Energy Transfer in Bacterial Reaction Center. *Sci. Adv.* **2017**, *3* (9). https://doi.org/10.1126/sciadv.1603141.

(21) Schröter, M.; Pullerits, T.; Kühn, O. Using Fluorescence Detected Two-Dimensional Spectroscopy to Investigate Initial Exciton Delocalization between Coupled Chromophores. *J. Chem. Phys.* **2018**, *149* (11). https://doi.org/10.1063/1.5046645.

(22) Tiwari, V.; Matutes, Y. A.; Gardiner, A. T.; Jansen, T. L. C.; Cogdell, R. J.; Ogilvie, J. P. Spatially-Resolved Fluorescence-Detected Two-Dimensional Electronic Spectroscopy Probes Varying Excitonic Structure in Photosynthetic Bacteria. *Nat. Commun.* **2018**, *9* (1). https://doi.org/10.1038/s41467-018-06619-x.

(23) Norris, D.; Bawendi, M. Measurement and Assignment of the Size-Dependent Optical Spectrum in CdSe Quantum Dots. *Phys. Rev. B - Condens. Matter Mater. Phys.* **1996**, *53* (24), 16338–16346. https://doi.org/10.1103/PhysRevB.53.16338.

(24) Lenngren, N.; Abdellah, M. A.; Zheng, K.; Al-Marri, M. J.; Zigmantas, D.; Žídek, K.; Pullerits, T. Hot Electron and Hole Dynamics in Thiol-Capped CdSe Quantum Dots Revealed by 2D Electronic Spectroscopy. *Phys. Chem. Chem. Phys.* **2016**, *18* (37), 26199–26204. https://doi.org/10.1039/c6cp04190f.

(25) Bullen, C. R.; Mulvaney, P. 0300.NanoLett.2004,4,2303.Pdf. **2004**.

(26) Zheng, K.; Žídek, K.; Abdellah, M.; Zhu, N.; Chábera, P.; Lenngren, N.; Chi, Q.; Pullerits, T. Directed Energy Transfer in Films of CdSe Quantum Dots: Beyond the Point Dipole Approximation. *J. Am. Chem. Soc.* **2014**, *136* (17), 6259–6268. https://doi.org/10.1021/ja411127w.

(27) Yu, W. W.; Qu, L.; Guo, W.; Peng, X. Erratum: Experimental Determination of the Extinction Coefficient of CdTe, CdSe and CdS Nanocrystals (Chemistry of Materials (2003) 15, 14 (2854-2860)). *Chem. Mater.* **2004**, *16* (3), 560. https://doi.org/10.1021/cm033007z.

(28) Murray, C. B.; Norris, D. J.; Bawendi, M. G. Synthesis and Characterization of Nearly Monodisperse CdE (E = S, Se, Te) Semiconductor Nanocrystallites. *J. Am. Chem. Soc.* **1993**, *115* (19), 8706–8715. https://doi.org/10.1021/ja00072a025.

(29) Norris, D. J.; Sacra, A.; Murray, C. B.; Bawendi, M. G. Measurement of the Size Dependent Hole Spectrum in CdSe Quantum Dots. *Phys. Rev. Lett.* **1994**, *72* (16), 2612–2615. https://doi.org/10.1103/PhysRevLett.72.2612.

(30) Klimov, V. I.; Mikhailovsky, A. A.; Xu, S.; Malko, A.; Hollingsworth, J. A.; Leatherdale, C. A.; Eisler, H. J.; Bawendi, M. G. Optical Gain and Stimulated Emission in Nanocrystal Quantum Dots. *Science (80-.).* **2000**, *290* (5490), 314–317. https://doi.org/10.1126/science.290.5490.314.

(31) Caram, J. R.; Zheng, H.; Dahlberg, P. D.; Rolczynski, B. S.; Griffin, G. B.; Dolzhnikov, D. S.; Talapin, D. V.; Engel, G. S. Exploring Size and State Dynamics in CdSe Quantum Dots Using Two-Dimensional Electronic Spectroscopy. *J. Chem. Phys.* **2014**, *140* (8). https://doi.org/10.1063/1.4865832.

(32) Norris, D.; Efros, A. L.; Rosen, M. Size Dependence of Exciton Fine Structure in CdSe Quantum Dots. *Phys. Rev. B - Condens. Matter Mater. Phys.* **1996**, *53* (24), 16347–16354. https://doi.org/10.1103/PhysRevB.53.16347.

(33) Ullrich, C. *Time-Dependent Density-Functional Theory: Concepts and Applications*; OUP Oxford, 2012.

(34) Köhler, J.; Wollenhaupt, M.; Bayer, T.; Sarpe, C.; Baumert, T. Zeptosecond Precision Pulse Shaping. *Opt. Express* **2011**, *19* (12), 11638. https://doi.org/10.1364/oe.19.011638.

(35) Vanacore, G. M.; Madan, I.; Berruto, G.; Wang, K.; Pomarico, E.; Lamb, R. J.; McGrouther, D.; Kaminer, I.; Barwick, B.; García De Abajo, F. J.; Carbone, F. Attosecond Coherent Control of Free-Electron Wave Functions Using Semi-Infinite Light Fields. *Nat. Commun.* **2018**, *9* (1). https://doi.org/10.1038/s41467-018-05021-x.

(36) Ipp, A.; Keitel, C. H.; Evers, J. Yoctosecond Photon Pulses from Quark-Gluon Plasmas. *Phys. Rev. Lett.* **2009**, *103* (15), 1–4. https://doi.org/10.1103/PhysRevLett.103.152301.

(37) Kythe, P. K. *Sinusoids: Theory and Technological Applications*; CRC Press, 2014.

(38) Laage, D.; Hynes, J. T. A Molecular Jump Mechanism of Water Reorientation. *Science (80-.).* **2006**, *311* (5762), 832–835. https://doi.org/10.1126/science.1122154.

(39) R. A. Harvey, P. C. champe, B. D. F. *Lippincott's Illustrated Reviews: Microbiology (Lippincott's Illustrated Reviews Series)*; Lippincott Williams and Wilkins, 2007.

(40) Cavalieri, A. L.; Müller, N.; Uphues, T.; Yakovlev, V. S.; Baltuška, A.; Horvath, B.; Schmidt, B.; Blümel, L.; Holzwarth, R.; Hendel, S.; Drescher, M.; Kleineberg, U.; Echenique, P. M.; Kienberger, R.; Krausz, F.; Heinzmann, U. Attosecond Spectroscopy in Condensed Matter. *Nature* **2007**, *449* (7165), 1029–1032. https://doi.org/10.1038/nature06229.

(41) Klaiber, M.; Hatsagortsyan, K. Z.; Keitel, C. H. Zeptosecond γ-Ray Pulses. **2007**, *1*, 2–5.

(42) Hernández-García, C.; Pérez-Hernández, J. A.; Popmintchev, T.; Murnane, M. M.; Kapteyn, H. C.; Jaron-Becker, A.; Becker, A.; Plaja, L. Zeptosecond High Harmonic KeV X-Ray Waveforms Driven by Midinfrared Laser Pulses. *Phys. Rev. Lett.* **2013**, *111* (3), 1–5. https://doi.org/10.1103/PhysRevLett.111.033002.

(43) W. Greiner, et al. *Physics:, Nuclear Future, Present And*; W. Greiner, Ed.; 2015.

(44) Kornowski, S. Lifetimes of Higgs , W and Z Bosons in the Scale-. **2015**.

(45) Steinhardt, R. G. THE DEFINITION OF " SPECTRUM ". **1952**, *1349*, 1952–1953.

(46) Thomas, N. C. The Early History of Spectroscopy. *J. Chem. Educ.* **1991**, *68* (8), 631–634. https://doi.org/10.1021/ed068p631.

(47) Tokmakoff, A. *Time-Dependent Quantum Mechanics and Spectroscopy*; Libre Texts, 2014.

(48) https://en.wikipedia.org/wiki/Spectroscopy.

(49) Isaac, S. Opticks : Opticks London : Sir Isaac Newton ’ s Advertisements. 1–111.

(50) Maxwell, J. C. *A Treatise on Electricity and Magnetism*; Clarendon Press, 1873.

(51) https://en.wikipedia.org/wiki/Quantum_mechanics.

(52) Committee, N. P. No Title https://www.nobelprize.org/prizes/lists/all-nobel-prizes/.

(53) American, S.; America, N.; American, S. : : S r e s a e s l u t r o h s a r t L. **2000**, *283* (3), 72–79.

(54) Sundström, V.; Pullerits, T.; Van Grondelle, R. Photosynthetic Light-Harvesting: Reconciling Dynamics and Structure of Purple Bacterial LH2 Reveals Function of Photosynthetic Unit. *J. Phys. Chem. B* **1999**, *103* (13), 2327–2346. https://doi.org/10.1021/jp983722+.

(55) Dostál, J.; Pšenčík, J.; Zigmantas, D. In Situ Mapping of the Energy Flow through the Entire Photosynthetic Apparatus. *Nat. Chem.* **2016**, *8* (7), 705–710. https://doi.org/10.1038/nchem.2525.

(56) Peter**,** C. Lewerenz, H. *Photoelectrochemical Water Splitting: Materials, Processes and Architectures*; The Royal Society of Chemistry, 2013.

(57) Kolano, C.; Helbing, J.; Kozinski, M.; Sander, W.; Hamm, P. Watching Hydrogen-Bond Dynamics in a β-Turn by Transient Two-Dimensional Infrared Spectroscopy. *Nature* **2006**, *444* (7118), 469–472. https://doi.org/10.1038/nature05352.

(58) Turner, D. B.; Nelson, K. A. Coherent Measurements of High-Order Electronic Correlations in Quantum Wells. *Nature* **2010**, *466* (7310), 1089–1091. https://doi.org/10.1038/nature09286.

(59) Hamm, P. *Concepts and Methods of 2D Infrared Spectroscopy*; 2011.

(60) Dietzek, B.; Christensson, N.; Kjellberg, P.; Pascher, T.; Pullerits, T.; Yartsev, A. Appearance of Intramolecular High-Frequency Vibrations in Two-Dimensional, Time-Integrated Three-Pulse Photon Echo Data. *Phys. Chem. Chem. Phys.* **2007**, *9* (6), 701–710. https://doi.org/10.1039/b614332f.

(61) Perdomo-Ortiz, A.; Widom, J. R.; Lott, G. A.; Aspuru-Guzik, A.; Marcus, A. H. Conformation and Electronic Population Transfer in Membrane-Supported Self-Assembled Porphyrin Dimers by 2D Fluorescence Spectroscopy. *J. Phys. Chem. B* **2012**, *116* (35), 10757–10770. https://doi.org/10.1021/jp305916x.

(62) Minhaeng Cho. *Two-Dimensional Optical Spectroscopy*; CRC Press; 1st edition, 2009.

(63) Minhaeng Cho. *Coherent Multidimensional Spectroscopy*; Minhaeng Cho, Ed.; 2019.

(64) Yurs, L. A.; Block, S. B.; Pakoulev, A. V.; Selinsky, R. S.; Jin, S.; Wright, J. Multiresonant Coherent Multidimensional Electronic Spectroscopy of Colloidal PbSe Quantum Dots. *J. Phys. Chem. C* **2011**, *115* (46), 22833–22844. https://doi.org/10.1021/jp207273x.

(65) Wright, J. C. Multiresonant Coherent Multidimensional Spectroscopy. *Annu. Rev. Phys. Chem.* **2011**, *62*, 209–230. https://doi.org/10.1146/annurev-physchem-032210-103551.

(66) Seibt, J.; Hansen, T.; Pullerits, T. 3D Spectroscopy of Vibrational Coherences in Quantum Dots: Theory. *J. Phys. Chem. B* **2013**, *117* (38), 11124–11133. https://doi.org/10.1021/jp4011444.

(67) Ruetzel, S.; Diekmann, M.; Nuernberger, P.; Walter, C.; Engels, B.; Brixner, T. Multidimensional Spectroscopy of Photoreactivity. *Proc. Natl. Acad. Sci. U. S. A.* **2014**, *111* (13), 4764–4769. https://doi.org/10.1073/pnas.1323792111.

(68) Gellen, T. A.; Lem, J.; Turner, D. B. Probing Homogeneous Line Broadening in CdSe Nanocrystals Using Multidimensional Electronic Spectroscopy. *Nano Lett.* **2017**, *17* (5), 2809–2815. https://doi.org/10.1021/acs.nanolett.6b05068.

(69) Rodriguez, Y.; Frei, F.; Cannizzo, A.; Feurer, T. Pulse-Shaping Assisted Multidimensional Coherent Electronic Spectroscopy. *J. Chem. Phys.* **2015**, *142* (21). https://doi.org/10.1063/1.4921793.

(70) Turner, D. B.; Arpin, P. C.; McClure, S. D.; Ulness, D. J.; Scholes, G. D. Coherent Multidimensional Optical Spectra Measured Using Incoherent Light. *Nat. Commun.* **2013**, *4*, 1–9. https://doi.org/10.1038/ncomms3298.

(71) Tollerud, J. O.; Davis, J. A. Coherent Multi-Dimensional Spectroscopy: Experimental Considerations, Direct Comparisons and New Capabilities. *Prog. Quantum Electron.* **2017**, *55* (July), 1–34. https://doi.org/10.1016/j.pquantelec.2017.07.001.

(72) Tollerud, J. O.; Hall, C. R.; Davis, J. A. Isolating Quantum Coherence Using Coherent Multi-Dimensional Spectroscopy with Spectrally Shaped Pulses. *Opt. Express* **2014**, *22* (6), 6719. https://doi.org/10.1364/oe.22.006719.

(73) Bruder, L.; Bangert, U.; Binz, M.; Uhl, D.; Vexiau, R.; Bouloufa-Maafa, N.; Dulieu, O.; Stienkemeier, F. Coherent Multidimensional Spectroscopy of Dilute Gas-Phase Nanosystems. *Nat. Commun.* **2018**, *9* (1). https://doi.org/10.1038/s41467-018-07292-w.

(74) Virk, K. S.; Sipe, J. E. Multidimensional Fourier Spectroscopy of Semiconductors. II. Decoherence Effects. *Phys. Rev. B - Condens. Matter Mater. Phys.* **2009**, *80* (16), 1–28. https://doi.org/10.1103/PhysRevB.80.165319.

(75) Chen, P. C. An Introduction to Coherent Multidimensional Spectroscopy. *Appl. Spectrosc.* **2016**, *70* (12), 1937–1951. https://doi.org/10.1177/0003702816669730.

(76) Zhang, W. M.; Chernyak, V.; Mukamel, S. Multidimensional Femtosecond Correlation Spectroscopies of Electronic and Vibrational Excitons. *J. Chem. Phys.* **1999**, *110* (11), 5011–5028. https://doi.org/10.1063/1.478400.

(77) Mukamel, S.; Richter, M. Multidimensional Phase-Sensitive Single-Molecule Spectroscopy with Time-and-Frequency-Gated Fluorescence Detection. *Phys. Rev. A - At. Mol. Opt. Phys.* **2011**, *83* (1), 1–10. https://doi.org/10.1103/PhysRevA.83.013815.

(78) Cundiff, S. T.; Mukamel, S. Optical Multidimensional Coherent Spectroscopy. *Phys. Today* **2013**, *66* (7), 44–49. https://doi.org/10.1063/PT.3.2047.

(79) Lomsadze, B.; Cundiff, S. T. Tri-Comb Multidimensional Coherent Spectroscopy. *IEEE Photonics Technol. Lett.* **2019**, *31* (23), 1886–1889. https://doi.org/10.1109/LPT.2019.2948342.

(80) Falvo, C.; Palmieri, B.; Mukamel, S. Coherent Infrared Multidimensional Spectra of the OH Stretching Band in Liquid Water Simulated by Direct Nonlinear Exciton Propagation. *J. Chem. Phys.* **2009**, *130* (18). https://doi.org/10.1063/1.3120771.

(81) Zhuang, W.; Hayashi, T.; Mukamel, S. Coherent Multidimensional Vibrational Spectroscopy of Biomolecules: Concepts, Simulations, and Challenges. *Angew. Chemie - Int. Ed.* **2009**, *48* (21), 3750–3781. https://doi.org/10.1002/anie.200802644.

(82) Oliver, T. A. A. Recent Advances in Multidimensional Ultrafast Spectroscopy. *R. Soc. Open Sci.* **2018**, *5* (1). https://doi.org/10.1098/rsos.171425.

(83) Lomsadze, B.; Smith, B. C.; Cundiff, S. T. Rapid and High-Resolution Multidimensional Coherent Spectroscopy Using Three Frequency Combs. *2019 Conf. Lasers Electro-Optics, CLEO 2019 - Proc.* **2019**, *1391* (September), 1389–1391. https://doi.org/10.23919/CLEO.2019.8749324.

(84) Smallwood, C. L.; Cundiff, S. T. Multidimensional Coherent Spectroscopy of Semiconductors. *Laser Photonics Rev.* **2018**, *12* (12), 1–21. https://doi.org/10.1002/lpor.201800171.

(85) Sanders, J. N.; Saikin, S. K.; Mostame, S.; Andrade, X.; Widom, J. R.; Marcus, A. H.; Aspuru-Guzik, A. Compressed Sensing for Multidimensional Spectroscopy Experiments. *J. Phys. Chem. Lett.* **2012**, *3* (18), 2697–2702. https://doi.org/10.1021/jz300988p.

(86) Scholes, G. D.; Fleming, G. R.; Olaya-Castro, A.; Van Grondelle, R. Lessons from Nature about Solar Light Harvesting. *Nat. Chem.* **2011**, *3* (10), 763–774. https://doi.org/10.1038/nchem.1145.

(87) Hayes, D.; Engel, G. S. Extracting the Excitonic Hamiltonian of the Fenna-Matthews-Olson Complex Using Three-Dimensional Third-Order Electronic Spectroscopy. *Biophys. J.* **2011**, *100* (8), 2043–2052. https://doi.org/10.1016/j.bpj.2010.12.3747.

(88) Schlau-Cohen, G. S.; Ishizaki, A.; Calhoun, T. R.; Ginsberg, N. S.; Ballottari, M.; Bassi, R.; Fleming, G. R. Elucidation of the Timescales and Origins of Quantum Electronic Coherence in LHCII. *Nat. Chem.* **2012**, *4* (5), 389–395. https://doi.org/10.1038/nchem.1303.

(89) Hayes, D.; Engel, G. S. Peak Shape Analysis of Diagonal and Off-Diagonal Features in the Two-Dimensional Electronic Spectra of the Fenna-Matthews-Olson Complex. *Philos. Trans. R. Soc. A Math. Phys. Eng. Sci.* **2012**, *370* (1972), 3692–3708. https://doi.org/10.1098/rsta.2011.0201.

(90) Konar, A.; Sechrist, R.; Song, Y.; Policht, V. R.; Laible, P. D.; Bocian, D. F.; Holten, D.; Kirmaier, C.; Ogilvie, J. P. Electronic Interactions in the Bacterial Reaction Center Revealed by Two-Color 2D Electronic Spectroscopy. *J. Phys. Chem. Lett.* **2018**, *9* (18), 5219–5225. https://doi.org/10.1021/acs.jpclett.8b02394.

(91) Arsenault, E. A.; Yoneda, Y.; Iwai, M.; Niyogi, K. K.; Fleming, G. R. Vibronic Mixing Enables Ultrafast Energy Flow in Light-Harvesting Complex II. *Nat. Commun.* **2020**, *11* (1), 1–8. https://doi.org/10.1038/s41467-020-14970-1.

(92) Turner, D. B.; Stone, K. W.; Gundogdu, K.; Nelson, K. A. Three-Dimensional Electronic Spectroscopy of Excitons in GaAs Quantum Wells. *J. Chem. Phys.* **2009**, *131* (14). https://doi.org/10.1063/1.3245964.

(93) Kuehn, W.; Reimann, K.; Woerner, M.; Elsaesser, T.; Hey, R. Two-Dimensional Terahertz Correlation Spectra of Electronic Excitations in Semiconductor Quantum Wells. *J. Phys. Chem. B* **2011**, *115* (18), 5448–5455. https://doi.org/10.1021/jp1099046.

(94) Davis, J. A.; Hall, C. R.; Dao, L. V.; Nugent, K. A.; Quiney, H. M.; Tan, H. H.; Jagadish, C. Three-Dimensional Electronic Spectroscopy of Excitons in Asymmetric Double Quantum Wells. *J. Chem. Phys.* **2011**, *135* (4). https://doi.org/10.1063/1.3613679.

(95) Butkus, V.; Zigmantas, D.; Abramavicius, D.; Valkunas, L. Distinctive Character of Electronic and Vibrational Coherences in Disordered Molecular Aggregates. *Chem. Phys. Lett.* **2013**, *587*, 93–98. https://doi.org/10.1016/j.cplett.2013.09.043.

(96) Kim, J.; Mukamel, S.; Scholes, G. D. Two-Dimensional Electronic Double-Quantum Coherence Spectroscopy. *Acc. Chem. Res.* **2009**, *42* (9), 1375–1384. https://doi.org/10.1021/ar9000795.

(97) Tanimura, Y.; Mukamel, S. Two-Dimensional Femtosecond Vibrational Spectroscopy of Liquids. *J. Chem. Phys.* **1993**, *99* (12), 9496–9511. https://doi.org/10.1063/1.465484.

(98) Cho, M.; Yu, J. Y.; Joo, T.; Nagasawa, Y.; Passino, S. A.; Fleming, G. R. The Integrated Photon Echo and Solvation Dynamics. *J. Phys. Chem.* **1996**, *100* (29), 11944–11953. https://doi.org/10.1021/jp9601983.

(99) Cho, M. Coherent Two-Dimensional Optical Spectroscopy. *Chem. Rev.* **2008**, *108* (4), 1331–1418. https://doi.org/10.1021/cr078377b.

(100) Garrett-Roe, S.; Hamm, P. Purely Absorptive Three-Dimensional Infrared Spectroscopy. *J. Chem. Phys.* **2009**, *130* (16). https://doi.org/10.1063/1.3122982.

(101) Borek, J. A.; Perakis, F.; Hamm, P. Testing for Memory-Free Spectroscopic Coordinates by 3D IR Exchange Spectroscopy. *Proc. Natl. Acad. Sci. U. S. A.* **2014**, *111* (29), 10462–10467. https://doi.org/10.1073/pnas.1406967111.

(102) Hamm, P.; Lim, M.; Degrado, W. F.; Hochstrasser, R. M. The Two-Dimensional IR Nonlinear Spectroscopy of a Cyclic Penta-Peptide in Relation to Its Three-Dimensional Structure. *Proc. Natl. Acad. Sci. U. S. A.* **1999**, *96* (5), 2036–2041. https://doi.org/10.1073/pnas.96.5.2036.

(103) Garrett-Roe, S.; Perakis, F.; Rao, F.; Hamm, P. Three-Dimensional Infrared Spectroscopy of Isotope-Substituted Liquid Water Reveals Heterogeneous Dynamics. *J. Phys. Chem. B* **2011**, *115* (21), 6976–6984. https://doi.org/10.1021/jp201989s.

(104) Seiler, H.; Palato, S.; Sonnichsen, C.; Baker, H.; Kambhampati, P. Seeing Multiexcitons through Sample Inhomogeneity: Band-Edge Biexciton Structure in CdSe Nanocrystals Revealed by Two-Dimensional Electronic Spectroscopy. *Nano Lett.* **2018**, *18* (5), 2999–3006. https://doi.org/10.1021/acs.nanolett.8b00470.

(105) De Camargo, F. V. A.; Grimmelsmann, L.; Anderson, H. L.; Meech, S. R.; Heisler, I. A. Resolving Vibrational from Electronic Coherences in Two-Dimensional Electronic Spectroscopy: The Role of the Laser Spectrum. *Phys. Rev. Lett.* **2017**, *118* (3), 1–6. https://doi.org/10.1103/PhysRevLett.118.033001.

(106) Tyagi, P.; Saari, J. I.; Walsh, B.; Kabir, A.; Crozatier, V.; Forget, N.; Kambhampati, P. Two-Color Two-Dimensional Electronic Spectroscopy Using Dual Acousto-Optic Pulse Shapers for Complete Amplitude, Phase, and Polarization Control of Femtosecond Laser Pulses. *J. Phys. Chem. A* **2013**, *117* (29), 6264–6269. https://doi.org/10.1021/jp400603r.

(107) Brixner, T.; Mančal, T.; Stiopkin, I. V.; Fleming, G. R. Phase-Stabilized Two-Dimensional Electronic Spectroscopy. *J. Chem. Phys.* **2004**, *121* (9), 4221–4236. https://doi.org/10.1063/1.1776112.

(108) Turner, D. B.; Hassan, Y.; Scholes, G. D. Exciton Superposition States in CdSe Nanocrystals Measured Using Broadband Two-Dimensional Electronic Spectroscopy. *Nano Lett.* **2012**, *12* (2), 880–886. https://doi.org/10.1021/nl2039502.

(109) Tekavec, P. F.; Lott, G. A.; Marcus, A. H. Fluorescence-Detected Two-Dimensional Electronic Coherence Spectroscopy by Acousto-Optic Phase Modulation. *J. Chem. Phys.* **2007**, *127* (21). https://doi.org/10.1063/1.2800560.

(110) Scheurer, C.; Mukamel, S. Design Strategies for Pulse Sequences in Multidimensional Optical Spectroscopies. *J. Chem. Phys.* **2001**, *115* (11), 4989–5004. https://doi.org/10.1063/1.1391266.

(111) TIWARI, V.; MATUTES, Y. A.; YU, Z.; PTASZEK, M.; BOCIAN, D. F.; HOLTEN, D.; KIRMAIER, C.; KONAR, A.; OGILVIE, J. P. Strongly Coupled Bacteriochlorophyll Dyad Studied Using Two-Dimensional Phase-Modulated Fluorescence-Detected Electronic Spectroscopy. *arXiv* **2018**, *26* (17), 22327–22341.

(112) Mueller, S.; Lüttig, J.; Malý, P.; Ji, L.; Han, J.; Moos, M.; Marder, T. B.; Bunz, U. H. F.; Dreuw, A.; Lambert, C.; Brixner, T. Rapid Multiple-Quantum Three-Dimensional Fluorescence Spectroscopy Disentangles Quantum Pathways. *Nat. Commun.* **2019**, *10* (1), 1–11. https://doi.org/10.1038/s41467-019-12602-x.

(113) De, A. K.; Monahan, D.; Dawlaty, J. M.; Fleming, G. R. Two-Dimensional Fluorescence-Detected Coherent Spectroscopy with Absolute Phasing by Confocal Imaging of a Dynamic Grating and 27-Step Phase-Cycling. *J. Chem. Phys.* **2014**, *140* (19). https://doi.org/10.1063/1.4874697.

(114) Karki, K. J.; Widom, J. R.; Seibt, J.; Moody, I.; Lonergan, M. C.; Pullerits, T.; Marcus, A. H. Coherent Two-Dimensional Photocurrent Spectroscopy in a PbS Quantum Dot Photocell. *Nat. Commun.* **2014**, *5* (1), 1–7. https://doi.org/10.1038/ncomms6869.

(115) Rahav, S.; Mukamel, S. Multidimensional Attosecond Photoelectron Spectroscopy with Shaped Pulses and Quantum Optical Fields. *Phys. Rev. A - At. Mol. Opt. Phys.* **2010**, *81* (6), 1–10. https://doi.org/10.1103/PhysRevA.81.063810.

(116) Roeding, S.; Brixner, T. Coherent Two-Dimensional Electronic Mass Spectrometry. *Nat. Commun.* **2018**, *9* (1), 1–9. https://doi.org/10.1038/s41467-018-04927-w.

(117) Augulis, R.; Zigmantas, D. Two-Dimensional Electronic Spectroscopy with Double Modulation Lock-in Detection: Enhancement of Sensitivity and Noise Resistance. *Opt. Express* **2011**, *19* (14), 13126. https://doi.org/10.1364/oe.19.013126.

(118) Myers, J. A.; Lewis, K. L.; Tekavec, P. F.; Ogilvie, J. P. Two-Color Two-Dimensional Fourier Transform Electronic Spectroscopy with a Pulse-Shaper. *Opt. Express* **2008**, *16* (22), 17420. https://doi.org/10.1364/oe.16.017420.

(119) Repository, Z. O.; Library, M. Infrared Spectroscopy Azide – Water Intermolecular Coupling Measured by Two – Color Two-Dimensional Infrared Spectroscopy. **2012**, *136*.

(120) Senlik, S. S.; Policht, V. R.; Ogilvie, J. P. Two-Color Nonlinear Spectroscopy for the Rapid Acquisition of Coherent Dynamics. *J. Phys. Chem. Lett.* **2015**, *6* (13), 2413–2420. https://doi.org/10.1021/acs.jpclett.5b00861.

(121) Borek, J. A.; Perakis, F.; Hamm, P. Azide-Water Intermolecular Coupling Measured by 2-Color 2D IR Spectroscopy. *EPJ Web Conf.* **2013**, *41*, 2–4. https://doi.org/10.1051/epjconf/20134106005.

(122) Cundiff, S. T. Optical Three Dimensional Coherent Spectroscopy. *Phys. Chem. Chem. Phys.* **2014**, *16* (18), 8193–8200. https://doi.org/10.1039/c4cp00176a.

(123) Voronine, D. V.; Abramavicius, D.; Mukamel, S. Manipulating Multidimensional Electronic Spectra of Excitons by Polarization Pulse Shaping. *J. Chem. Phys.* **2007**, *126* (4). https://doi.org/10.1063/1.2424706.

(124) Chachisvilis, M.; Fidder, H.; Sundström, V. Electronic Coherence in Pseudo Two-Colour Pump-Probe Spectroscopy. *Chem. Phys. Lett.* **1995**, *234* (1–3), 141–150. https://doi.org/10.1016/0009-2614(95)00041-2.

(125) Dawlaty, J. M.; Bennett, D. I. G.; Huxter, V. M.; Fleming, G. R. Mapping the Spatial Overlap of Excitons in a Photosynthetic Complex via Coherent Nonlinear Frequency Generation. *J. Chem. Phys.* **2011**, *135* (4). https://doi.org/10.1063/1.3607236.

(126) Gelzinis, A.; Butkus, V.; Songaila, E.; Augulis, R.; Gall, A.; Büchel, C.; Robert, B.; Abramavicius, D.; Zigmantas, D.; Valkunas, L. Mapping Energy Transfer Channels in Fucoxanthin-Chlorophyll Protein Complex. *Biochim. Biophys. Acta - Bioenerg.* **2015**, *1847* (2), 241–247. https://doi.org/10.1016/j.bbabio.2014.11.004.

(127) Konar, A.; Sechrist, R.; Song, Y.; Policht, V. R.; Laible, P. D.; Bocian, D. F.; Holten, D.; Kirmaier, C.; Ogilvie, J. P. Electronic Interactions in the Bacterial Reaction Center Revealed by Two-Color 2D Electronic Spectroscopy. *J. Phys. Chem. Lett.* **2018**, *9* (18), 5219–5225. https://doi.org/10.1021/acs.jpclett.8b02394.

(128) Gelzinis, A.; Augulis, R.; Butkus, V.; Robert, B.; Valkunas, L. Two-Dimensional Spectroscopy for Non-Specialists. *Biochim. Biophys. Acta - Bioenerg.* **2019**, *1860* (4), 271–285. https://doi.org/10.1016/j.bbabio.2018.12.006.

(129) Li, X.; Nakayama, H.; Arakawa, Y. Phonon Bottleneck in Quantum Dots: Role of Lifetime of the Confined Optical Phonons. *Phys. Rev. B - Condens. Matter Mater. Phys.* **1999**, *59* (7), 5069–5073. https://doi.org/10.1103/PhysRevB.59.5069.

(130) Urayama, J.; Norris, T. B.; Singh, J.; Bhattacharya, P. Observation of Phonon Bottleneck in Quantum Dot Electronic Relaxation. *Phys. Rev. Lett.* **2001**, *86* (21), 4930–4933. https://doi.org/10.1103/PhysRevLett.86.4930.

(131) Meerifield, R. E. Propagation of Electronic Excitation in Insulating Crystals. *J. Chem. Phys.* **1958**, *28* (4), 647–650. https://doi.org/10.1063/1.1744206.

(132) Trlifaj, M. The Diffusion of the Excitation Energy in Molecular Crystals. *Czechoslov. J. Phys.* **1958**, *8* (5), 510–520. https://doi.org/10.1007/BF01602895.

(133) Aslangul, C.; Al., E. Density Operator Description of Excitons in Molecular Aggregates... *Phys. Rev. B* **1974**, *10*.

(134) Cohen-Tannoudji, C. Theorie Quantique Du Cycle de Pompage Optique Verification Experimentale Des Nouveaux Effets Prevus. **1962**, 1–72.

(135) Turner, D. B.; Scholes, G. D. Comparison of Electronic and Vibrational Coherence Measured by Two-Dimensional Electronic Spectroscopy. *Opt. InfoBase Conf. Pap.* **2011**, 1904–1911. https://doi.org/10.1364/ls.2011.ltue1.

(136) Caram, J. R.; Zheng, H.; Dahlberg, P. D.; Rolczynski, B. S.; Griffin, G. B.; Fidler, A. F.; Dolzhnikov, D. S.; Talapin, D. V.; Engel, G. S. Persistent Interexcitonic Quantum Coherence in CdSe Quantum Dots. *J. Phys. Chem. Lett.* **2014**, *5* (1), 196–204. https://doi.org/10.1021/jz402336t.

(137) Pullerits, T.; Zigmantas, D.; Sundström, V. Beatings in Electronic 2D Spectroscopy Suggest Another Role of Vibrations in Photosynthetic Light Harvesting. *Proc. Natl. Acad. Sci. U. S. A.* **2013**, *110* (4), 1148–1149. https://doi.org/10.1073/pnas.1221058110.

(138) Butkus, V.; Zigmantas, D.; Valkunas, L.; Abramavicius, D. Vibrational vs. Electronic Coherences in 2D Spectrum of Molecular Systems. *Chem. Phys. Lett.* **2012**, *545*, 40–43. https://doi.org/10.1016/j.cplett.2012.07.014.

(139) Collini, E.; Gattuso, H.; Levine, R. D.; Remacle, F. Ultrafast Fs Coherent Excitonic Dynamics in CdSe Quantum Dots Assemblies Addressed and Probed by 2D Electronic Spectroscopy. *J. Chem. Phys.* **2021**, *154* (1). https://doi.org/10.1063/5.0031420.

(140) Seibt, J.; Pullerits, T. Beating Signals in 2D Spectroscopy: Electronic or Nuclear Coherences? Application to a Quantum Dot Model System. *J. Phys. Chem. C* **2013**, *117* (36), 18728–18737. https://doi.org/10.1021/jp406103m.

(141) Cui, J.; Beyler, A. P.; Coropceanu, I.; Cleary, L.; Avila, T. R.; Chen, Y.; Cordero, J. M.; Heathcote, S. L.; Harris, D. K.; Chen, O.; Cao, J.; Bawendi, M. G. Evolution of the Single-Nanocrystal Photoluminescence Linewidth with Size and Shell: Implications for Exciton-Phonon Coupling and the Optimization of Spectral Linewidths. *Nano Lett.* **2016**, *16* (1), 289–296. https://doi.org/10.1021/acs.nanolett.5b03790.

(142) Candès, E. J. Compressive Sampling. *Int. Congr. Math. ICM 2006* **2006**, *3*, 1433–1452. https://doi.org/10.4171/022-3/69.

(143) Candès, E. J.; Romberg, J.; Tao, T. Robust Uncertainty Principles: Exact Signal Reconstruction from Highly Incomplete Frequency Information. *IEEE Trans. Inf. Theory* **2006**, *52* (2), 489–509. https://doi.org/10.1109/TIT.2005.862083.

(144) Candes, E. J.; Wakin, M. B. An Introduction To Compressive Sampling. *IEEE Signal Process. Mag.* **2008**, *25* (2), 21–30. https://doi.org/10.1109/msp.2007.914731.

(145) Duarte, M. F.; Davenport, M. A.; Takhar, D.; Laska, J. N.; Sun, T.; Kelly, K. F.; Baraniuk, R. G. Single-Pixel Imaging via Compressive Sampling. *IEEE Signal Process. Mag.* **2008**, *25* (2), 83–91. https://doi.org/10.1109/msp.2007.914730.

(146) Tibshirani, R. Regression Shrinkage and Selection Via the Lasso. *J. R. Stat. Soc. Ser. B* **1996**, *58* (1), 267–288. https://doi.org/10.1111/j.2517-6161.1996.tb02080.x.

(147) Roeding, S.; Klimovich, N.; Brixner, T. Optimizing Sparse Sampling for 2D Electronic Spectroscopy. *J. Chem. Phys.* **2017**, *146* (8). https://doi.org/10.1063/1.4976309.

(148) Kazimierczuk, K.; Orekhov, V. Y. Accelerated NMR Spectroscopy by Using Compressed Sensing. *Angew. Chemie - Int. Ed.* **2011**, *50* (24), 5556–5559. https://doi.org/10.1002/anie.201100370.

(149) Dunbar, J. A.; Osborne, D. G.; Anna, J. M.; Kubarych, K. J. Accelerated 2D-IR Using Compressed Sensing. *J. Phys. Chem. Lett.* **2013**, *4* (15), 2489–2492. https://doi.org/10.1021/jz401281r.

(150) Swärd, J.; Adalbjörnsson, S. I.; Jakobsson, A. High Resolution Sparse Estimation of Exponentially Decaying N-Dimensional Signals. *Signal Processing* **2016**, *128*, 309–317. https://doi.org/10.1016/j.sigpro.2016.04.002.